

# Chiral Luttinger liquids at the fractional quantum Hall edge

A. M. Chang\*

*Department of Physics, Purdue University, West Lafayette, Indiana 47907-1396, USA*

(Published 13 November 2003)

The edges of quantum Hall fluids behave as one-dimensional conductors. This article reviews electron transport into these edge states, covering both the theory based on the chiral Luttinger liquid and the experimental findings using electron tunneling as the probe. The first part of the review presents a basic description of this theory, including a derivation of the density of states, to provide a framework and language for discussing the experimental observations. The signature of the chiral Luttinger liquid is a power-law behavior for the density of states and the tunneling conductances. Experimentally, two techniques have been applied to study the tunneling conductance, using a gated point contact between two quantum Hall edges, or using a cleaved-edge barrier between an edge and a normal conductor. The point-contact method exhibits resonant tunneling, which appears to show some aspects of the Luttinger liquid, and the cleaved-edge method has yielded clear power-law dependences in the off-resonance conductances. Power-law behavior over many orders of magnitude is observed, confirming the Luttinger-liquid character of the edge states. However, the power-law exponents, while in agreement with finite-size numerical calculations, can differ from the universal values predicted by the Chern-Simon field theory. This disagreement is still not well understood. The review concludes with a brief survey of other one-dimensional conductors that have been studied to look for characteristics of the nonchiral Tomonaga-Luttinger liquid.

## CONTENTS

I. Introduction	1449	IV. Other Luttinger-Liquid Systems	1495
II. Theoretical Background	1451	A. Ballistic single-channel wires	1496
A. Breakdown of the Fermi-liquid picture in one dimension and the Tomonaga-Luttinger liquid	1452	B. Carbon nanotubes	1496
1. Bosonization	1454	C. One-dimensional gold atom chains	1497
2. Power-law behavior in the single-particle Green's function	1455	D. Quasi-one-dimensional conductors	1498
3. $g$ -ology	1457	Acknowledgments	1500
B. Chiral Luttinger liquid	1460	References	1500
1. Wen's hydrodynamic formulation	1461		
2. 1D effective-field theory of the chiral Luttinger liquid	1464		
3. Role of disorder	1466		
4. Compressible fluid edges	1466		
5. Scaling functions for electron tunneling	1468		
6. Resonant tunneling	1472		
7. Shot noise and fractional charge: quasiparticle tunneling	1474		
8. Finite-size numerical investigations	1475		
III. Experiments on Chiral Luttinger Liquids—Tunneling into the Fractional Quantum Hall Edge	1475		
A. Measurement techniques	1478		
B. Point-contact experiments	1479		
C. Cleaved-edge experiments	1480		
1. Crystal and sample preparation	1480		
2. Tunneling conductances at $\nu=1/3$	1482		
3. Tunneling conductances at $\nu=1/2$	1485		
4. Power-law exponents and universality	1486		
5. Resonant tunneling into a biased fractional quantum Hall edge	1489		
D. Discussion: Is the chiral Luttinger liquid exponent universal?	1490		
E. Shot-noise characteristics and fractional charges	1493		
		I. INTRODUCTION	

This article deals with electron transport in a new state of matter, specifically, electron tunneling into the chiral Luttinger liquid (CLL). The chiral Luttinger liquid, also known as the chiral Tomonaga-Luttinger liquid,<sup>1</sup> is a particularly simple form of strongly interacting one-dimensional (1D) metallic conductor. Its theoretical definition is a one-dimensional metal having elementary excitations which propagate or circulate along the boundary in one direction only; its practical realization is by the edge states of quantum Hall effect conductors. The CLL is distinguished from conventional three-dimensional (3D) metals by the absence of a single-particle pole in the spectral density. Instead, the usual pole is replaced by power-law dependences in momentum and frequency. Experimentally, what this means is that in a transport measurement where electrons are injected into or removed from the 1D correlated metal across a tunneling barrier, a power-law behavior is observed. This behavior occurs either in the tunnel current or in the differential conductance as a function of energy, where this energy may be set by a bias voltage or

<sup>1</sup>See, for example, Wen, 1990a, 1990b, 1991a, 1991b, 1992, 1995; Moon *et al.*, 1993; Kane *et al.*, 1994; Fendley *et al.*, 1995a, 1995b; Kane and Fisher, 1995; Chang *et al.*, 1996, 2001; Grayson *et al.*, 1998.

\*Present address: Department of Physics, Duke University, Durham, NC 27708. Electronic address: yingshe@phy.duke.edu

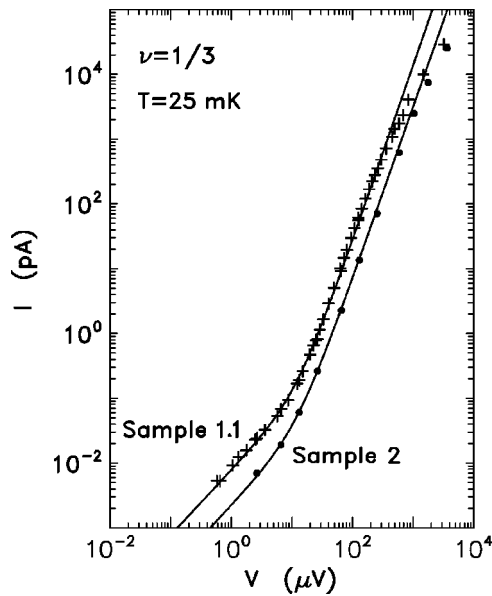


FIG. 1. Current-voltage ( $I$ - $V$ ) characteristics for tunneling from the bulk-doped  $n$ +GaAs into the edge of a  $\nu=1/3$  fractional quantum Hall effect: +, sample 1.1 in a log-log plot at  $B=13.4$  T; ●, sample 2 at  $B=10.8$  T. The solid curves represent fits to the theoretical universal scaling form of Eq. (178) for  $\alpha=2.7$  and 2.65, respectively. From Chang, Pfeiffer, and West (1996).

by temperature. From the perspective of measurements, the CLL is an extremely clean system. Residing at the one-dimensional edge of the two-dimensional fractional quantum Hall fluid, the CLL is realized in devices grown by the molecular-beam epitaxy (MBE) growth technique, which offers extremely precise, atomic-scale control. This control extends beyond the growth of the metallic electron system itself to include the tunnel barrier as well. Furthermore, the nature of the CLL can be tuned by changing the magnetic field and hence the filling factor of the fractional quantum Hall fluid. This tunability leads to a rich variety of similar yet different Luttinger liquids. In Fig. 1, we show the first set of current-voltage ( $I$ - $V$ ) data with sufficient dynamic range to establish a power-law dependence, obtained for electron tunneling from a 3D, highly doped bulk GaAs metal into the edge of a  $\nu=1/3$  fractional quantum Hall fluid (Chang *et al.*, 1996). Note that in the log-log plot, the low-bias voltage range below  $15 \mu\text{eV}$  is dominated by the thermal energy and is therefore linear. Above this regime a power-law behavior with a range exceeding three decades in current and 1.5 decades in voltage is observable. This power law stands in direct contrast to conventional metals, which exhibit an energy-independent tunneling conductance and a linear  $I$ - $V$  relationship in the clean limit, reflecting the energy-independent tunneling density of states. To date, both on-resonance tunneling and off-resonance tunneling have revealed signatures of this unusual power-law behavior (Chang *et al.*, 1996, 1998, 2001; Grayson *et al.*, 1998, 2001).

The present strong interest in Luttinger liquids comes from two major directions. First of all, interacting 1D and quasi-1D systems are extremely interesting in their own right, particularly in light of recent observations of anomalous behaviors such as dc and frequency-dependent conductivities, photoemission spectra, nuclear magnetic resonance (NMR) relaxation, etc. The systems in which they occur are quite diverse and include the CLL, 1D ballistic semiconductor wires (Tarucha *et al.*, 1995; Yacoby *et al.*, 1996; Auslaender *et al.*, 2000), 1D organic conductors (Basista *et al.*, 1990; Dardel *et al.*, 1993; Zwick *et al.*, 1997; Schwartz *et al.*, 1998), blue-bronze-type conductors (Dardel *et al.*, 1991; Denlinger *et al.*, 1999; Sing *et al.*, 1999), and carbon nanotubes (Bockrath *et al.*, 1999; Yao *et al.*, 1999; Bachtold *et al.*, 2001). Second, phenomenologically there appear to be considerable and unmistakable similarities between the high-temperature superconductors (Bednorz and Muller, 1986; Wu *et al.*, 1987) in their normal state (Anderson, 1987, 1990, 1992; Varma *et al.*, 1989; Harris *et al.*, 1992; Ando *et al.*, 1995) and the 1D Luttinger liquids. Most notable of these is the absence of a single-particle pole as determined from angle-resolved photoemission measurements (Anderson, 1987, 1990, 1992; Ding *et al.*, 1997; Shen and Schrieffer, 1997). This unambiguous and unusual feature has led to a tremendous amount of speculation and investigation on two-dimensional Luttinger-like correlated systems in which the coupling to a gauge field (Baskaran and Anderson, 1988; Zou and Anderson, 1988; Kopietz, 1996; Lee *et al.*, 1998) leads to power-law correlations (Ren and Anderson, 1993; Rantner and Wen, 2001). Models have also been proposed which assume outright the existence of coupled-1D Luttinger stripes (Emery *et al.*, 1999; Carlson *et al.*, 2000) where the stripes form as a result of phase separation.

One-dimensional Luttinger liquids could also prove to be of interest down the road because of their possible relevance to  $1+1$ -dimensional conformal field theories (see, for example, Voit, 1995). Conformal field theories are central to the theory of superstrings, which are modeled as one-dimensional objects. Furthermore, it is not entirely unthinkable that the physics associated with the chiral Luttinger liquid which exists at the edge of the two-dimensional quantum Hall fluid may bear similarity to the embedding of our  $3+1$ -dimensional space-time at the boundary of higher-dimensional spaces. Indeed, such a possibility has recently been explored (Zhang and Hu, 2001).

The CLL belongs to a larger class of new, correlated systems that are collectively termed non-Fermi-liquid systems. By a non-Fermi-liquid, we mean in general terms interacting fermion systems in which the elementary excitations cannot be described by the venerable Fermi-liquid picture of long-lived quasiparticles, related to bare electrons by a one-to-one correspondence via the adiabatic principle. Non-Fermi-liquids come in many varieties and are encountered in diverse systems. Outstanding examples include (1) 1D Luttinger liquids and Hubbard models, (2) 2D systems coupled to gauge

fields, (3) systems with strong Fermi-surface nesting, (4) composite-fermion systems in the fractional quantum Hall fluids, (5) systems in the vicinity of critical fluctuations or soft modes, and (6) Kondo systems or Anderson Hamiltonian systems in which a local degree of freedom couples to a continuum.

It is the purpose of this article to review the current status of the field of chiral Luttinger liquids in a manner that is intended to be self-contained and readily accessible to experimentalists and theorists alike. To accomplish this it is necessary to include, in addition to the major experimental results, a theory section in order to provide the framework for the key concepts and novel features associated with a Luttinger liquid. Written from an experimentalist's perspective, it is hoped that this theory section could also serve as a starting point for those readers interested in more in-depth theoretical studies. The experimental sections will discuss the techniques and advantages of the CLL system both from the perspective of the phenomenon itself and from the perspective of device realization, highlighting the major results and the unusual power-law tunneling density of states observed in both off-resonance and on-resonance conditions. We shall also discuss recent tunneling current noise measurements which shed light on the quasiparticle fractional charge, and briefly survey other 1D systems such as 1D quantum wires, carbon nanotubes, and quasi-1D organic and blue-bronze conductors.

This review is organized as follows: Section II introduces the basic theoretical framework for understanding a chiral Luttinger liquid. Section III summarizes the major experimental results in electron tunneling into the fractional quantum Hall edge. This section includes a discussion of the conditions under which the existence of a chiral Luttinger liquid is established, particularly with regard to the edge of the  $\nu=1/3$  fractional Hall fluid. We present evidence that Luttinger-liquid-like tunneling behavior is not restricted to the edge of the special, incompressible fractional quantum Hall fluid given by the Laughlin (1983), hierarchical (Haldane, 1983; Halperin, 1984), or Jain series (Jain, 1989a, 1989b, 1990), but can be observed at general filling fractions, including those corresponding to compressible fluids. We discuss the clear evidence of non-Fermi-liquid behavior in resonant tunneling (as opposed to off-resonance tunneling), where a resonant impurity level mediates the tunneling process. Furthermore, we describe quantum shot-noise measurements that probe the fractional charge of the quasiparticles (De-Picciotto *et al.*, 1997; Saminadayar *et al.*, 1997; Reznikov *et al.*, 1999). In Sec. IV, the review concludes with a survey of the latest developments in other 1D conducting systems such as quantum wires, single-walled nanotubes, and quasi-1D organic and blue-bronze conductors.

## II. THEORETICAL BACKGROUND

This section is devoted to an introductory review of the key theoretical concepts used to describe a chiral Luttinger liquid, presented from the point of view of an

experimentalist. The hope is to provide an appreciation, particularly for those readers who are not familiar with the theory of 1D interacting systems, of the unusual aspects of this new type of correlated electron fluid.

A chiral Luttinger liquid in one dimension is characterized by bosonic elementary excitations (plasmons) rather than the familiar Fermi-liquid quasiparticle/hole excitations, and by the absence of a single-particle pole, which is replaced by power-law behavior in the correlation functions. The difference can be subtle. In particular, in the sector of Hilbert space spanning neutral excitations at low energy ( $\omega \rightarrow 0$ ) and small wave vector ( $\mathbf{q} \rightarrow 0$ ), a Fermi-liquid description is still workable (Castellani *et al.*, 1994; Carmelo and Castro Neto, 1996; Ng, 1997; Castellani and Di Castro, 1999). However, in the charge sector in which the addition or removal of charged carriers (electrons or holes) is involved, the Fermi-liquid description breaks down, as evidenced in the destruction of the quasiparticle pole and the vanishing of the quasiparticle renormalization factor  $z_{\mathbf{k}}$ .

The basic and familiar picture of a Landau Fermi liquid (Landau, 1956, 1957, 1958) will not be reviewed here partially due to space constraints. Instead the reader is referred to discussions in standard textbooks (Abrikosov *et al.*, 1963; Nozières, 1964; Mahan, 2000). For a discussion with continuity to this review, see Chang (2002). We begin our discussion with a summary of the main reasons the Fermi-liquid picture breaks down in one dimension, placing emphasis on the unusual phase-space structure which leads to the formation of a Tomonaga-Luttinger liquid, or Luttinger liquid for short. We describe Haldane's formulation (Haldane, 1979, 1981) based on the bosonization technique (Tomonaga, 1950; Matthis and Lieb, 1965; Luther and Peschel, 1974; Haldane, 1981), which solves the original Luttinger model (Tomonaga, 1950; Luttinger, 1963) exactly, and the alternative  $g$ -ology model renormalization-group analysis of the Luttinger fixed point (Solyom, 1979; Voit, 1995; Metzner *et al.*, 1998). From there we proceed to a consideration of the essential aspects of the theory of the chiral Luttinger liquid. We start with the seminal, effective-field formulation due to Wen (1990a, 1990b, 1991a, 1991b, 1992, 1995) for incompressible fractional Hall fluid edges, and discuss the role of disorder (Kane *et al.*, 1994; Kane and Fisher, 1995) before moving to a discussion of the compressible fractional fluids (Shytov *et al.*, 1998; Levitov *et al.*, 2001). We summarize the universal scaling functions for the tunneling current and conductance and in particular the Chamon-Fradkin scaling function (Chamon and Fradkin, 1997) for off-resonance tunneling. This scaling function, which covers the entire range from weak to strong tunneling for the case of incoherent, multiple point contacts, has proven extremely useful in providing systematic fits to the experimental data and extracting reliable power-law exponents. Lastly we touch on the case of on-resonance tunneling through an impurity level (Chamon and Wen, 1993; Kane and Fisher, 1994; Fendley *et al.*, 1995b; Geller *et al.*, 1996; Kane, 1998). In view of the existing discrepancy between experiment and certain predictions

of these effective-field theories, we conclude with a discussion of recent numerical results on finite-size systems (Goldman and Tsiper, 2001; Mandal and Jain, 2001, 2002; Wan *et al.*, 2002).

Although the field of the chiral Luttinger liquid at the fractional quantum Hall edge is relatively young, approximately 12 years old, the study of the Luttinger liquid has had a long history dating back to the 1950s and 1960s, at least as far as theory is concerned. Many authors have contributed to this exciting field and more complete reviews of different aspects are available (Emery, 1979; Solyom, 1979; Schulz, 1991, 1995; Voit, 1995; Metzner *et al.*, 1998). Excellent reviews of the theory of the chiral Luttinger liquid can also be found in the articles of Wen (1992, 1995). Once again, our goal here is to provide a self-contained, fairly complete overview of the transport properties, with an emphasis on describing the key ideas in relatively simple terms. For more thorough discussions of the theoretical issues we refer the reader to these excellent reviews.

#### A. Breakdown of the Fermi-liquid picture in one dimension and the Tomonaga-Luttinger liquid

The familiar Fermi-liquid picture in three dimensions is based on the existence of long-lived quasiparticle/quasihole excitations as the energy of excitation approaches zero or equivalently as the energy approaches the Fermi energy. These quasiparticles (quasiholes) can be traced back to bare electrons (holes) with a one-to-one correspondence, starting from the noninteracting situation followed by adiabatic turning on of the electron-electron interaction. Phenomenologically supposing the existence of such low-energy excitations, Landau was able to account for a rich variety of physical phenomena exhibited by conventional metals in the presence of non-negligible interactions (Landau 1956, 1957, 1958). The Fermi-liquid picture finds more rigorous justification in many-body perturbation theory (Abrikosov *et al.*, 1963; Nozières, 1964) through in-depth analysis of (i) the quasiparticle lifetime, which varies as  $|k - k_F|^{-2}$  when  $k$  approaches  $k_F$  for  $D \geq 2$ , or as  $|E - E_F|^{-2}$  when  $E$  approaches the Fermi energy  $E_F$  (Luttinger, 1960), and (ii) the interaction operators  $\gamma$  and  $\Gamma$  (reduced operator), leading to the well-known Ward identities reflecting underlying conservation laws—e.g., continuity equations reflecting the conservation of charge and enabling us to relate vertex functions and interaction operators to the Landau parameters. The slow rate of decay for excitations near  $E_F$  is central to the success of the Fermi-liquid picture.

The Fermi-liquid picture breaks down in one dimension. This is a direct consequence of the unique phase-space structure in one dimension, notably the fact that the Fermi surface consists of two discrete points ( $\pm k_F$ ) rather than a line or surface (or multiple lines or surfaces), and that for each branch of the momentum-energy dispersion—left- or right-moving—the 1D wave

vector uniquely determines the energy. Some of the most significant, interrelated consequences include the following:

- (1) The reduced 1D phase space leads to a quasiparticle scattering rate  $(\text{Im}[\Sigma(\mathbf{k}, \omega)]) \propto |k - k_F|$  and  $\propto \omega$ , rather than the  $|k - k_F|^2$  and  $\omega^2$  dependences in two and three dimensions, and to a logarithmic divergence in  $\text{Re}(\Sigma)$  at  $E = E_F$  ( $\omega \rightarrow 0$ ) (Luttinger, 1960; Voit, 1995; Metzner *et al.*, 1998). Here  $\Sigma$  denotes the self-energy. Note that the real and imaginary parts of  $\Sigma$  are related by the Kramers-Kronig relations.
- (2) Logarithmic divergences appear in the two-particle interaction operator commencing in second-order perturbation theory related to (1) above.
- (3) A logarithmic divergence at  $E_F$  directly implies that the quasiparticle renormalization, or quasiparticle weight, vanishes:  $z_{\mathbf{k}}|_{k_F} \sim (1 + \partial[\text{Re}[\Sigma]/\partial\omega])^{-1}|_{E_F} \sim 1/\ln(\omega) \rightarrow 0!$  Hence the one-to-one correspondence of the unperturbed  $\mathbf{k}$ -electron state to the elementary excitations of the interacting system is lost.
- (4) Low-energy electron-hole excitations arising from interactions can occur about the two discrete Fermi points at  $\pm k_F$  with small momentum transfer,  $q \ll k_F$ , or across the Fermi sea with momentum transfer  $q \approx 2k_F$ . This indicates that as the excitation energy approaches zero, there is a forbidden region for electron-hole excitations at  $0 < q < 2k_F$ . Generalizations to multiple electron-hole processes yield a series of forbidden regions,  $2(n-1)k_F < q < 2nk_F$ , where  $n$  denotes the number of electron-hole pairs.
- (5) Spin-charge separation occurs, i.e., the spin and charge bosonic elementary excitations propagate at different velocities. The presence of low-energy, ungapped bosonic charge and spin modes is a direct consequence of the finite spin and charge-density responses at low  $q$  and  $\omega$ .

All of these well-known behaviors point to the inescapable fact that the Fermi-liquid picture is not appropriate in 1D once electron-electron interaction is turned on. The Fermi liquid cannot serve as an adequate starting point for understanding certain aspects of this strongly correlated system, particularly those processes involving the so-called charge and spin sectors where injection or removal of bare electrons takes place. In contrast, thermodynamic properties, which depend on the neutral excitations (e.g.,  $e$ - $h$  pairs, collective modes, plasmons, etc.) at low  $\omega$ , and  $\mathbf{q}$  ( $\omega \ll \epsilon_F, q \ll k_F$ ), can still adequately be described by the Fermi liquid, albeit with the caveat that the quasiparticle to bare electron one-to-one correspondence is lost (Solyom, 1979; Schulz, 1991, 1995; Voit, 1995; Carmelo and Castro Neto, 1996; Ng, 1997; Metzner *et al.*, 1998; Castellani and Di Castro, 1999).

Historically there have been two major parallel and complementary approaches to the theoretical investigation of interacting metallic 1D systems, with their focus centered on the idealized Tomonaga-Luttinger models

(Tomonaga, 1950; Luttinger, 1963). One approach is based on the bosonization technique (Tomonaga, 1950; Matthis and Lieb, 1965; Luther and Emery, 1974; Luther and Peschel, 1974; Haldane, 1981), and the other on the so-called  $g$ -ology model in connection with renormalization-group treatment (Menyhard and Solyom, 1973; Solyom, 1979; Metzner *et al.*, 1998). Note that related models in the field-theoretic context have also been explored (Heidenreich *et al.*, 1975). A general discussion of the topic of interaction in 1D encompasses a rather diverse range of systems and phenomena. In addition to metallic systems, other related systems such as the 1D Hubbard model or models with strong backscattering are of great interest in their own right. Here we confine our attention to metallic systems with weak backscattering to avoid complications introduced by insulating tendencies or by gapped behavior in the spectrum of low-energy excitation. The bosonization approach, first introduced by Tomonaga (1950), and Matthis and Lieb (1965), and later on expanded upon by Luther and Peschel (1974) and Haldane (1979, 1981), indicates that a bosonic description is appropriate in one dimension for interacting systems dominated by forward scattering. The renormalization-group approach is basically a method for going beyond perturbation theory and in many instances has the effect of summing up the most relevant (logarithmically divergent) diagrams in a systematic and controlled way. Because its implementation is invariably founded on many-body perturbation theory, the usual many-body techniques play a natural and useful role. These include using the Ward identities arising out of conservation laws to connect the vertex functions with physically measurable quantities, equation-of-motion methods, and others. As a consequence, this type of analysis has proven helpful in elucidating the relation between a Fermi liquid and a Tomonaga-Luttinger liquid, while at the same time allowing clear-cut differentiation of the two systems. The aforementioned signature difficulties in conventional treatments of the 1D problem are simply indicative of the fact that the fermion representation is not the appropriate basis for describing the essential low-energy physics and dynamics.

The Tomonaga and Luttinger models are idealized interacting 1D models that are soluble. Their solubility is based on (i) linearized dispersion about the two Fermi points at  $\pm k_F$ ; and (ii) a forward-scattering interaction only, with no backscattering terms. These original models do not include electron spin. Generalization to include spin is straightforward and will be discussed in the  $g$ -ology model. Specifically the Tomonaga Hamiltonian is given in second-quantized form by (Tomonaga, 1950; Dzyaloshinskii and Larkin, 1973)

$$H_{Tomonaga} = \sum_k \frac{k^2}{2m} a_k^\dagger a_k + \frac{1}{2} \sum_{k,k',q} \lambda_q a_k^\dagger a_{k+q} a_{k'}^\dagger a_{k'-q}, \quad (1)$$

where  $q$  is restricted to  $|q| \ll 2k_F$ , or equivalently  $\lambda_q$  is appreciable only for small  $q$  values and approaches zero when  $q$  is of order  $2k_F$ . The Luttinger model intro-

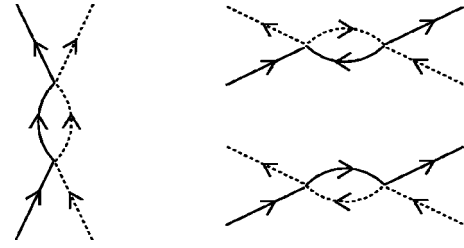


FIG. 2. Cooper (left) and zero-sound (right) diagrams for one dimension: solid lines, the unrenormalized propagator for right-moving electrons; dashed lines, the left-moving electrons.

duces massless Dirac fermions with linear dispersion, which renders the problem more mathematically tractable. The introduction of Dirac fermions and a sea of negative energy states does not qualitatively change the low-energy physics, since excitations to the Fermi level require large energies. The Luttinger Hamiltonian defined on a line of length  $L$  is given by (Luttinger, 1963; Matthis and Lieb, 1965; Luther and Peschel, 1974)

$$H_{Luttinger} = H_o + H_I, \quad (2)$$

$$\begin{aligned} H_o &= v_F \int_0^L \Psi^\dagger(x) \sigma_z p \Psi(x) dx \\ &= v_F \int_0^L [\psi_r^\dagger(x) p \psi_r(x) - \psi_l^\dagger(x) p \psi_l(x)] dx \\ &= v_F \sum_k k (a_{r,k}^\dagger a_{r,k} - a_{l,k}^\dagger a_{l,k}), \end{aligned} \quad (3)$$

$$H_I = 2 \frac{\lambda v_F}{L} \sum_{k,k',q} u_q (a_{r,k}^\dagger a_{r,k+q} a_{l,k'}^\dagger a_{l,k'-q}). \quad (4)$$

Here  $v_F$  is the magnitude of the Fermi velocity,  $\Psi^\dagger = (\psi_l, \psi_r)$ ,  $\sigma_z$  is the  $z$  component of the Pauli spin matrix, and the subscripts  $l$  and  $r$  refer to the left- and right-moving branches of the energy-momentum dispersion, respectively. Note that there are no backscattering terms of the form  $a_{r,k}^\dagger a_{l,k+q} a_{l,k'}^\dagger a_{r,k'-q}$  which scatter particles between left- and right-moving branches. The second-order perturbation calculation for the self-energy  $\Sigma$ , corresponding to a diagram of the type shown in Fig. 2, yields the well-known results that  $\text{Im}[\Sigma] \sim \omega$  and  $\text{Re}[\Sigma] \sim \omega \ln \omega$ , leading to the vanishing of the quasiparticle normalization factor,  $z \rightarrow 0$  (Luttinger, 1960; Metzner *et al.*, 1998). This is a clear sign that conventional perturbative treatment, so successful in demonstrating the validity of the Fermi liquid in three dimensions, is no longer valid in one dimension.

The two models exhibit essentially the same low-energy physics. Tomonaga demonstrated that this type of 1D interacting model supports bosonic sound-wave excitations, which are plasmon oscillations with a linear dispersion  $\omega = v_q q$  where the interaction-dependent velocity is given by

$$v_q = \sqrt{v_F^2 + \frac{2v_F}{\pi} \lambda_q}. \quad (5)$$

A similar conclusion was reached by Matthis and Lieb (1965) for the Luttinger model. The Tomonaga and Luttinger models can be solved two ways, by bosonization (Tomonaga, 1950; Matthis and Lieb, 1965; Luther and Peschel, 1974; Haldane, 1979, 1981) and by nonperturbative many-body techniques such as renormalization-group analysis and the use of Ward identities (Dzyaloshinskii and Larkin, 1973; Everts and Schulz, 1974; Solyom, 1979; Metzner and Di Castro, 1993; Voit, 1995; Metzner *et al.*, 1998). It is convenient to work with the Luttinger model since the introduction of massless Dirac fermions allows a fully rigorous mathematical solution of the problem.

### 1. Bosonization

In a sense, bosonization is a natural way to address the 1D interacting system since, for models dominated by forward scattering, the elementary excitations are linearly dispersing boson modes. The key idea of bosonization lies in the central role played by the density operator:

$$\rho_{i,q} = \sum_k a_{i,k+q}^\dagger a_{i,k}, \quad (6)$$

$$\rho_{i,-q} = \sum_k a_{i,k-q}^\dagger a_{i,k}, \quad (7)$$

where  $q \geq 0$  and  $i=l,r$ . This definition is not fully rigorous and leads to ambiguities for  $q=0$ , as pointed out by Haldane (1979, 1981). For  $q=0$  it is sufficient to subtract out the expectation value of  $\rho_{i,0}$  in the ground state of the filled Fermi sea:

$$\rho_{i,q=0} = \sum_k [a_{i,k+q}^\dagger a_{i,k} - \langle 0 | a_{i,k+q}^\dagger a_{i,k} | 0 \rangle]. \quad (8)$$

This well-defined operator also uniquely and correctly accounts for quantities arising from the cancellation of two divergent terms when the continuum limit is taken to reflect infinite degrees of freedom. When used to compute commutation relations between operators, this subtraction is equivalent to a normal ordering with respect to the ground state of a filled Fermi sea; operators that annihilate the ground state are placed to the right before the cancellation of divergent quantities is carried out (Matthis and Lieb, 1965; Haldane, 1979, 1981). In so doing one obtains the all-important commutation relation for the  $\rho$ 's:

$$[\rho_{i,q}, \rho_{j,-q'}] = -\frac{\text{sgn}(i)Lq}{2\pi} \delta_{i,j} \delta_{q,q'}, \quad (9)$$

where  $\text{sgn}(i)=+1$  for  $i=r$ , and  $\text{sgn}(i)=-1$  for  $i=l$ . This commutation relation immediately leads to the definition of harmonic-oscillator-type raising and lowering operators for  $q>0$ :

$$a_q^\dagger = \sqrt{\frac{2\pi}{L|q|}} \rho_{r,q}, \quad a_{-q}^\dagger = \sqrt{\frac{2\pi}{L|q|}} \rho_{l,-q}, \quad (10)$$

and

$$a_q = \sqrt{\frac{2\pi}{L|q|}} \rho_{r,-q}, \quad a_{-q} = \sqrt{\frac{2\pi}{L|q|}} \rho_{l,q}, \quad (11)$$

respectively. The lowering operators annihilate the ground state. Note that there is no  $q=0$  bosonic mode. The  $q=0$  mode is represented by the number operator in each of the two left- and right-moving branches given above in Eq. (8). After normal ordering to properly subtract out divergent contributions, the kinetic term of the Hamiltonian,  $H_o = v_F \sum_k k [a_{r,k}^\dagger a_{r,k} - a_{l,k}^\dagger a_{l,k}]$ , can be written in terms of the boson raising and lowering operators as

$$H_o = v_F \sum_{q>0} |q| (a_q^\dagger a_q + a_{-q}^\dagger a_{-q}) + \frac{v_F}{L} [(N_r)^2 + (N_l)^2]. \quad (12)$$

A generalized interaction term of the Tomonaga-Luttinger type describing forward scattering only,  $H_{for}$ , can be written as

$$H_{for} = \frac{\pi}{L} \sum_q [V_q (\rho_{r,q} \rho_{r,-q} + \rho_{l,q} \rho_{l,-q}) + U_q (\rho_{r,q} \rho_{l,-q} + \rho_{r,-q} \rho_{l,q})]. \quad (13)$$

In terms of the boson operators, the total Hamiltonian takes the quadratic form (Haldane, 1981)

$$H = H_o + H_{for} = -\frac{1}{2} \sum_q v_F |q| \left[ v_N \left( \frac{k_F L}{\pi} + N_r + N_l \right)^2 + v_J (N_r - N_l)^2 \right] + \frac{1}{2} \sum_q |q| [(v_F + V_q) (a_q^\dagger a_q + a_q a_q^\dagger) + U_q (a_q^\dagger a_{-q}^\dagger + a_q a_{-q})], \quad (14)$$

where the velocities  $v_N = v_F + V_0 + U_0$  and  $v_J = v_F + V_0 - U_0$  characterize the propagation of the charge and current modes associated with the symmetric and antisymmetric combinations of  $N_r$  and  $N_l$  respectively, at low energies, with  $N = (k_F L)/\pi + N_r + N_l$  and  $J = N_r - N_l$ . This quadratic form is readily diagonalized by a Bogoliubov transformation:

$$b_q^\dagger = \cosh(\phi_q) a_q^\dagger - \sinh(\phi_q) a_{-q}, \quad (15)$$

with  $\phi_q = \frac{1}{2} \tanh^{-1}[-U_q/(v_F + V_q)]$ , yielding a Hamiltonian of noninteracting boson modes:

$$H = \sum \omega_q b_q^\dagger b_q + \frac{1}{2} \sum_q (\omega_q - v_F |q|) + \frac{\pi}{2L} [v_N N^2 + v_J J^2], \quad (16)$$

where  $\omega_q = \sqrt{(v_F + V_q)^2 - U_q^2} |q|$ , while the boson (plasmon) velocity,  $v_q \rightarrow v_o = \sqrt{(v_F + V_0)^2 - U_0^2}$  as  $q \rightarrow 0$ . Note that the relationship  $v_o^2 = v_N v_J$  holds. This relation is important and will remain valid in the case of the Luttinger liquid when interactions between boson modes are

present. For this Hamiltonian both the quantum numbers  $N$ , reflecting total charge, and  $J$ , reflecting the total current, are conserved. This form of the Hamiltonian clearly illustrates that the low-energy excitations of this 1D interacting fermion system are bosonic modes. Furthermore, it can be shown that the boson representation generates a complete Hilbert space, equivalent to the original fermionic Hilbert space (Overhauser, 1965; Haldane, 1981). What remains is the need to introduce a well-defined fermion operator,  $\psi_i(x)$ , in terms of the boson operators. Luther and Peschel (1974) first discovered such a representation. Although the original expression suffers from some ambiguities, it is nevertheless useful for illustrating the main features of such an operator. The Luther-Peschel expression for the fermion field,  $\psi_{LP,i}(x)$ , is given by

$$\psi_{LP,i}(x) = \frac{1}{\sqrt{2\pi a}} \exp[ik_F x + i\phi_i(x)], \quad (17)$$

where  $i=r,l$  and

$$\phi_i(x) = \frac{-2\pi i}{L} \sum_{q>0} \frac{e^{-aq/2}}{q} [\rho_{i,-q} e^{iqx} - \rho_{i,q} e^{-iqx}]. \quad (18)$$

Note that the density operator in real space,  $\rho_i(x)$ , can be written as

$$\begin{aligned} \rho_i(x) &= \frac{1}{L} \sum_{q>0} [\rho_{i,-q} e^{iqx} + \rho_{i,q} e^{-iqx}] \\ &= \lim_{a \rightarrow 0} \left( \frac{1}{2\pi} \partial_x \phi_i \right). \end{aligned} \quad (19)$$

The above expression for the fermion field can readily be shown to obey the appropriate anticommutation relation by utilizing the standard identity,  $e^A e^B = e^{[A,B]} e^B e^A$  for  $[A,B]$  equaling multiple of the identity. From such an expression it is possible to deduce all the power-law correlations in the single-particle and multi-particle Green's functions (Theumann, 1967; Dover, 1968; Luther and Peschel, 1974; Efetov and Larkin, 1975; Finkelstein, 1977). The quantity  $\phi_q$ , utilized in the Bogoliubov transformation, governs the power law at large distances. For the single-particle Green's function, the power-law exponent  $\alpha$  is given by

$$\alpha = \cosh(2\phi_o) = \frac{v_F + V_o}{\sqrt{(v_F + V_o)^2 - U_o^2}}. \quad (20)$$

We shall derive this result utilizing the alternative equation-of-motion method in Sec. I.A.2 below. The Luther-Peschel expression is in some ways ambiguous, as it is necessary to take the limit of  $a \rightarrow 0$ . A full, well-defined expression that properly takes into account the  $q=0$  mode is quite involved and will not be discussed here. Instead, we refer the interested reader to the original papers by Haldane (1979, 1981).

## 2. Power-law behavior in the single-particle Green's function

Ward identities derivable from either the equations of motion (Everts and Schulz, 1974) or from skeleton dia-

grams in a perturbation diagrammatic analysis (Dzyaloshinskii and Larkin, 1973) enable us to solve the correlation functions, e.g., Green's functions, in closed form. These Ward identities are direct consequences of conservation laws in the Tomonaga-Luttinger model. In addition to the usual conservation of total charge, the separate conservation of charge in the left- and right-moving channels, as a result of an absence of back-scattering processes coupling the two channels, leads to additional Ward identities that together make an exact solution possible. To illustrate these points, consider the charge density in the left or right channel,  $\rho_i(x)$ ,  $i=r,l$ :

$$\rho_i(x) = \frac{1}{L} \sum_q \rho_{i,q} e^{-iqx}. \quad (21)$$

The evolution of this operator is governed by the equation of motion,

$$i \frac{\partial \rho_i(x)}{\partial t} = [\rho_i(x), H]. \quad (22)$$

Using the commutation relation between  $\rho_{i,q}$  and the fermion operators,  $a_{i,q}$ ,

$$[\rho_{i,q}, a_{i',q'}] = -\delta_{i,i'} a_{q'-q}, \quad (23)$$

and the commutator for the  $\rho_{i,q}$ 's [Eq. (9)] yields the continuity equations

$$i \frac{\partial \rho_r(x)}{\partial t} = -q[(v_F + V_q)\rho_{r,q} + U_q \rho_{l,q}], \quad (24)$$

$$i \frac{\partial \rho_l(x)}{\partial t} = q[(v_F + V_q)\rho_{l,q} + U_q \rho_{r,q}], \quad (25)$$

where the currents in the right and left channels are proportional to the respective  $\rho_{i,q}$ 's. These equations reflecting separate right- and left-channel charge conservation give rise to the important Ward identities for the density correlation functions  $R_i(k_1, t_1; q, t; k_2, t_2)$ :

$$\begin{aligned} R_i(k_1, t_1; q, t; k_2, t_2) \\ = \langle 0 | T \{ a_{r,k_1}(t_1) \rho_{i,q}(t) a_{r,k_2}^\dagger(t_2) \} | 0 \rangle, \quad (k_1, k_2) > 0, \end{aligned} \quad (26)$$

and

$$\begin{aligned} R_i(k_1, t_1; q, t; k_2, t_2) \\ = \langle 0 | T \{ a_{l,k_1}(t_1) \rho_{i,q}(t) a_{l,k_2}^\dagger(t_2) \} | 0 \rangle, \quad (k_1, k_2) < 0. \end{aligned} \quad (27)$$

Note that we are only interested in  $k_1$  and  $k_2$  in the neighborhood of  $k_F$ . This restriction also avoids complications from the positron branch, which is irrelevant to the physics of interest. To arrive at the Ward identities we again use the usual relationship,  $i\partial\hat{O}(t)/\partial t = [\hat{O}, H]$  on the  $R_i$ 's, and Eqs. (24) and (25) to find

$$\begin{aligned}
& [i\partial_t + \text{sgn}(i)q(v_F + V_q)]R_i(k_1, t_1; q, t; k_2, t_2) \\
& + qU_q R_j(k_1, t_1; q, t; k_2, t_2) \\
& = \delta_{i,r} \delta_{k_2, k_1 - q} [\delta(t - t_1)G(k_2, t_1 - t_2) \\
& - \delta(t - t_2)G(k_1, t_1 - t_2)], \quad (k_1, k_2) > 0, \quad (28)
\end{aligned}$$

and

$$\begin{aligned}
& [i\partial_t - \text{sgn}(i)q(v_F + V_q)]R_i(k_1, t_1; q, t; k_2, t_2) \\
& + qU_q R_j(k_1, t_1; q, t; k_2, t_2) \\
& = \delta_{i,l} \delta_{k_2, k_1 - q} [\delta(t - t_1)G(k_2, t_1 - t_2) \\
& - \delta(t - t_2)G(k_1, t_1 - t_2)], \quad (k_1, k_2) < 0, \quad (29)
\end{aligned}$$

where  $(i, j) = \{r, l\}$  but  $i \neq j$ ,  $\text{sgn}(i=r) = +1$ ,  $\text{sgn}(i=l) = -1$ , and  $G(k, t)$  is the single-particle Green's function. The right-hand side in the equations comes from the discontinuity of the time-ordered product evaluated at equal times. Here the single-particle Green's function is given by

$$G(k, t) = i\langle 0 | T \{ a_{r,k}(t) a_{r,k}^\dagger(0) \} | 0 \rangle, \quad k > 0, \quad (30)$$

and

$$G(k, t) = i\langle 0 | T \{ a_{l,k}(t) a_{l,k}^\dagger(0) \} | 0 \rangle, \quad k < 0. \quad (31)$$

These Ward identities for the single-particle density correlation function  $R$ , in conjunction with the usual equations of motion for the single-particle Green's function (Nozières, 1964, Chap. 3),

$$\begin{aligned}
& [i\partial_t - v_F k + \mu]G(k, t) \\
& = -\delta(t) + i\frac{\pi}{L} \sum_q [V_q(R_r(k - q, t^+; -q, t; k, 0) \\
& + R_r(k + q, t^-; q, t; k, 0) + U_q R_l(k - q, t^+; -q, t; k, 0) \\
& + R_l(k + q, t^-; q, t; k, 0)], \quad (k \pm q, k) > 0, \quad (32)
\end{aligned}$$

and

$$\begin{aligned}
& [i\partial_t - |v_F k| + \mu]G(k, t) \\
& = -\delta(t) + i\frac{\pi}{L} \sum_q [V_q(R_l(k - q, t^+; -q, t; k, 0) \\
& + R_l(k + q, t^-; q, t; k, 0) + U_q R_r(k - q, t^+; -q, t; k, 0) \\
& + R_r(k + q, t^-; q, t; k, 0)], \quad (k \pm q, k) < 0, \quad (33)
\end{aligned}$$

form a closed set of equations. Here we are interested in the situation where  $|k| \sim k_F$ , and  $|q| \ll k_F$ . Upon transforming into  $\omega$ -Fourier representation and eliminating the  $R$ 's, one finds an integral equation for the single-particle Green's function (Dzyaloshinskii and Larkin, 1973; Everts and Schulz, 1974; Voit, 1995; Metzner *et al.*, 1998):

$$\begin{aligned}
& [\omega + |v_F k| - \mu]G(k, \omega) \\
& = 1 + i\frac{1}{L} \sum_{q>0} \int d\omega' G(k - q, \omega - \omega') \\
& \times \frac{V_q[\omega' + \text{sgn}(k)q(v_F + V_q)] - \text{sgn}(k)qU_q^2}{-\omega^2 + q^2(v_F + V_q)^2 - q^2U_q^2}. \quad (34)
\end{aligned}$$

In the simplest case where the  $q$  dependence of  $V_q$  and  $U_q$  are neglected but an ultraviolet cutoff  $\Lambda$  is introduced, this integral equation is solved by transforming to real space-time with

$$\tilde{G}(x, t) = \int \frac{d\omega}{2\pi} \int \frac{dk}{2\pi} G(k, \omega) e^{ikx - i\omega t} \quad (35)$$

and

$$\begin{aligned}
\tilde{K}(x, t) & = \int \frac{d\omega}{2\pi} \int \frac{dk}{2\pi} \\
& \times \frac{V_q[\omega' + \text{sgn}(k)q(v_F + V_q)] - \text{sgn}(k)qU_q^2}{-\omega^2 + q^2(v_F + V_q)^2 - q^2U_q^2} \\
& \times e^{ikx - i\omega t}, \quad (36)
\end{aligned}$$

yielding

$$[\partial_t \pm v_F \partial_x] \tilde{G}(x, t) = \delta(t) \delta(x) + \tilde{K}(x, t) \tilde{G}(x, t). \quad (37)$$

Equation (37) is solved by the ansatz

$$\tilde{G}(x, t) = \exp[L(x, t) - L(0, 0)] \tilde{G}_o(x, t) \quad (38)$$

with

$$\begin{aligned}
L(x, t) & = \ln[r - v_F t + is(t)/\Lambda] \\
& - [(\alpha + 1)/2] \ln[x - v_o t + is(t)/\Lambda] \\
& - [(\alpha - 1)/2] \ln[x + v_o t + is(t)/\Lambda]. \quad (39)
\end{aligned}$$

Here  $L(0, 0) = \eta \ln(\Lambda)$ , and

$$\tilde{G}_o(x, t) = \frac{1}{2\pi} \frac{1}{x - v_F t + i0^+ s(t)}, \quad (40)$$

with  $s(t) = +1$  for  $t > 0$ , and  $-1$  for  $t < 0$ . The final form for  $\tilde{G}(x, t)$  exhibits the well-known power-law behavior:

$$G(x,t) = \frac{1}{2\pi\Lambda^{\alpha-1}} \frac{1}{[x-ut+is(t)/\Lambda]^{(\alpha+1)/2}[x+ut+is(t)/\Lambda]^{(\alpha-1)/2}} \quad (41)$$

with the renormalized velocity  $v_o = \sqrt{(v_F + V_o)^2 - U_o^2}$ , where  $V_o = V_q$ ,  $q \rightarrow 0$  and  $U_o = U_q$ ,  $q \rightarrow 0$ , and the exponent  $\alpha$  is given by

$$\alpha = 1 + \frac{1}{2v_o} [v_F + V_o - v_o]. \quad (42)$$

The resulting density of states,  $D(\omega)$ , also exhibits the hallmark power-law behavior:

$$D(\omega) \propto \omega^{\alpha-1}. \quad (43)$$

Straightforward generalization to include spin yields

$$G(x,t) = \frac{1}{2\pi\Lambda_q^{\alpha_c + \alpha_s}} \frac{1}{[x - v_c t + is(t)/\Lambda]^{(\alpha_c + 1)/4} [x + v_c t + is(t)/\Lambda_q]^{(\alpha_c - 1)/4}} \times \frac{1}{[x - v_s t + is(t)/\Lambda]^{(\alpha_s + 1)/4} [x + v_s t + is(t)/\Lambda_q]^{(\alpha_s - 1)/4}}, \quad (44)$$

where the indices  $c$  and  $s$  refer to the charge and spin modes, respectively.

Extensions beyond the idealized Tomonaga-Luttinger model to take into account nonlinear energy-momentum dispersion and weak backscattering lead to generalized models that can be analyzed either by bosonization (Luther and Emery, 1974; Haldane, 1981; Voit, 1995; Metzner *et al.*, 1998) or by the many-body techniques of renormalization-group analysis and Ward identities (Solyom, 1979; Metzner and Di Castro, 1993; Metzner *et al.*, 1998). The name ‘‘Luttinger liquid’’ was coined to reflect the fact that the nonidealities lead to an interaction between the boson modes away from  $q=0$ , much in the same way that interaction between quasiparticles arises in a Fermi liquid (Nozières, 1964; Haldane, 1981). The interested reader is referred to the literature for details.

Bosonization has been further utilized in two directions, (i) to analyze the effect of nonlinear dispersion (Haldane, 1981) and (ii) to solve a specific type of backscattering problem (Luther and Emery, 1974; Haldane, 1979). By introducing a quadratic energy-momentum dispersion plus a third-order term to ensure the stability of the Luttinger-liquid state, Haldane showed that a Hamiltonian can be written in terms of the boson operators,  $b_q$ , and number and current operators,  $N$  and  $J$ . Nevertheless, several key features of the Luttinger model are preserved for situations where  $J$  is still a good quantum number. Haldane further argued that even if  $J$  is not a good quantum number, the low-energy structure is preserved: (1)  $v_o = \sqrt{v_N v_J}$ ; (2)  $v_N = v_o \exp(-2\phi_o)$ ; (3)  $v_J = v_o \exp(2\phi_o)$ ; and (4)  $\phi_o$  still controls the power-law falloff of Fermi Green’s functions at large distance. However, the Fermi velocity is renormalized and becomes  $q$  dependent.

### 3. $g$ -ology

The alternative route to a similar conclusion on general, 1D interacting systems including weak backscatter-

ing is based on renormalization-group analysis. As previously mentioned, forward scattering in the Tomonaga-Luttinger model leads to a logarithmic contribution in the second-order perturbative calculation of the self-energy, and a logarithmic divergence in the interaction operator at low energies,  $\Gamma \propto \ln(\omega/\Lambda)$ . The effect of renormalization is to re-sum the perturbation series to all orders, rendering the divergent physical quantities finite, by rescaling the divergences away with some cutoff-dependent factors. The success of the renormalization in this context of 1D interacting systems relies heavily on Ward identities reflecting conservation laws and skeleton diagram analysis in many-body theory.

A successful renormalization-group analysis, called *g-ology* for the study of the running coupling  $g$ , was first put forth as an ansatz by Solyom (1979) and co-workers (Menyhard and Solyom, 1973; Solyom, 1973; Solyom and Zawadowski, 1974). They used a bandwidth renormalization scheme within a model of linearized energy-momentum dispersion about the two Fermi points and a model with a spin-dependent Hamiltonian, which may include a backscattering term ( $H_1$ ). This is in addition to the usual forward-scattering terms  $H_2$  and  $H_4$ , where  $H_2$  contains density operators for both the right- and left-moving branches,  $\rho_{r,q,\sigma} = \sum_k a_{r,k+q,\sigma}^\dagger a_{r,k,\sigma}$  and  $\rho_{l,q,\sigma} = \sum_k a_{l,k+q,\sigma}^\dagger a_{l,k,\sigma}$ , respectively,  $\sigma$  denotes the spin, and  $H_4$  involves density operators in one branch only. Umklapp processes ( $H_3$ ) relevant for lattice Hubbard-type models at half filling will not be included here. The Hamiltonian is given by (Solyom, 1979; Metzner and Di Castro, 1993; Metzner *et al.*, 1998)

$$H = H_o + H_1 + H_2 + H_4, \quad (45)$$

where

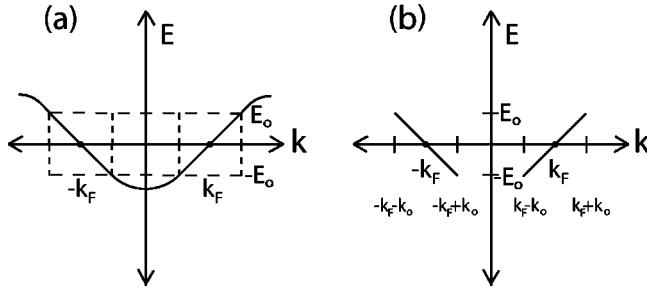


FIG. 3. Linearized dispersion for Tomonaga-Luttinger model, about the Fermi points at  $\pm k_F$ . For convenience the Fermi energy is set to zero. The bandwidth  $2E_o$  is equal to  $2v_F k_o$ . The allowed momenta are restricted to the regions within  $|k \pm k_F| \leq k_o$  [left and right dashed boxed regions in (a)]. (a) The energy dispersion before linearization. (b) Linearized dispersion for the two regions within the left and right dashed boxes of (a), corresponding to the left- and right-moving branches, respectively.

$$H_o = \sum_{\sigma} \sum_{k_F - k_o < k < k_F + k_o} v_F k a_{r,k,\sigma}^{\dagger} a_{r,k,\sigma} - \sum_{\sigma} \sum_{-k_F - k_o < k < -k_F + k_o} v_F k a_{l,k,\sigma}^{\dagger} a_{l,k,\sigma}, \quad (46)$$

$$H_1 = L^{-1} \sum_{\sigma, \sigma'} \sum_q g_{1\perp} \delta_{\sigma, -\sigma'} \sum_k a_{r,k+q,\sigma}^{\dagger} a_{l,k-2k_F,\sigma} \times \sum_{k'} a_{l,k'-q,\sigma'}^{\dagger} a_{r,k'+2k_F,\sigma'}, \quad (47)$$

$$H_2 = (L)^{-1} \sum_{\sigma, \sigma'} \sum_q [g_{2\parallel} \delta_{\sigma, \sigma'} + g_{2\perp} \delta_{\sigma, -\sigma'}] \times \sum_k a_{r,k+q,\sigma}^{\dagger} a_{r,k,\sigma} \sum_{k'} a_{l,k'-q,\sigma'}^{\dagger} a_{l,k',\sigma'} = L^{-1} \sum_{\sigma, \sigma'} \sum_q [g_{2\parallel} \delta_{\sigma, \sigma'} + g_{2\perp} \delta_{\sigma, -\sigma'}] \times \rho_{r,q,\sigma} \rho_{l,-q,\sigma'}, \quad (48)$$

$$H_4 = (2L)^{-1} \sum_{\sigma, \sigma'} \sum_q [g_{4\parallel} \delta_{\sigma, \sigma'} + g_{4\perp} \delta_{\sigma, -\sigma'}] \times \left\{ \sum_{k_1} a_{r,k_1+q,\sigma}^{\dagger} a_{r,k_1,\sigma} \sum_{k_2} a_{r,k_2-q,\sigma'}^{\dagger} a_{r,k_2,\sigma'} + \sum_{k'_1} a_{l,k'_1+q,\sigma}^{\dagger} a_{l,k'_1,\sigma} \sum_{k'_2} a_{l,k'_2-q,\sigma'}^{\dagger} a_{l,k'_2,\sigma'} \right\} = (2L)^{-1} \sum_{\sigma, \sigma'} \sum_q [g_{4\parallel} \delta_{\sigma, \sigma'} + g_{4\perp} \delta_{\sigma, -\sigma'}] \times [\rho_{r,q,\sigma} \rho_{r,-q,\sigma'} + \rho_{l,q,\sigma} \rho_{l,-q,\sigma'}]. \quad (49)$$

Here for the right branch the summation is over  $k_F - k_o < k < k_F + k_o$ ; while for the left branch, it is over  $-k_F - k_o < k < -k_F + k_o$ , with a bandwidth cutoff of  $E_o = v_F k_o$ . See Fig. 3. The notations  $\parallel$  and  $\perp$  denote

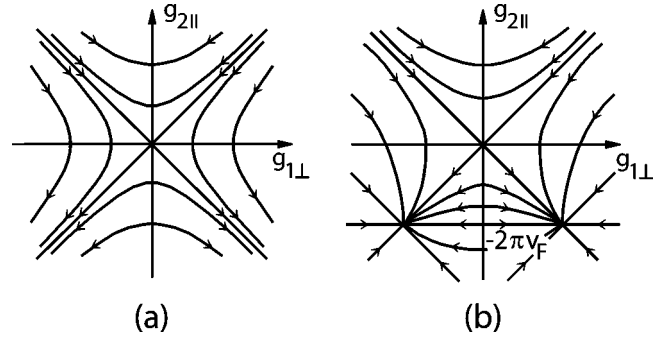


FIG. 4. Renormalization-group flow diagram for the  $g_{2\parallel}$ ,  $g_{1\perp}$ ,  $g_4$   $g$ -ology model, in a cut within the  $g_{2\parallel}$ - $g_{1\perp}$  plane from (a) second-order perturbation calculations, and (b) third-order calculations. For  $|g_{1\perp}| < g_{2\parallel}$  corresponding to weak backscattering, the trajectories scale to the Tomonaga-Luttinger fixed line, for which  $g_{1\perp} = 0$  (no backscattering). For large  $|g_{1\perp}|$ , the trajectories flow away from the Tomonaga-Luttinger fixed line into regimes where the perturbation calculations are no longer valid. From Solyom, 1979.

scattering processes between parallel and antiparallel spins, respectively. The bandwidth cutoff  $E_o$  turns out to generate a multiplicative renormalization, which was shown to hold, order by order, using perturbation theory. The renormalization involves the multiplicative parameters  $z$ , associated with the renormalization of the single-particle Green's function  $G$ , and the  $z_j$ 's, associated with the renormalization of the various dimensionless interaction vertices  $\Gamma_j$ ,  $j=1,2,4$ :

$$G \rightarrow z G, \quad (50)$$

and

$$\Gamma_j \rightarrow z_j^{-1} \Gamma_j, \quad (51)$$

when the bandwidth cutoff is reduced from  $E_o$  to  $E'_o$ . The coupling constants  $g_j$  then transform as  $g_j \rightarrow z^{-2} z_j g_j$ . The renormalizability amounts to demonstrating that the quantities  $z$  and  $z_j$  depend only on the ratio  $E'_o/E_o$ , and are independent of the energy and momentum variables  $(\omega, \mathbf{k})$ , while  $G$  and the  $\Gamma_i$ 's preserve their analytic form before and after the renormalization transformation. Even with the scaling analysis, the computed scaling trajectories are valid only in the weak-coupling limit of weak backscattering,  $|g_{1\perp}| \leq g_{2\parallel}$ , while strong coupling flows out of the range of validity of the scaling hypothesis. (See Fig. 4 and its caption below.)

A full, modern-day renormalization-group analysis is discussed by Metzner and Di Castro (1993) and Metzner *et al.* (1998). Only two renormalization parameters,  $z$  and  $z_\rho$ , in addition to the coupling constants  $g_i$ , are necessary to renormalize the most singular correlation functions of the fermion, boson (density-density), and mixed types:

$$G^{2n,l}(\{k_i, t_i, k'_i, t'_i\}; \{q_j, t''_j\}) = (-i)^{n+l} \langle 0 | T \{ a_{k_1}(t_1) \cdots a_{k_n}(t_n) \times a_{k'_n}^{\dagger}(t'_n) \cdots a_{k'_1}^{\dagger}(t'_1) \rho_{q_1}(t''_1) \cdots \rho_{q_l}(t''_l) \} | 0 \rangle. \quad (52)$$

It is convenient to work in the Fourier-transformed representation using the associated vertex functions  $\Gamma^{2n,l}(K,\Omega)$ , which equal the  $G^{2n,l}(K,\Omega)$  divided by the external legs. Here  $(K,\Omega)$  denotes all the incoming and outgoing external energy-momenta. It turns out that only the four most singular vertices,  $\Gamma^2$ ,  $\Gamma^4$ ,  $\Gamma^{(0,2)}$ , and  $\Gamma^{(2,1)}$ , need to be renormalized since all other higher-order vertices do not exhibit logarithmic divergences in a perturbation series. The renormalization is defined by

$$G^{-1} \rightarrow z G^{-1}; \Gamma^{(2)} \rightarrow z \Gamma^{(2)}, \quad (53)$$

$$\Gamma^{(4)} \rightarrow z^2 \Gamma^{(4)}, \quad (54)$$

$$\Gamma^{(0,2)} \rightarrow z_\rho^2 \Gamma^{(0,2)}, \quad (55)$$

$$\Gamma^{(2,1)} \rightarrow z^2 z_\rho \Gamma^{(2,1)}, \quad (56)$$

$$g \rightarrow \bar{g}, \quad (57)$$

where the renormalization occurs as the energy-momentum cutoff is changed from  $\Lambda$  to  $\Lambda'$ , and the renormalization factors  $z$  and  $z_\rho$ , and the couplings  $g_i$ , depend only on  $g_i$  and the ratio  $\Lambda'/\Lambda$ , and not on the external energy-momenta  $(K,\Omega)$ , i.e.,

$$z = z(\Lambda'/\Lambda, \bar{g}). \quad (58)$$

The renormalization group is defined by

$$\begin{aligned} \tilde{\Gamma}^{2n,l}(K,\Omega; \bar{g}, \lambda) \\ \equiv \lim_{\Lambda \rightarrow \infty} z^n(\bar{g}, \lambda/\Lambda) z_\rho^l(\bar{g}, \lambda/\Lambda) \Gamma^{2n,l}(K,\Omega; g, \Lambda), \end{aligned} \quad (59)$$

with

$$\begin{aligned} \tilde{\Gamma}^{2n,l}(K,\Omega; \bar{g}', \lambda') \\ = z^n(\bar{g}, \lambda'/\lambda) z_\rho^l(\bar{g}, \lambda'/\lambda) \tilde{\Gamma}^{2n,l}(K,\Omega; \bar{g}, \lambda), \end{aligned} \quad (60)$$

and

$$z(g, \lambda'/\lambda) = \lim_{\Lambda \rightarrow \infty} z(\bar{g}, \lambda'/\Lambda) / z(\bar{g}, \lambda/\Lambda). \quad (61)$$

The differential form for the renormalization-group flow follows from Eqs. (60) and (61) when one considers infinitesimal changes,  $\lambda' = \lambda + \partial\lambda$ :

$$[\lambda \partial_\lambda + \beta(\bar{g}) \partial_{\bar{g}} - n \gamma(\bar{g}) + l \gamma_\rho(\bar{g})] \tilde{\Gamma}^{(2n,l)}(K,\Omega; \bar{g}, \lambda) = 0 \quad (62)$$

with  $\beta(\bar{g}) = \partial \bar{g}' / \partial(\lambda'/\lambda)|_{\lambda'=\lambda}$ ,  $\gamma(\bar{g}) = \partial \ln z / \partial(\lambda'/\lambda)|_{\lambda'=\lambda}$ , and  $\gamma_\rho(\bar{g}) = \partial \ln z_\rho / \partial(\lambda'/\lambda)|_{\lambda'=\lambda}$ . Note that a fixed point of the renormalization group signifies that  $\bar{g}$  does not change with  $\lambda$ , or  $\beta=0$ . Under such circumstances the renormalization-group flow immediately yields

$$\tilde{\Gamma}^{(2n,l)}(K,\Omega; \bar{g}, \lambda) = \lambda^n \gamma(\bar{g}^*) - l \gamma_\rho(\bar{g}^*), \quad (63)$$

where  $\bar{g}^*$  is the fixed point. The removal of all divergences with this finite number of renormalization parameters indicates the renormalizability of the theory.

In this renormalization-group analysis, full usage is made of the Ward identities reflecting the separate conservation of charge and spin in the right and left branches, which severely constrains the theory and number of free parameters. Renormalization is usually com-

puted perturbatively. For the simple case of only  $g_2$  coupling with all other couplings equal to zero (a special case of the Tomonaga-Luttinger model), computation to second order (two loops) leads to unrenormalized  $g_2$  and  $z_\rho$  and a renormalization of  $z$  (Solyom, 1979; Metzner and Di Castro, 1993; Metzner *et al.*, 1998):

$$z(\lambda/\Lambda, g) = 1 + \frac{g_2^2}{8\pi^2 v_F^2} \ln \frac{\lambda}{\Lambda} + O(g^3). \quad (64)$$

It turns out that for  $g_1=0$  ( $g_{1\perp}=0$ ), the set of arbitrary  $g_2$  and  $g_4$ , namely, the Tomonaga-Luttinger model, forms a fixed line of the  $g$ -ology model. For the general case, however, all couplings scale (Solyom, 1979):

$$\frac{dg_{2\parallel}}{dx} = \frac{1}{x} \left( \frac{1}{\pi v_\sigma} g_{1\perp}^2 + \frac{1}{2\pi^2 v_\sigma^2} g_{1\parallel} g_{1\perp}^2 + \dots \right), \quad (65)$$

$$\frac{dg_{1\perp}}{dx} = \frac{1}{x} \left( \frac{1}{\pi v_\sigma} g_{2\parallel} g_{1\perp} + \frac{1}{4\pi^2 v_\sigma^2} (g_{2\parallel}^2 g_{1\perp} + g_{1\perp}^3) + \dots \right), \quad (66)$$

$$\frac{d(g_{2\parallel} - 2g_2)}{dx} = 0, \quad (67)$$

$$\frac{d(g_{4\parallel} - g_{4\perp})}{dx} = \frac{1}{x} \left( \frac{1}{2\pi^2 v_F^2} g_{2\parallel} g_{1\perp}^2 + \dots \right), \quad (68)$$

and

$$\frac{d(g_{4\parallel} + g_{4\perp})}{dx} = 0, \quad (69)$$

where the last two expressions imply

$$\frac{dg_{4\perp}}{dx} = -\frac{1}{x} \left( \frac{1}{4\pi^2 v_F^2} g_{1\parallel} g_{1\perp}^2 + \dots \right). \quad (70)$$

These scaling trajectories plotted for a cut in the  $g_{2\parallel}$ - $g_{1\perp}$  plane are shown in Fig. 4. For weak coupling (weak backscattering), where  $|g_{1\perp}| \leq g_{2\parallel}$ , the trajectories scale to the Tomonaga-Luttinger fixed line of no backscattering, i.e.,  $g_{1\perp}^* = 0$ . On the other hand, for strong coupling, the trajectories scale away to a regime where the perturbative treatment is no longer valid. Intuitively, under sufficiently strong backscattering, insulating behavior can be expected. For a specific strong-coupling (strong-backscattering) problem, in particular under the condition of

$$\frac{-g_{2\parallel}}{2\pi v_F + g_{4\parallel} - g_{4\perp}} = \frac{3}{5}, \quad (71)$$

Luther and Emery (1974) showed that there is a decoupling of the charge and spin sectors, resulting in a gapped behavior in the spin excitation spectrum. It has, however, been argued that the Luther-Emery problem does not represent a true backscattering problem (Haldane, 1979). In addition to the solution of the weak-backscattering problem, renormalization-group analysis has been successful in showing that nonlinear energy-momentum dispersion can be scaled away as it generates irrelevant terms in the renormalization-group sense (Metzner and Di Castro, 1993).

## B. Chiral Luttinger liquid

The chiral Luttinger liquid (CLL) theory of the fractional quantum Hall edge, pioneered by Wen (1990a, 1990b, 1991a, 1991b, 1992, 1995), provides an effective way to describe the low-energy dynamics at the boundary of the strongly correlated 2D electron-gas system. This theory is based on a model in which the 2D physics of the fractional quantum Hall fluid is adequately described by the Chern-Simon effective-field theories (Girvin and MacDonald, 1987; Read, 1989; Zhang *et al.*, 1989; Wen and Niu, 1990; Frohlich and Zee, 1991; Wen, 1995), and the electron correlation built into the bulk 2D system is assumed to extend all the way to the boundary. In the case of incompressible fluids, such as the Laughlin or the hierarchical states, the bulk excitation contains an energy gap and the edge is truly one dimensional in nature. Tomonaga-Luttinger-liquid-type behavior, characterized by power-law correlations and gapless bosonic excitations, arises as a natural consequence of strong correlation and one dimensionality. Here, in contrast to the ordinary case, the magnetic field introduces a sense of rotation in the propagation of edge modes, dictated by the motion of semiclassical skipping orbits at the boundary in the direction given by  $\mathbf{E} \times \mathbf{B}$ , where  $\mathbf{E}$  is the effective electric field and includes the contribution of the edge confinement potential. The resulting Tomonaga-Luttinger liquid is therefore chiral. A unique feature of the idealized chiral Luttinger liquid investigated in effective-field theories is the universality of the electron-tunneling exponent  $\alpha$ . For incompressible fractional Hall fluids belonging to the Laughlin fractions,  $\nu = 1/m$ , where  $\nu$  is the filling factor and  $m$  is an odd integer,  $\alpha$  [defined by the tunneling current-voltage ( $I$ - $V$ ) relationship  $I \propto V^\alpha$ ,] is believed to be given by the dimensionless Hall resistance,  $\alpha = \rho_{xy}/(h/e^2)$ . For  $1/m$  fractional fluids  $\alpha$  is exactly equal to  $m$ . In other words, for the  $\nu = 1/3$  Laughlin fluid,  $\alpha$  would equal 3 exactly. This line of thought is based on the topological properties and characterizations of the fractional quantum Hall states (Blok and Wen, 1990a, 1990b; Frohlich and Zee, 1991; Wen and Zee, 1992; Wen, 1995) and as such is insensitive to the specific form of the electron-electron interaction potential.

In complex incompressible fractional Hall fluids involving the hierarchical sequence (Haldane, 1983; Halperin, 1984; Jain, 1989a, 1989b, 1990), tunneling characteristics have been proposed as an effective way to classify and distinguish different states based on the topological order of those states. This topological order embodied in the  $K$ -matrix formulation (Frohlich and Zee, 1991; Wen and Zee, 1992; Wen, 1995) in principle enables us to differentiate among incompressible fluids exhibiting the same Hall resistance (conductance). The tunneling exponents for many hierarchical states with complex, multibranch edge modes are *a priori* nonuniversal. The value of the exponent depends on the details of the intermode mixing interaction. However, Kane, Fisher, and Polchinski (Kane *et al.*, 1994; Kane and Fisher, 1995) have shown that residual disorder can re-

store the exponent to universal values when sufficiently strong. In particular, for the Jain sequence  $\nu = n/(np + 1)$ , where  $n = 1, 2, 3$ , etc., and  $p$  is an even integer, mode mixing gives rise to one charged mode and  $(n - 1)$  neutral modes. In this universal limit, the charged mode propagates at one velocity while the  $(n - 1)$  neutral modes, obeying an  $SU(N)$  symmetry, where  $N = n$ , all propagate at a different but shared velocity. The charged and neutral modes thus behave analogously to the charge and spin modes in the ordinary 1D Tomonaga-Luttinger-liquid case. When all modes co-propagate (i.e., travel in the same direction), e.g., for  $p = 2$ , and  $1 \leq n \leq \infty$  corresponding to  $1/3 \leq \nu \leq 1/2$ , the exponent remains constant and equal to  $p + 1$ , in this case 3. On the other hand, for  $p = -2$ , before mixing the outermost edge mode and inner holelike modes propagate in opposite directions. For example, at  $\nu = 2/3$  the outermost edge mode is the usual electron mode familiar from the integer quantum Hall fluid, while a  $1/3$  charged, inner holelike branch propagates in the opposing direction. These counterpropagating modes, when mixed, lead to a shake-up process and to a renormalization of the exponent, which at a given filling fraction tends to a universal value when sufficient disorder is present.

The experimental observation of Luttinger-liquid-like behavior for compressible states (Chang *et al.*, 1998) came as somewhat of a surprise. At present the most internally consistent theoretical description for the edge dynamics of compressible Hall fluids and for their edge tunneling characteristics is that put forth by Shytov, Levitov, and Halperin (Shytov *et al.*, 1998; Levitov *et al.*, 2001), based on a composite-fermion, Chern-Simon effective-field-theory formulation. The result is a Luttinger-liquid-like edge dynamic in which the finite, nonzero diagonal resistivity  $\rho_{xx}$  of the compressible fluid slightly changes the exponent from the universal value valid for  $\rho_{xx} = 0$ . The idea is as follows. Since for high-quality samples  $\rho_{xx}$  is typically small, of order  $(1/10)\rho_{xy}$  or less regardless of whether the fractional Hall fluid is compressible or incompressible, the corresponding diagonal conductance,  $\sigma_{xx} = \rho_{xx}/[\rho_{xx}^2 + \rho_{xy}^2]$ , is also small,  $\sigma_{xx} \leq 0.1\sigma_{xy}$ , where  $\sigma_{xy} = \rho_{xy}/[\rho_{xx}^2 + \rho_{xy}^2] \approx 1/\rho_{xy}$  is the Hall conductance. As a result, when an external electron is injected at the edge, its spreading proceeds much faster along the boundary than in the perpendicular direction into the bulk. Therefore the tunneling will still appear Luttinger-liquid-like. For compressible fluids residual disorder or interaction also tends to drive the exponent to universal values. The inclusion of disorder results in an exponent for electron tunneling,  $\alpha$ , which when plotted as a function of reduced Hall resistance,  $\rho_{xy}/(h/e^2)$ , exhibits steplike plateaus on which it is roughly constant, while varying in a linear fashion between plateaus. The plateaus are not perfectly flat due to the nonzero  $\rho_{xx}$ , and they occur when all edge modes co-propagate, whereas the linear regions occur when counterpropagating modes are present. The functional dependence is an extension of the Kane-Fisher (Kane *et al.*, 1994; Kane and Fisher, 1995) result to continuous values of the Hall resistance.

What is summarized above constitutes the “effective-field” description of the theory of the fractional quantum Hall edge. This description is expected to hold rigorously when the wave function is of the Laughlin form or its hierarchical derivatives, even in the presence of the boundary. This means that nominally the interaction between electrons is of the extreme short-ranged form of  $\delta''(\mathbf{r})$ , a second derivative of a delta function. The leap to realistic, long-ranged Coulomb or partially screened (e.g., dipolar) interactions can only be treated in an approximate way (Imura and Nagaosa, 1997; Zheng and Yu, 1997; Zülicke and MacDonald, 1997; Levitov *et al.*, 2001). Based on the topological nature of the quantum Hall fluids, it is usually argued that the range of the interaction is irrelevant. This remains an open and extremely important issue, however. Recent cumulative experimental evidence and suggestive numerical results are raising the possibility of deviations from universality, which will be fully discussed below in Secs. II.B.8 and III.D.

### 1. Wen’s hydrodynamic formulation

As was seen in Sec. II.A, for the Tomonaga-Luttinger liquids in one dimension, the commutator relationship between density operators,  $[\rho_q, \rho_{q'}] = cq \delta_{q, -q'}$ , where  $c$  is a constant (the so-called Kac-Moody algebra), and the existence of a well-defined fermion operator,  $\Psi(x) \sim e^{i\phi(x)}$ , where  $\phi(x)$  is a boson operator related to  $\rho(x)$  by  $\partial_x \phi = 2\pi\rho(x)$ , lead to bosonic soundlike low-energy neutral excitations and power-law correlations in the charged sector when electrons are added or removed, provided forward scattering dominates and backscattering is irrelevant. The one-dimensional edge of the fractional quantum Hall fluid is a strongly interacting system in which backscattering is nearly completely suppressed, particularly in the quantized regime. Therefore the existence of Luttinger-liquid-like edge dynamics is quite natural.

Wen introduced several equivalent formulations to motivate and derive the effective low-energy physics of the fractional quantum Hall edge, based on hydrodynamics or gauge invariance of the effective-field theory. The most intuitive is the hydrodynamic approach, which we shall describe in this section. We start with the simplest case of the  $\nu = 1/m$  Laughlin Hall fluid, in which  $m$  is an odd integer. Based on the observation that the fractional Hall fluid is an irrotational, incompressible fluid, Wen first wrote down a classical hydrodynamic theory for a surface wave that travels in one direction only, followed by canonical quantization of the momentum and coordinate variables to obtain a quantum theory. Using the 1D edge density  $\rho(x)$ , he described the propagation of the disturbance depicted in Fig. 5, by the wave equation

$$\partial_t \rho(x) - v \partial_x \rho(x) = 0. \tag{72}$$

In an incompressible fluid, the vanishing of dissipation (longitudinal conductivity  $\sigma_{xx} \rightarrow 0$ ) and the presence of a

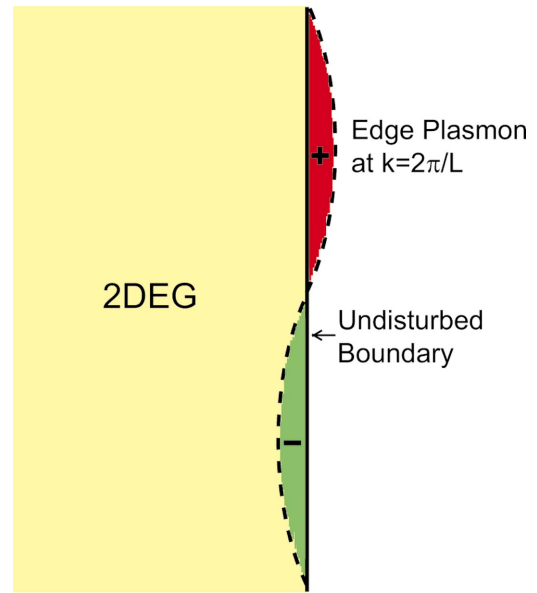


FIG. 5. (Color) Edge density plasmon wave at the boundary of a fractional quantum Hall fluid. In the absence of a density disturbance the boundary is depicted as a straight line. In the presence of a plasmon wave at wave vector  $k = 2\pi/L$ , where  $L$  is the length of the boundary, some regions accumulate excess charge while others suffer a depletion of charge.

nonzero Hall conductance,  $\sigma_{Hall} = \sigma_{xy}$ , generates a persistent current along the edge due to the boundary electric field:

$$\mathbf{j} = \sigma_{xy} \hat{z} \times \mathbf{E} = \sigma_{xy} \hat{z} \times [-\nabla V], \quad \mathbf{E} = -\nabla V, \quad \sigma_{xy} = \nu \frac{e^2}{h}, \tag{73}$$

where  $V$  is the edge potential. At the boundary the electrons execute semiclassical skipping orbits and drift with the velocity  $v = (E/B)c$ . Introducing the vertical displacement  $h(x)$  at position  $x$  along the edge, related to the edge density by

$$h(x) = \rho(x)n, \quad n = \nu \frac{eB}{hc}, \tag{74}$$

where  $n$  is the fractional Hall fluid average bulk density, we obtain the Hamiltonian associated with the chiral edge wave,

$$\begin{aligned} H &= \int dx \frac{1}{2} e \rho(x) h(x) E \\ &= \frac{1}{2} \int dx [\rho(x)]^2 \frac{e}{n} \\ &= \pi \hbar \frac{v}{\nu} \int dx [\rho(x)]^2. \end{aligned} \tag{75}$$

Transforming to a momentum representation where

$$\rho_q = \frac{1}{\sqrt{L}} \int dx e^{iqx} \rho(x), \tag{76}$$

$$\rho(x) = \frac{1}{\sqrt{L}} \sum_q \rho_q e^{-iqx}, \tag{77}$$

we have

$$H = 2\pi\hbar \frac{v}{\nu} \sum_{q>0} \rho_q \rho_{-q}. \quad (78)$$

This yields a corresponding wave equation in  $k$  space of

$$\dot{\rho}_q = -ivq\rho_q. \quad (79)$$

Hamilton's equations for coordinates and momenta,

$$\dot{q}_q = \frac{\partial H}{\partial p_q}, \quad \dot{p}_q = -\frac{\partial H}{\partial q_q}, \quad (80)$$

allow us to identify

$$q_q = \rho_q, \quad k>0, \quad p_q = \frac{i\hbar}{\nu q} \rho_{-q}, \quad k<0. \quad (81)$$

The final step is to quantize the Hamiltonian by requiring the canonical commutation relation

$$[q_q, p_{q'}] = i\hbar \delta_{q,q'}, \quad (82)$$

giving

$$[\rho_q, \rho_{q'}] = \frac{\nu}{2\pi} q \delta_{q,-q'}, \quad (83)$$

$$[H, \rho_q] = -qv\rho_q. \quad (84)$$

Aside from the extra factor  $\nu$  in Eq. (83), these expressions bear considerable similarity to the corresponding expressions for the ordinary Luttinger liquid. We can indeed draw parallels with the ordinary Luttinger liquid. Expressing the density operator in terms of fermion creation-annihilation operators,

$$\rho_q = \frac{1}{\sqrt{L}} \sum_k c_{k+q}^\dagger c_k, \quad (85)$$

$$\rho(x) = \frac{1}{\sqrt{L}} \sum_q \rho_q e^{-iqx}, \quad (86)$$

and writing the fermion field operator  $\psi(x)$  in terms of the annihilation operator,

$$\psi(x) = \frac{1}{\sqrt{L}} \sum_k c_k e^{ikx}, \quad (87)$$

we arrive at the important commutation relation

$$[\rho(x), \psi(x')] = -\delta(x-x')\psi(x), \quad (88)$$

which is satisfied by a representation of  $\psi(x)$  in the form  $\tilde{\psi}(x)$ :

$$\tilde{\psi}(x) \propto e^{i(1/\nu)\phi}, \quad \partial_x \phi = 2\pi\hbar\rho, \quad (89)$$

where  $\phi(x)$  obeys the commutation relation

$$[\phi(x), \phi(x')] = -i\pi\nu \operatorname{sgn}(x-x'). \quad (90)$$

Note the similarity of Eq. (89) with Eqs. (17) and (19) for the ordinary Luttinger liquid. For this form to be a valid fermionic operator,  $\tilde{\psi}(x)$  must satisfy the usual anticommutation relation,  $\{\tilde{\psi}(x), \tilde{\psi}(x')\} = 0$ . Making use of the operator identity

$$e^A e^B = e^{[A,B]} e^B e^A \quad (91)$$

between two operators  $A$  and  $B$  when their commutator,  $[A, B]$ , is a  $c$  number, we find

$$\tilde{\psi}(x)\tilde{\psi}(x') = (-1)^{1/\nu} \tilde{\psi}(x')\tilde{\psi}(x), \quad (92)$$

which requires  $1/\nu$  to be an odd integer, consistent with the condition for a simple fractional Hall fluid of the Laughlin type (Tsui *et al.*, 1982; Laughlin, 1983). As in the case of the ordinary Luttinger liquid, the Green's functions can be evaluated in terms of the  $\phi$  boson fields (Luther and Peschel, 1974; Wen, 1992, 1995). For the  $1/m$  Laughlin fluids, we have

$$\begin{aligned} \langle \phi(x,t)\phi(0,0) \rangle &= \langle 0 | e^{iHt} \phi(x) e^{-iHt} \phi(0) | 0 \rangle \\ &= \langle 0 | e^{-i[(v/i)\partial_x]t} \phi(x) \phi(0) | 0 \rangle \\ &= \langle 0 | e^{-i[vp_x]t} \phi(x) \phi(0) | 0 \rangle \\ &= -\nu \ln(x-vt) + \text{const.} \end{aligned} \quad (93)$$

The single-particle Green's function is then given by

$$\begin{aligned} \langle 0 | T \{ \psi^\dagger(x,t) \psi(0,0) \} | 0 \rangle \\ = \exp\left( \frac{1}{\nu^2} \langle \phi(x,t)\phi(0,0) \rangle \right) \propto \frac{1}{(x-vt)^{1/\nu}}, \end{aligned} \quad (94)$$

established using the operator relations

$$e^A e^B = e^{A+B+[A,B]/2} \quad (95)$$

and

$$\langle e^A \rangle = e^{\langle A^2 \rangle / 2}, \quad (96)$$

where  $A$  and  $B$  are linear combinations of harmonic-oscillator-type creation and annihilation operators, and the average is in a harmonic-oscillator-type ensemble. Notice that for the  $\nu=1$  integer fluid edge, the propagator is the conventional fermion propagator, and the edge dynamics are Fermi-liquid-like, albeit still chiral. On the other hand, for  $\nu<1$  or  $m>1$ , the propagator exhibits the unusual, power-law correlation that is the hallmark of Luttinger-liquid behavior. In the  $(k, \omega)$  representation, the single-particle Green's function takes the form

$$G(k, \omega) \propto \frac{(vk + \omega)^{m-1}}{vk - \omega}, \quad (97)$$

leading to a power-law density of states with the universal exponent value of  $m-1$ :

$$D(\omega) \propto |\omega|^{m-1}. \quad (98)$$

In particular, for the strongest, most robust fractional Hall fluid,  $\nu=1/3$ ,  $m=3$ , this theory predicts an exact value of 2 for the exponent in the electron-tunneling density of states. This in turn leads to an exponent  $\alpha$  of exactly 3 in the current-voltage ( $I$ - $V$ ) characteristics for tunneling from a normal metal into the  $\nu=1/3$  fractional fluid edge. This is a central result and a dramatic prediction of the chiral Luttinger liquid model of edge dynamics within the effective-field theory.

It is possible to generalize this type of dynamics to the edges of more complex fractional Hall fluids. The sim-

plest examples are the spin-polarized  $\nu=2/5$  and  $\nu=2/3$  fluids, each of which contains two fluid components resulting in two edge modes. In the case of the  $2/5$  fluid consisting of a  $\nu_1=1/3$  outer component and a  $\nu_2=1/15$  inner component of quasiparticle condensate ( $2/5=1/3+1/15$ ), the edge modes consist of an  $e/3$ -charged outer mode closest to the boundary and an  $e/5$ -charged inner mode with both modes propagating in the same direction. In the case of the  $2/3$  fluid, the outer component is a  $\nu_1=1$  fluid, while the inner component consists of a  $\nu_h=1/3$ ,  $|e|/3$  quasihole condensate corresponding to an  $e/3$  quasiparticle condensate at  $\nu_2=-1/3$ . Therefore the edge modes consist of an outer,  $e$ -charged electron, while the inner mode is an  $e/3$  quasiparticle mode which propagates in the opposite direction from the outer mode (MacDonald, 1990; Wen, 1992, 1995; Kane *et al.*, 1994; Kane and Fisher, 1995). Note this important distinction of co-propagating versus counterpropagating modes in the two cases. For instance, in the  $2/5$  fluid it does not matter whether the modes propagate both in the positive or negative directions, e.g., under magnetic field reversal, or for a hole rather than an electron gas. What matters is that they propagate in the same direction. Generalizing the edge Hamiltonian, we have (for convenience, from here on we suppress the constant  $\hbar$ )

$$H=2\pi\sum_I\frac{v_I}{v_I}\sum_{q>0}\rho_{I,q}\rho_{I,-q}, \quad (99)$$

where  $I=1,2$  and refers to the  $I$ th edge mode, and  $\sum_I\nu_I=\nu$ . For the Hamiltonian to be bounded from below to yield a well-defined ground state, it is necessary to have the condition  $\nu_I\nu_I>0$ . The commutation relationship between  $\rho_{I,q}$ 's is given by

$$[\rho_{I,q},\rho_{J,q'}]=\frac{\nu_I}{2\pi}q\delta_{I,J}\delta_{q,-q'}. \quad (100)$$

The electron field operators can be written as

$$\Psi_I(x)=e^{i(1/\nu_I)\phi_I(x)}, \quad (101)$$

where  $\rho_I(x)=(1/2\pi)\partial\phi_I(x)$ . A straightforward computation of the electron propagators yields

$$\begin{aligned} &\langle 0|T\{\Psi_I^\dagger(x,t)\Psi_I(0,0)\}|0\rangle \\ &= \langle 0|\exp\left(\frac{1}{v_I^2}\langle\phi_I(x,t)\phi_I(0,0)\rangle\right)|0\rangle \\ &= e^{ik_Ix}\frac{1}{(x-v_I t)^{1/\nu_I}}, \end{aligned} \quad (102)$$

where  $k_I=r_I/l_o^2$  and  $l_o=\sqrt{\hbar c/eB}$ , the magnetic length. Being charged, the two edges can interact either through Coulomb forces or through the mediation of disorder, giving rise to an interaction term between  $\rho_1$  and  $\rho_2$ . The resulting total Hamiltonian can be written as

$$H=2\pi\left(\sum_I U_{II}\sum_{q>0}\rho_{I,q}\rho_{I,-q}+\sum_{I\neq J} V_{IJ}\sum_{q>0}\rho_{I,q}\rho_{J,-q}\right), \quad (103)$$

where  $U$  contains the diagonal elements only and  $V$  con-

tains the off-diagonal elements, i.e.,  $V_{II}=0$ . At this point it is convenient to introduce the scaled density operators,

$$\tilde{\rho}_I\equiv\frac{1}{\sqrt{|v_I|}}\rho_I. \quad (104)$$

The Hamiltonian becomes

$$\begin{aligned} H &= 2\pi\left(\sum_I U_{II}|v_I|\sum_{q>0}\tilde{\rho}_{I,q}\tilde{\rho}_{I,-q}\right. \\ &\quad \left. + \sum_{I\neq J} V_{IJ}\sqrt{|v_I v_J|}\sum_{q>0}\tilde{\rho}_{I,q}\tilde{\rho}_{J,-q}\right) \\ &= 2\pi\left(\sum_I u_{II}\sum_{q>0}\tilde{\rho}_{I,q}\tilde{\rho}_{I,-q} + \sum_{I\neq J} v_{IJ}\sum_{q>0}\tilde{\rho}_{I,q}\tilde{\rho}_{J,-q}\right), \end{aligned} \quad (105)$$

where the matrix elements  $u_{II}=U_{II}|v_I|$  and  $v_{IJ}=V_{IJ}\sqrt{|v_I v_J|}$  have the units of velocity. The commutation relation becomes

$$[\tilde{\rho}_{I,q},\tilde{\rho}_{J,q'}]=\frac{\text{sgn}(v_I)}{2\pi}q\delta_{I,J}\delta_{q,-q'}. \quad (106)$$

$H$  can be rediagonalized with the following transformation of the  $\tilde{\rho}$ 's while preserving the above form of the commutation relation:

$$\tilde{R}_{1,q}=\cos(\sqrt{\eta}\theta)\tilde{\rho}_{1,q}+\frac{1}{\sqrt{\eta}}\sin(\sqrt{\eta}\theta)\tilde{\rho}_{2,q}, \quad (107)$$

$$\tilde{R}_{2,q}=-\sqrt{\eta}\sin(\sqrt{\eta}\theta)\tilde{\rho}_{1,q}+\cos(\sqrt{\eta}\theta)\tilde{\rho}_{2,q}, \quad (108)$$

where

$$\tan(2\sqrt{\eta}\theta)=2\frac{\sqrt{|\eta|}v_{12}}{u_{11}-\eta u_{22}}, \quad (109)$$

with  $\eta=\text{sgn}(v_1 v_2)$  and the convention that  $\sqrt{-1}=i$ . The resulting Hamiltonian and commutation relations are given by

$$H=2\pi\sum_I\text{sgn}(v_I)V_I\sum_{q>0}\tilde{R}_{I,q}\tilde{R}_{I,-q}, \quad (110)$$

$$[\tilde{R}_{I,q},\tilde{R}_{J,q'}]=\frac{\text{sgn}(v_I)}{2\pi}q\delta_{I,J}\delta_{q,-q'}, \quad (111)$$

where the velocities of the two modes of the rediagonalized edge excitations are

$$\begin{aligned} \text{sgn}(v_I)V_I &= \frac{1}{\cos(2\sqrt{\eta}\theta)}[\cos^2(\sqrt{\eta}\theta)u_{II} \\ &\quad - \eta\sin^2(\sqrt{\eta}\theta)u_{JJ}] \end{aligned} \quad (112)$$

for  $J\neq I$ . These new velocities preserve the direction of propagation for the corresponding modes before rediagonalization. The electron propagator for the  $I$ th mode takes the form

$$\langle 0|T\{\Psi_I(x,t)\Psi_I^\dagger(0,0)\}|0\rangle = e^{ik_Ix} \frac{1}{(x-V_I t)^{(1/|\nu_I|)\cos^2(\sqrt{\eta}\theta)}} \times \frac{1}{(x-V_I t)^{(1/|\nu_I|)\eta\sin^2(\sqrt{\eta}\theta)}}, \quad (113)$$

for  $J \neq I$ . The most general electron propagation process may be accompanied by a transfer of any integer number  $n$  of quasiparticles between the inner and outer edges across the outer fractional fluid. In the 2/5 case, the outer fluid is a  $\nu_1 = 1/3$  condensate and the quasiparticles have charge  $e/3$ , while for the 2/3 case, the outer fluid is a  $\nu_1 = 1$  condensate with  $e$ -charged quasiparticles. The quasiparticle transfer operator  $T_{\nu_1}$  may be written as

$$T_{\nu_1} = [\Psi_1 \Psi_2^\dagger]^{\nu_1}. \quad (114)$$

The most general electron field operator  $\Psi$  then can be formed as a linear combination of terms containing a product of the  $\Psi_I$ 's and  $T_{\nu_1}^n$ :

$$\Psi = \Psi_1 \sum_n c_n T_{\nu_1}^n. \quad (115)$$

From Eq. (101), and noting that  $n$  may take on negative values, we have  $\Psi_I^\dagger = [\Psi_I]^{-1}$ . Therefore  $\Psi_2 = \Psi_1 T_{\nu_1}^{-1/\nu_1}$ . The propagator  $\langle T[\Psi(x,t)\Psi(0,0)] \rangle$  contains the terms  $\langle T[(\Psi_1 T_{\nu_1}^n)(\Psi_1 T_{\nu_1}^m)^\dagger] \rangle$

$$\propto \delta_{n,m} e^{i[k_1 + n\nu_1(k_2 - k_1)]x} (x - V_1 t)^{-\gamma_{1n}} (x - V_2 t)^{-\gamma_{2n}}. \quad (116)$$

The exponents  $\gamma_{In}$  are given by

$$\gamma_{1n} = \left[ \left( n + \frac{1}{|\nu_1|} \right) \sqrt{|\nu_1|} \cos(\sqrt{\eta}\theta) - \frac{n\nu_1}{\nu_2} \sqrt{|\nu_2|} \sqrt{\eta} \sin(\sqrt{\eta}\theta) \right]^2, \quad (117)$$

$$\gamma_{2n} = \left[ \left( n + \frac{1}{|\nu_1|} \right) \sqrt{|\nu_1|} \sqrt{\eta} \sin(\sqrt{\eta}\theta) + \frac{n\nu_1}{\nu_2} \sqrt{|\nu_2|} \cos(\sqrt{\eta}\theta) \right]^2, \quad (118)$$

satisfying the sum rule

$$\sum_I \text{sgn}(\nu_I) \gamma_{In} \equiv \lambda_n = \left( n + \frac{1}{|\nu_1|} \right)^2 \nu_1 + \frac{n^2 \nu_1^2}{\nu_2}. \quad (119)$$

The exponent for an electron-tunneling measurement is given by the process with the minimum exponent. For 2/5, the tunneling density of states behaves as  $D(\omega) \propto \omega^{\alpha-1}$  where  $\alpha = 3$ . In other words, the edge of the 2/5 fluid, a daughter condensate from the 1/3 fluid, should exhibit a universal value of tunneling exponent  $I \propto V^3$ . This results from the fact that although there are now two edge modes, they co-propagate. Consequently the

exponent suffers no renormalization. On the other hand, for the 2/3 fluid which supports counterpropagating edge modes, the sum rule alone does not supply sufficient constraint to guarantee a unique, universal value of the exponent. However, strong Coulomb interactions (Wen, 1992) or residual disorder (Kane *et al.*, 1994; Kane and Fisher, 1995), which mix the counterpropagating modes, drive the exponent to a universal value of  $\alpha = 2$  as discussed in the next section. One final remark is in order: for  $\tilde{\psi}(x)$  to satisfy the anticommutation relation,  $\{\tilde{\psi}(x), \tilde{\psi}(x')\} = 0$ , the topological quantum numbers  $\lambda_n$  must be odd integers, yielding

$$\tilde{\psi}(x)\tilde{\psi}(x') = (-1)^{1/\lambda_n} \tilde{\psi}(x')\tilde{\psi}(x) = -\tilde{\psi}(x')\tilde{\psi}(x). \quad (120)$$

## 2. 1D effective-field theory of the chiral Luttinger liquid

For other fillings corresponding to incompressible fluids, in particular, the Jain series, one can generalize the previous type of discussion. To proceed in the most expedient and rigorous way, it is necessary to introduce a generalized chiral boson description in terms of the boson fields  $\phi_i$ 's arising as a natural extension of the  $\phi$  fields above. The chiral boson action is given by (Wen, 1992, 1995)

$$S_{edge} = \frac{1}{4\pi} \int dt dx [K_{IJ} \partial_t \phi_I \partial_x \phi_J - U_{IJ} \partial_x \phi_I \partial_x \phi_J - V_{IJ} \partial_x \phi_I \partial_x \phi_J], \quad (121)$$

with the Hamiltonian

$$H = \frac{1}{4\pi} \int dx [U_{IJ} \partial_x \phi_I \partial_x \phi_J + V_{IJ} \partial_x \phi_I \partial_x \phi_J] = \frac{1}{4\pi} \int dx W_{IJ} \partial_x \phi_I \partial_x \phi_J, \quad (122)$$

where the matrix  $W_{IJ}$ , given by

$$W_{IJ} \equiv U_{IJ} \delta_{IJ} + V_{IJ}, \quad (123)$$

is a positive-definite symmetric matrix with positive-definite eigenvalues to ensure that  $H$  is bounded from below. This edge action is derived from the the  $K$ -matrix formulation of the bulk 2D effective action of fractional Hall fluids (Blok and Wen, 1990a, 1990b; Frohlich and Zee, 1991; Wen and Zee, 1992; Wen, 1995) in terms of the gauge fields  $a_{I\mu}$ , after inputting the information about the boundary potential via the  $U_{IJ}$ ,  $V_{IJ}$  terms,

$$S_{bulk} = -\frac{1}{2\pi} \int dt dx dy \times \left[ \frac{1}{2} K_{IJ} a_{I\mu} \partial_\nu a_{J\lambda} \epsilon^{\nu\lambda} + e t_I A_\mu \partial_\nu a_{I\lambda} \epsilon^{\mu\nu\lambda} \right]. \quad (124)$$

By identifying the edge densities  $\rho_I$ 's with the derivative of the boson fields,  $\rho_I = (1/2\pi) \partial_x \phi_I$ , one recovers the Hamiltonian form of Eq. (122) above. Here  $K$  is an

$n \times n$  matrix with integer elements containing information about the topological properties of the  $n$  condensates and  $n$  different varieties of quasiparticle contained in the fractional Hall fluid.  $t$  is an  $n$ -component charge vector from which the fluid filling factor  $\nu$  can be computed:

$$\nu = t_I^T [K^{-1}]_{IJ} t_J. \quad (125)$$

$A_\nu$  is an external potential coupled to the electron 3-current:

$$j^\mu = \frac{1}{2\pi} t_I \partial \nu a_{I\lambda} \epsilon^{\mu\nu\lambda}. \quad (126)$$

In the ‘‘symmetric’’ basis for Abelian fractional Hall fluids, i.e., fluids with quasiparticle excitations obeying Abelian statistics,  $K$  is a symmetric matrix with odd-integer diagonal elements, while  $t_I = 1$ , i.e.,  $t^T = (1, 1, \dots, 1)$ , yielding

$$\nu = \sum_{IJ} [K^{-1}]_{IJ}. \quad (127)$$

For the  $\nu = n/(np + 1)$  Jain series, where  $n$  is a positive integer and  $p$  an even integer,  $K$  is of dimension  $n$  with  $K_{IJ} = \delta_{IJ} + p$ . For instance, the  $2/5$  fluid is represented by  $n = 2$ ,  $p = 2$  with  $K$  given by

$$(K_{11}, K_{12}; K_{21}, K_{22}) = (3, 2; 2, 3), \quad (128)$$

while the  $2/3$  ‘‘hole fluid’’ with  $\nu = -2/3$  is represented by  $n = 2$ ,  $p = -2$  with

$$(K_{11}, K_{12}; K_{21}, K_{22}) = (-1, -2; -2, -1). \quad (129)$$

(Note that the  $2 \times 2$  matrix of the  $\nu = 1 - 1/m$  fractional Hall electron fluid can also be represented with  $K_{11} = 1$ ,  $K_{22} = -m$  and zero off-diagonal elements.) In the edge dynamics,  $n$  also gives the number of edge modes while the signs of the eigenvalues of the  $K$  matrix give the relative direction of propagation for the modes. In the  $2/5$  case, the eigenvalues  $\lambda_1 = 1$ ,  $\lambda_2 = 5$  are both positive, and the two edge modes co-propagating, while in the  $2/3$  fluid the eigenvalues of  $\lambda_1 = 1$ ,  $\lambda_2 = -3$  indicate that the modes counterpropagate.

The edge action, Eq. (121), together with the Hamiltonian (122), describes the low-energy dynamics of the  $n$  edge modes associated with the  $n$  condensates, where the edge density of the  $I$ th condensate is given by

$$\rho_I = \frac{1}{2\pi} \partial_x \phi_I. \quad (130)$$

The  $\rho$ 's satisfy the Kac-Moody commutation relation,

$$[\rho_{Ik}, \rho_{J-k'}] = [K^{-1}]_{IJ} \frac{k}{2\pi} \delta_{k,k'}. \quad (131)$$

The electron charge density is

$$\rho_e = e \sum_I \rho_I. \quad (132)$$

The quasiparticle operator  $\Psi_I(x)$  associated with the  $I$ th condensate satisfies the relation

$$[\rho_I(x), \Psi_I(x')] = l_I [K^{-1}]_{IJ} \delta(x - x') \Psi_I(x), \quad (133)$$

where the elements of the  $n$ -component  $l$  vector  $l_I$  are integers, and the quasiparticle carries a charge

$$Q_I = e \sum_{IJ} l_I [K^{-1}]_{IJ} t_J. \quad (134)$$

In terms of the chiral boson fields  $\phi_I$ 's,  $\Psi_I$  has the representation

$$\Psi_I \propto \exp(i \phi_I l_I). \quad (135)$$

In particular the electron operator is given by

$$\Psi_{eL} \propto \exp\left(i \sum_I \phi_I l_I\right), \quad (136)$$

with the requirement

$$l_I = \sum_J K_{IJ} L_J, \quad \sum_I L_I = 1 \quad (137)$$

to yield a unit charge. There are many possible choices for the  $n$ -component vector  $L$  with integer-valued elements. The true electron operator  $\Psi_e$  can be written as a linear combination of such operators,  $\Psi_{eL}$ . The requirement of anticommutation for the electron operator yields  $\lambda = \sum_{IJ} L_I K_{IJ} L_J = \text{odd integer}$ .

Because both the  $K$  matrix and the  $W$  matrix ( $W_{IJ} = U_{IJ} \delta_{IJ} + V_{IJ}$ ) are symmetric in the symmetric basis while  $W$  is positive definite, it is possible to simultaneously diagonalize them using transforms:

$$W \rightarrow SWS^T, \quad K \rightarrow SKS^T. \quad (138)$$

The  $S$  transformation is a product of orthogonal transforms and diagonal transforms containing positive-valued diagonal elements that rescale the  $\rho$  fields. The resultant  $I$ th eigenvalue of the transformed  $K$  matrix carries a sign,  $\sigma_I$ , which indicates the direction of propagation of the  $I$ th mode, while the corresponding eigenvalue of the transformed  $W$  matrix yields the corresponding velocity (speed of sound),  $\sigma_I \tilde{V}_I = |\tilde{V}_I|$ . In terms of the transformed  $\tilde{R}_I$ 's,

$$\tilde{R}_I = \sum_{IJ} S_{IJ} \rho_I, \quad (139)$$

the Hamiltonian and  $\tilde{R}_I$  commutation are given by

$$H = 2\pi \sum_{I,k} |\tilde{V}_I| \tilde{R}_{I,k} \tilde{R}_{I,-k} \quad (140)$$

and

$$[\tilde{R}_{I,k}, \tilde{R}_{J,-k'}] = \sigma_I \frac{k}{2\pi} \delta_{I,J} \delta_{k,k'}. \quad (141)$$

The propagator for the  $I$ th quasiparticle takes the form

$$\langle 0 | T \{ \Psi_I(x, t) \Psi_I^\dagger(0, 0) \} | 0 \rangle \propto e^{i l_I k x} \prod_I (x - V_I t + i \sigma_I \delta)^{-\gamma_I}, \quad (142)$$

where

$$\sqrt{\gamma_I} = \sum_J l_J [S^{-1}]_{IJ}, \tag{143}$$

and  $\gamma_I$  satisfies the sum rule

$$\sum_I \sigma_I \gamma_I \equiv \lambda_I = \sum_{IJ} l_I [K^{-1}]_{IJ} l_J. \tag{144}$$

For electron tunneling in the Jain sequence, for which the  $n \times n$   $K$  matrix takes the form  $K_{IJ} = \delta_{IJ} + p$ , with  $[K^{-1}]_{IJ} = \delta_{IJ} - p/(np+1)$ , the tunneling process is dominated by the smallest exponent. When  $p > 0$ , e.g., the  $1/3, 2/5, 3/7, 4/9, \dots$  series, all modes co-propagate, i.e., move in the same direction. The minimum exponent constrained by the sum rule corresponds to  $l_I = p, I \neq n, l_n = p + 1$ , with the exponent value  $\alpha = p + 1$ . For the above Jain series,  $p = 2$ , and all fluids within this series are predicted to exhibit the identical, universal exponent value of  $\alpha = 3$ . On the other hand, for the electron-hole symmetric,  $p = -2$  series,  $2/3, 3/5, 4/7, \dots$ , the presence of counterpropagating modes means that the sum rule no longer constrains the exponent to a universal value, even for a given fluid, e.g.,  $2/3$ . In fact, it is necessary to include the effect of residual disorder to drive the exponents to universal values, as discussed by Kane, Fisher, and Polchinski (Kane *et al.*, 1994; Kane and Fisher, 1995). Long-range Coulomb interaction may also have a similar effect (Wen, 1992). What is required is a mechanism to equilibrate the edge modes, in particular, those that propagate in opposite directions, leading to a universal exponent value for each fluid in the  $p < 0$  Jain sequence given by (Kane and Fisher, 1995)

$$\alpha = 1 + |p| - \frac{2}{n}. \tag{145}$$

Note that for the above series,  $\alpha$  approaches the value 3 as  $\nu \rightarrow 1/2$  ( $n \rightarrow \infty$ ).

### 3. Role of disorder

Here we summarize only the basic ideas about the role of disorder in the edge modes. A detailed mathematical analysis which demonstrates that residual disorder drives the exponent to the universal values given by Eq. (145) for the  $p < 0$  Jain series, as a consequence of the equilibration of the edge modes, is beyond the scope of this article.

First, we note the existence of an  $SU(N)$  symmetry among the neutral modes, which are decoupled from the single charged mode. Starting from the action for the edge dynamics, Eq. (121), Kane and Fisher showed that if the interaction term characterized by the  $W$  matrix is separated into a diagonal contribution  $D, D_{IJ} = v \delta_{IJ}$ , and a traceless contribution  $\tilde{W}, \tilde{W}_{IJ} = W_{IJ} - v \delta_{IJ}$ , the action containing the  $K$  matrix and  $D$  matrix,

$$S_o = \frac{1}{4\pi} \int dt dx \sum_{IJ} [K_{IJ} \partial_t \phi_I \partial_x \phi_J + v \delta_{IJ} \partial_x \phi_I \partial_x \phi_J], \tag{146}$$

describes edge modes that can be transformed via an orthogonal transformation  $O$  into a single charged

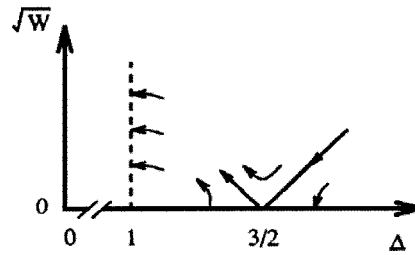


FIG. 6. Kosterlitz-Thouless-type phase transition for the  $\nu = 2/3$  composite edge. When the disorder  $W$  is weak ( $\sqrt{W}$  small), the scaling trajectories flow to nonuniversal values of the interaction parameter  $\Delta$ . On the other hand, when  $\sqrt{W}$  is sufficiently large, the system scales to the universal value of  $\Delta = 1$ . Here  $\Delta$  is related to the tunneling exponent. From Kane, Fisher, and Polchinski, 1994.

mode,  $\phi_\rho = \sqrt{n} \Phi_n = \sum_I \phi_I$  and the  $n - 1$  neutral modes. This mode is decoupled from the neutral modes with boson fields,  $\Phi_I, I = 1, \dots, n - 1$ , where  $\Phi_I = O_{IJ} \phi_J$ . The resultant action is

$$S_o = S_{charge} + S_{neu}, \tag{147}$$

$$S_{charge} = \frac{1}{4\pi} \int dt dx \left( \frac{1}{\nu} \partial_t \phi_\rho \partial_x \phi_\rho + v \partial_x \phi_\rho \partial_x \phi_\rho \right), \tag{148}$$

and

$$S_{neu} = \frac{1}{4\pi} \int dt dx \sum_{i=1}^{n-1} [\partial_t \Phi_i \partial_x \Phi_i + v \partial_x \Phi_i \partial_x \Phi_i]. \tag{149}$$

Note that since  $p < 0$  therefore  $\nu < 0$ , and the charge and neutral modes propagate in opposite directions, while all neutral modes propagate at the same velocity  $v$ . Introduction of an auxiliary field completes the  $SU(N)$  symmetry of the neutral sector.

In a remarkable result, it can be shown that adding randomness to the action  $S_o$  does not destroy the  $SU(N)$  symmetry (Kane and Fisher, 1995). Furthermore, the remaining mode-mode coupling through the traceless  $\tilde{W} = W - vI$  matrix is either absorbed into a velocity renormalization of the charged mode, or is an irrelevant perturbation. In the absence of disorder, however, these terms are relevant and change the exponent of the propagators. Therefore disorder has the effect of restoring the  $SU(N)$  symmetry of the neutral modes and maintaining the decoupling between the charged and neutral sectors. This disorder-driven approach to universality occurs as a Kosterlitz-Thouless phase transition in the disorder parameter, as is shown in Fig. 6 for the edge of the  $2/3$  fluid.

### 4. Compressible fluid edges

Thus far, we have focused exclusively on edge tunneling into the edge of incompressible fractional quantum Hall fluids, specifically into the Laughlin (1983) and Jain series (Jain, 1989a, 1989b, 1990; see also the Haldane/Halperin series, Haldane, 1983; Halperin, 1984). One of the early experimental surprises was the observation of

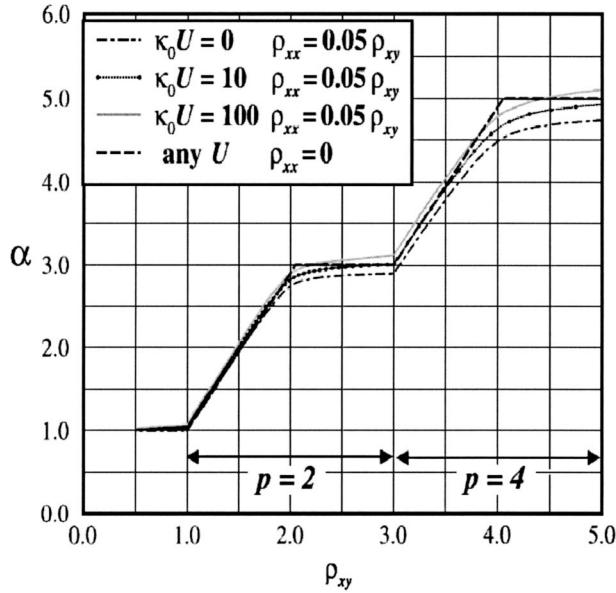


FIG. 7. The electron-tunneling exponent  $\alpha$ , as a function of the dimensionless Hall resistance  $\rho_{xy}$ . A constant Hall angle,  $\tan^{-1}[\rho_{xy}/\rho_{xx}]$ , is assumed. For  $\rho_{xx}=0.05\rho_{xy}$ ,  $\alpha$  is plotted for three values of the short-range interaction  $U=1/\kappa-1/\kappa_o$ . Note that at  $\rho_{xx}=0$  the exponent is universal (no  $U$  dependence), but at finite  $\rho_{xx}$  it can be either larger or smaller than the universal result. From Shytov, Levitov, and Halperin, 1998.

power-law tunneling characteristics for electron tunneling into the compressible,  $\nu=1/2$  composite-fermion fluid edge (Chang, 1998). At first sight it was not entirely clear that electron tunneling into the composite-fermion edge would necessarily entail an orthogonality catastrophe. To account for the experimental findings and to investigate the tunneling behavior for general fillings, compressible or incompressible, Shytov, Levitov, and Halperin (Shytov *et al.*, 1998; Levitov *et al.*, 2001) proposed a theory based on an effective edge action derived from the bulk 2D composite-fermion effective action and computed the equal-space single-particle Green's function relevant for electron tunneling. They found an approximate power-law behavior for all fillings. The behavior of the exponent exhibits plateaus (steps) when plotted against the dimensionless Hall resistance  $\rho_{xy}/(h/e^2)$ , as shown in Fig. 7, and is driven close to universal values by residual disorder in between steps, varying in an approximately linear manner. Small deviations from the universal values arise from interaction and a nonzero longitudinal resistivity,  $\rho_{xx} \geq 0$ . Note that for compressible fluids  $\rho_{xy}/(h/e^2) \approx 1/\nu$ , where  $\nu$  is the Landau-level filling. The result of Shytov, Levitov, and Halperin thus basically fills in the continuous sections between the discrete points of incompressible fluids previously investigated by Wen (1992) and Kane and Fisher (1995). This somewhat surprising result of a power-law behavior at all fillings  $\nu$  has its origin in the fact that, for high-quality samples such as those used in experiment, the longitudinal resistance is invariably small,  $\rho_{xx} \leq 0.1\rho_{xy}$ , in the fractional quantum Hall regime. Therefore a charge introduced into the edge necessarily

propagates a large distance along the boundary before it is able to penetrate into the 2D bulk.

The actual computation is extremely technical (Shytov *et al.*, 1998; Levitov *et al.*, 2001). We shall merely sketch the ideas. For a model of short-ranged electron-electron interaction,

$$U(\mathbf{r}) = U \delta(\mathbf{r}), \quad (150)$$

with an effective composite-fermion interaction

$$U_{CF}(\mathbf{r}) = \left( U + \frac{1}{\kappa_o} \delta(\mathbf{r}) \right), \quad (151)$$

where  $\kappa_o = 2\pi m^*/\hbar^2$  is the free composite-fermion compressibility. Integrating out the degree of freedom perpendicular to the edge yields an action for the edge

$$S_{edge} = \sum_{\omega, k} \frac{1}{2} \left[ \sigma_{xx} |\omega| \left( k^2 + \frac{|\omega|}{U + \frac{1}{\kappa_o}} \right) + i \sigma_{xy} \omega k \right] \times \phi_{-\omega, -k} \phi_{\omega, k} + J(-\omega, -k) \phi_{\omega, k}, \quad (152)$$

where  $\phi_{\omega, k}$  is the  $(\omega, k)$  Fourier transform of the boundary boson field,  $\phi(x, t)$ , and  $J$  is the Fourier transform of the source term  $J(x, t) = e \delta(x - x_o) [\delta(t - t_1) - \delta(t - t_2)]$  at the boundary. This action reduces to the standard expression, Eq. (121), in the limit of incompressibility where  $\sigma_{xx} = 0$ .

The equal-space electron single-particle Green's function relevant for electron-tunneling processes is computed using the composite-fermion Green's function coupled to the gauge field  $a^\mu$ :

$$G(t_1, t_2, a_\mu) = G_{CF}(t_2 - t_1) \times \exp \left( i \int_{-\infty}^{\infty} d^2 r dt a^\mu(\mathbf{r}, t) j_\mu^{free}(\mathbf{r}, t) \right), \quad (153)$$

where  $G_{CF}(t) \approx 1/t$  is the composite-fermion Green's function in the absence of slow gauge-field fluctuations, and  $j_\mu^{free}(\mathbf{r}, t)$  is a current describing the spreading of free composite-fermion density. The electron single-particle Green's function is approximated by

$$G(t) = G_{CF}(t) \exp \{ i [S_{edge}(t) - S_{free}(t)] \}, \quad (154)$$

where the subscript “free” refers to the action of noninteracting composite fermions. The end result yields an expression for the electron-tunneling exponent:

$$\alpha = 1 + \frac{2}{\pi} \left[ \tan^{-1} \left( \frac{\rho_{xy}}{\rho_{xx}} \right) \tilde{\rho}_{xy} - \tan^{-1} \left( \frac{\rho_{xy}^o}{\rho_{xx}^o} \right) \tilde{\rho}_{xy}^o \right] + \frac{\tilde{\rho}_{xx}}{\pi} \ln[(1 + \kappa_o U)] \frac{\sigma_{xx}}{\sigma_{xx}^o}, \quad (155)$$

with

$$\rho_{xy} = \rho_{xy}^o + p h/e^2 = h/\nu e^2, \quad \rho_{xx} = \rho_{xx}^o, \quad (156)$$

$p$  being the number of flux quanta attached to the composite fermions, and

$$\tilde{\rho}_{xx} = \frac{\rho_{xx}}{e^2/h}, \quad (157)$$

$$\tilde{\rho}_{xy} = \frac{\rho_{xy}}{e^2/h} \quad (158)$$

being the dimensionless diagonal and Hall resistivities (see Fig. 7). Accounting for the long-range Coulomb interaction only slightly modifies the exponent  $\alpha$ . In particular, a logarithmic correction is found and the effective exponent increases as the energy associated with the tunneling decreases. For edge tunneling from a normal metal into a  $\nu=1/3$  fractional fluid edge, this predicts that the exponent will exceed 3 as the energy decreases towards 0.

### 5. Scaling functions for electron tunneling

To probe the chiral Luttinger liquid, transport measurements of electron tunneling into the edge of a fractional quantum Hall fluid can be made by placing contacts on opposite sides of the tunnel barrier as shown in Fig. 16 below in the experimental section (Sec. III.D). Several measurement schemes are possible: (i) a direct measurement of the tunneling current through the barrier  $I_{tun}$  for a voltage bias  $V$  applied between the two sides to deduce the current-voltage ( $I$ - $V$ ) characteristics. This should yield a power-law dependence  $I_{tun} \propto V^\alpha$  reflecting the power-law tunneling density of states,  $D(\omega) \propto \omega^{\alpha-1}$ ; (ii) a differential conductance measurement,  $dI/dV \propto V^{\alpha-1}$ ; and (iii) a zero-bias measurement of the linear tunneling conductance  $G(T)$ , which should exhibit a nonlinear,  $G \propto T^{\alpha-1}$ , dependence on the temperature  $T$ , again reflecting the power-law tunneling density of states. The value  $\alpha$  extracted from all these measurements must be consistent.

The experimental finding that the tunneling behavior as a function of  $V$  and temperature  $T$  does indeed obey a universal scaling form predicted by theory represents an extremely significant result. Therefore, to make contact with experiments, it is necessary to compute the tunneling current under conditions in which the energy scale is set either by  $V$  ( $E=eV$ ), or by  $T$  ( $E=kT$ ). The tunnel current response is usually computed in perturbation theory by considering an operator that annihilates an electron on one side of the tunnel barrier at an initial time  $t$ , and creates it on the opposite side at a different time  $t'$ ,  $\psi_1(x,y,t)\psi_2^\dagger(x',y',t')$ . To be specific and make contact with the experimental results presented in the experimental section (on electron tunneling from a heavily doped, 3D  $n$ +GaAs metal into the edge of a fractional quantum Hall fluid), we shall use the convention that the subscript 1 refers to the normal metal and subscript 2 to the edge of the fractional Hall fluid. The direction  $x$  ( $x'$ ) parametrizes the direction along the boundary, while  $y$  ( $y'$ ) is the direction perpendicular to the boundary. A tunneling event must conserve momentum parallel to the interface (boundary). For instance in the Landau gauge,  $\nabla \cdot \mathbf{A} = \mathbf{0}$ , the wave function  $\phi(x,y)$  takes the form of a running wave in the  $x$  direction,  $e^{ikx}$ ,

where the wave vector  $k$  is proportional to the  $y$  position of the guidance center,  $y_o$ ,  $k=y_o/l_o^2$ , where  $l_o = \sqrt{\hbar c/eB}$  is the magnetic length with a value of 8.1 nm at  $B=10$  T. Tunneling across the barrier involves a change in the position of  $y$ , and therefore a change in the momentum of  $x$ . If the system is completely clean and without defects or impurities, translational invariance in this parallel direction alone would suppress tunneling. Therefore it is essential to mediate tunneling via processes that do not conserve momentum. The presence of impurities and point defects can mediate tunneling at pointlike (size  $\leq l_o$ ) positions. Point tunneling efficiently mediates tunneling, since it necessarily involves a broad range of momenta as dictated by the uncertainty principle. Therefore the tunneling probability, which in the general case can be  $k$  dependent, must be averaged over  $k$ . In other words, the spectral density function  $A_\pm(\omega,k)$  will be averaged, yielding the tunneling density of states

$$D_\pm(\omega) = \int A_\pm dk, \quad (159)$$

where  $\pm$  denote the tunneling of electrons and holes, respectively. Note that the power-law dependence is expected to be the same for the tunneling of electrons and holes [Eqs. (97) and (98)]. The task at hand is therefore to compute the tunneling current for point tunneling.

The simplest approximation to point tunneling is made by setting the coordinates equal to the respective values at the tunneling point,  $(x,y)=(0,y_1),(x',y')=(0,y_2)$ , where for convenience we have chosen  $x=x'=0$ , and  $|y_2-y_1|=b$ , the barrier width. As a further approximation, the effect of the final barrier width  $b$  is incorporated in the “bare” tunneling amplitude  $\Gamma$  only. Suppressing the  $y$  coordinates and choosing the initial time,  $t=0$ , we obtain the tunnel coupling

$$H_{tun} = \Gamma \psi_2^\dagger(0)\psi_1(0) + \text{H.c.} \quad (160)$$

The current response to an applied bias  $V$  at zero temperature is given in the weak-coupling (weak-tunneling) limit by first-order perturbation theory (Schrieffer *et al.*, 1963; Wen, 1991b):

$$\begin{aligned} I_{tun}(t) = e\Gamma^2 \int_{-\infty}^{\infty} dt' \theta(t) \\ \times \{ e^{i\int_t^{t'} eV(t'') dt''} \langle [A(t), A^\dagger(0)] \rangle \\ - e^{-i\int_t^{t'} eV(t'') dt''} \langle [A^\dagger(t), A(0)] \rangle \}, \quad (161) \end{aligned}$$

where  $A(t) = c_2(0,t)c_1^\dagger(0,t)$ , and  $c_1, c_2$  are the electron operators on the edges 1 and 2. In general, the electron propagator for the  $i$ th edge can be written as

$$G_i(x=0,t) = a_i^{-1} \omega_i^{-\alpha} t^{-\alpha}, \quad (162)$$

where  $a_i$  is a cutoff length and  $\omega_i$  a cutoff frequency. Note that this is an equal-space propagator. For the Laughlin series with filling factor  $\nu=1/m$ , where  $m$  is an odd integer, and  $\alpha=1/\nu$ ,

$$\langle c_{1,2}^\dagger(x,t)c_{1,2}(0) \rangle \propto (x \pm v_{1,2}t)^{-\alpha_{1,2}} e^{\mp(i/\nu_{1,2})k_{F_{1,2}}x}. \quad (163)$$

This form leads to

$$\langle A(t)A^\dagger(0) \rangle = \frac{1}{a_1 a_2} \frac{1}{[-\omega_1(t-i\delta)]^{\alpha_1}} \frac{1}{[\omega_2(t-i\delta)]^{\alpha_2}}, \quad (164)$$

$$\langle A^\dagger(0)A(t) \rangle = \frac{1}{a_1 a_2} \frac{1}{[-\omega_1(t+i\delta)]^{\alpha_1}} \frac{1}{[\omega_2(t+i\delta)]^{\alpha_2}}, \quad (165)$$

$$\begin{aligned} \langle A(x,t)A^\dagger(0,0) \rangle &= a_1^{\alpha_1-1} a_2^{\alpha_2-1} \\ &\times \frac{1}{[x-v_1(t-i\delta)]^{\alpha_1}} \frac{1}{[x+v_2(t-i\delta)]^{\alpha_2}} \\ &\times e^{(i/\nu_1)k_{F_1}x} e^{(i/\nu_2)k_{F_2}x}, \end{aligned} \quad (166)$$

$$\begin{aligned} \langle A^\dagger(0,0)A(x,t) \rangle &= a_1^{\alpha_1-1} a_2^{\alpha_2-1} \\ &\times \frac{1}{[x-v_1(t+i\delta)]^{\alpha_1}} \frac{1}{[x+v_2(t+i\delta)]^{\alpha_2}} \\ &\times e^{-(i/\nu_1)k_{F_1}x} e^{-(i/\nu_2)k_{F_2}x}. \end{aligned} \quad (167)$$

The zero-temperature tunneling current is then given by

$$\begin{aligned} I_{tun}(V) &= -2e\Gamma^2 \text{Im} \left[ -i \frac{\pi}{(\alpha_1 + \alpha_2 - 1)!} \right. \\ &\times \left. \int d\omega \times f(\omega, t) \frac{a_1^{\alpha_1-1} a_2^{\alpha_2-1}}{v_1^{\alpha_1} v_2^{\alpha_2}} \omega^{\alpha_1 + \alpha_2 - 1} \right], \end{aligned} \quad (168)$$

where  $f(\omega, t)$  is defined by

$$e^{i\int_t^t eV(t'')dt''} = \int d\omega f(\omega, t) e^{i\omega(t-t')}. \quad (169)$$

For a dc bias this expression simplifies to

$$\begin{aligned} I_{tun}(V) &= -2e\Gamma^2 \text{Im} \\ &\times \left[ -i \frac{\pi}{(\alpha_1 + \alpha_2 - 1)!} \left( \frac{a_1^{\alpha_1-1} a_2^{\alpha_2-1}}{v_1^{\alpha_1} v_2^{\alpha_2}} V^{\alpha_1 + \alpha_2 - 1} \right) \right]. \end{aligned} \quad (170)$$

At finite temperature, the expressions become

$$\begin{aligned} \langle A(0,t)A^\dagger(0,0) \rangle &= \frac{a_1^{\alpha_1-1} a_2^{\alpha_2-1}}{v_1^{\alpha_1} v_2^{\alpha_2}} (\pi T)^{\alpha_1 + \alpha_2} \\ &\times \frac{1}{[-\sinh(\pi Tt)]^{\alpha_1}} \frac{1}{\sinh[\pi Tt]^{\alpha_2}} \\ &\times e^{i\pi[(\alpha_1 + \alpha_2)/2] \text{sgn}(t)}, \end{aligned} \quad (171)$$

$$\begin{aligned} \langle A^\dagger(0,0)A(0,t) \rangle &= \frac{a_1^{\alpha_1-1} a_2^{\alpha_2-1}}{v_1^{\alpha_1} v_2^{\alpha_2}} (\pi T)^{\alpha_1 + \alpha_2} \\ &\times \frac{1}{[-\sinh(\pi Tt)]^{\alpha_1}} \frac{1}{\sinh[\pi Tt]^{\alpha_2}} \\ &\times e^{-i\pi[(\alpha_1 + \alpha_2)/2] \text{sgn}(t)}, \end{aligned} \quad (172)$$

yielding a tunnel current

$$\begin{aligned} I_{tun} &= 2e\Gamma^2 \frac{a_1^{\alpha_1-1} a_2^{\alpha_2-1}}{v_1^{\alpha_1} v_2^{\alpha_2}} (2\pi T)^{\alpha_1 + \alpha_2 - 1} \\ &\times B\left(\alpha_{12} - i \frac{\omega}{2\pi T}, \alpha_{12} - i \frac{\omega}{2\pi T}\right) \frac{\sin \pi\left(\alpha_{12} + i \frac{\omega}{2\pi T}\right)}{\cos \pi\alpha_{12}}, \end{aligned} \quad (173)$$

where  $\alpha_{12} = (\alpha_1 + \alpha_2)/2$ , and  $B$  is the beta function.

Explicit expressions for a dc current can be obtained, first, in the limit of  $eV \ll 2\pi T$ , where the current is linear in  $V$  and obeys a power law in  $T$ :

$$\begin{aligned} I_{tun} &\propto \frac{a_1^{\alpha_1-1} a_2^{\alpha_2-1}}{v_1^{\alpha_1} v_2^{\alpha_2}} \frac{\pi}{\Gamma(2\alpha_{12})} T^\alpha [\Gamma(\alpha_{12})]^2 \frac{eV}{2\pi T} \\ &\propto T^{\alpha-1} eV, \end{aligned} \quad (174)$$

and second, for  $eV \gg 2\pi T$ , where the current exhibits a power law in  $V$ ,

$$I_{tun} \propto \frac{a_1^{\alpha_1-1} a_2^{\alpha_2-1}}{v_1^{\alpha_1} v_2^{\alpha_2}} \frac{\pi}{\Gamma(2\alpha_{12})} T^\alpha \left(\frac{eV}{2\pi T}\right)^\alpha \propto (eV)^\alpha. \quad (175)$$

Here  $\alpha = 2\alpha_{12} - 1 = \alpha_1 + \alpha_2 - 1$ ;  $\Gamma(s)$  denotes the gamma function with argument  $s$ , and note that we have set the Boltzmann constant  $k_B$  to 1 for convenience. Correspondingly, the differential conductance  $G_{tun}$  in the two limits is given by

$$\begin{aligned} G_{tun} &\equiv \frac{dI_{tun}}{dV} \\ &\propto \frac{a_1^{\alpha_1-1} a_2^{\alpha_2-1}}{v_1^{\alpha_1} v_2^{\alpha_2}} \frac{\pi}{\Gamma(2\alpha_{12})} T^\alpha [\Gamma(\alpha_{12})]^2 \frac{e}{2\pi T} \propto T^{\alpha-1} \end{aligned} \quad (176)$$

and

$$\frac{a_1^{\alpha_1-1} a_2^{\alpha_2-1}}{v_1^{\alpha_1} v_2^{\alpha_2}} \frac{\pi}{\Gamma(2\alpha_{12})} T^\alpha \frac{ae}{2\pi T} \left(\frac{eV}{2\pi T}\right)^{\alpha-1} \propto (eV)^{\alpha-1}. \quad (177)$$

The dimensionless variable,  $x = eV/2\pi T$ , appears as a natural variable for which the condition  $x = 1$  denotes an approximate crossover condition. In one direction, the energy scale for tunneling is determined by the thermal energy ( $x < 1$ ) and the tunneling current approaches linearity in the bias voltage  $V$ , while obeying a power law in temperature,  $I \propto T^{\alpha-1}$ . In the opposite situation, the energy scale is set by  $eV$  ( $x > 1$ ) and  $I$  is nonlinear in  $V$ ,

approaching the power-law  $I \propto V^\alpha$  functional form. For the differential conductance,  $G$  approaches a  $V$ -independent form while proportional to  $T^{\alpha-1}$  for  $x < 1$ , and a power-law bias voltage form,  $G \propto V^{\alpha-1}$ , for  $x > 1$ . By measuring the voltage-bias power law for  $x \gg 1$  and the temperature power law for  $x \ll 1$  in two independent measurements, one can check the consistency of the values deduced for the exponent  $\alpha$ .

Besides dc characteristics, based on Eq. (168), under an additional ac excitation at frequencies akin to the Josephson frequency,  $\omega = e^*V/\hbar$ , interesting resonance structures in the tunneling current and in the tunneling-current quantum shot noise are predicted to be observable. At typical accessible base temperatures of a few tens of milli-Kelvin, excitation voltages in the  $\mu\text{V}$  range corresponding to Josephson frequencies in the GHz regime are needed to exceed the thermal-energy scale.

A similar but alternative formulation of the scaling expressions due to Wen has been put forth by Kane and Fisher based on a renormalization-group analysis of the backscattering between left- and right-moving Luttinger-liquid channels for a single impurity. They uncovered a duality relation between the strong- and weak-tunneling limits. In the weak-tunneling limit relevant to the experimental conditions discussed in this review, Kane and Fisher (1992b, 1992c) give an alternative expression of

$$I \propto [\Gamma(\alpha_{12})]^2 x + x^\alpha. \quad (178)$$

This expression exhibits the same limiting behaviors for  $x \ll 1$  and  $x \gg 1$  as Eqs. (174) and (175). The crossover voltage where the linear and power-law contributions are equal to each other is given by  $eV = [\Gamma(\alpha_{12})]^{2/(\alpha-1)} (2\pi T)$ . For tunneling between  $\nu_1 = 1$  and  $\nu_2 = 1/3$ ,  $\alpha_{12} = 2$ , implying  $\Gamma(\alpha_{12}) = 1! = 1$ , and the crossover occurs at  $eV = 2\pi T$ .

It turns out that for tunneling through a single impurity or contact point within this effective-field theory, a complete solution with a full universal curve spanning the entire range of weak and strong coupling (tunneling) can also be obtained based on the Bethe ansatz. Fendley, Ludwig, and Saleur (1995a, 1995b) were able to demonstrate the integrability of the problem for tunneling between chiral Luttinger edges at filling fractions between  $1/4$  and  $1$ , assuming a single edge mode for each edge, while at the same time proving the exact duality relation between weak and strong tunneling. Note for  $\nu < 1/4$ , the model needs fine-tuning to achieve integrability. In the context of the fractional Hall edge, the duality corresponds to the physical situation of electron tunneling in the weak limit and quasiparticle tunneling in the strong limit. It turns out that even in the presence of backscattering between the left- and right-moving  $\nu$  channels, with coupling occurring at a point via an impurity or point contact, the problem is integrable and can be mapped onto known field-theory models of the boundary sine-Gordon type (Ghoshal and Zamolodchikov, 1994), which in turn is directly related to the Kondo problem. This entire class of problems is soluble via the Bethe ansatz. As a consequence of this integrability and the associated presence of an underlying quantum criti-

cal point, the differential conductance can be expressed in terms of two dimensionless variables,  $eV/T$  and  $T_K/T$ , formed out of the three energy scales, the bias voltage  $V$ , the temperature  $T$ , and the Kondo energy scale  $T_K$  which characterizes the strength of the point-contact coupling:

$$G = \frac{dI}{dV} = G\left(\frac{eV}{T}, \frac{T_K}{T}\right). \quad (179)$$

In the limit for weak coupling for which  $eV, T \ll T_K$ , the expression for the current has the functional form of Eq. (178) with the scale of the current set by  $T_K$ :

$$I_{\text{tun}} = \nu \frac{e^2}{h} \frac{T_K}{2\{\Gamma[(\alpha+1)/2]\}^2} \left(\frac{2\pi T}{T_K}\right)^\alpha \times (\{\Gamma[(\alpha+1)/2]\}^2 x + x^\alpha). \quad (180)$$

In the special case of tunneling between two  $\nu = 1/2$  edges, the entire scaling curve can be expressed in closed form (Kane and Fisher, 1992c; Fendley *et al.*, 1995b):

$$I_{\text{tun}} = \int_{-\infty}^{\infty} \frac{d\omega}{2\pi} \frac{\omega^2}{\omega^2 + \left(\frac{T_K}{2}\right)^2} [f(\omega - \omega_o) - f(\omega)] \quad (181)$$

and

$$G_{\text{tun}} = \frac{1}{2} \frac{e^2}{h} \int_{-\infty}^{\infty} d\omega \frac{\omega^2}{\omega^2 + \left(\frac{T_K}{2}\right)^2} [-f'(\omega - \omega_o)], \quad (182)$$

where  $\omega_o = eV/2$  and  $f$  is the Fermi-Dirac distribution. These expressions can be recast in terms of the digamma function  $\psi$  and its derivative (Fendley *et al.*, 1995b). For general values of  $\nu$ , in the  $T=0$  limit these solutions yield (Chamon and Fradkin, 1997):

$$G = \nu \frac{e^2}{h} \begin{cases} \sum_1^{\infty} c_n(1/\nu) \left(\frac{V}{2T_K}\right)^{2n(1/\nu-1)}, & \left(\frac{V}{2T_K}\right) < e^\delta \\ 1 - \sum_1^{\infty} c_n(\nu) \left(\frac{V}{2T_K}\right)^{2n(\nu-1)}, & \left(\frac{V}{2T_K}\right) > e^\delta, \end{cases} \quad (183)$$

where

$$c_n(\nu) = (-1)^{n-1} \frac{\Gamma(n\nu+1)}{\Gamma(n+1)} \frac{\Gamma(1/2)}{\Gamma[n(\nu-1)+1/2]}, \quad (184)$$

and  $\delta = [\nu \ln \nu + (1-\nu) \ln(1-\nu)]/2(\nu-1)$ .

To further tie in with experiments in which tunneling takes place between a 3D  $n + \text{GaAs}$  normal metal and a chiral Luttinger edge, Chamon and Fradkin (1997; Fradkin, 2000) made extensive use of the exact solutions provided by Fendley, Ludwig, and Saleur, applied to a case of multiple, weak-coupling point contacts that were incoherent with each other. They first mapped the 3D metal to a  $\nu_1 = 1$  chiral fermion mode, resulting in an action for tunneling at a point contact into a  $\nu_2 = 1/m$  chiral Luttinger mode [see Chklovskii and Halperin (1998) for a somewhat different view of such a mapping]:

$$\begin{aligned}
 S = \frac{1}{4\pi} \int dt dx & \left( \frac{1}{v_1} (\partial_t \phi_1 - v_1 \partial_x \phi_1) \partial_x \phi_1 \right. \\
 & + \frac{1}{v_2} (\partial_t \phi_2 - v_2 \partial_x \phi_2) \partial_x \phi_2 \\
 & \left. + \Gamma \delta(x) e^{i\omega t} e^{-i\{(1/v_1)\phi_1(0,t) - (1/v_2)\phi_2(0,t)\} + \text{H.c.}} \right), \quad (185)
 \end{aligned}$$

where the two Luttinger edge modes interact at the point  $x=0$  and live in different spaces of  $x \geq 0$  and  $x \leq 0$ , respectively. As a result the  $x$  coordinate for each field can be rescaled to yield the same velocity for the two modes,  $v = v_1 = v_2$ . The electron operator for each mode is given by  $\psi_l(x,t) = e^{i(1/v_l)\phi_l}$ . An orthogonal transformation,

$$\tilde{\phi}_1 = \cos \theta \phi_1 + \sin \theta \phi_2, \quad (186)$$

$$\tilde{\phi}_2 = -\sin \theta \phi_1 + \cos \theta \phi_2, \quad (187)$$

where

$$\cos \theta = \frac{1}{\sqrt{2}} \frac{\sqrt{1/v_1} + \sqrt{1/v_2}}{\sqrt{1/v_1 + 1/v_2}}, \quad (188)$$

$$\sin \theta = \frac{1}{\sqrt{2}} \frac{\sqrt{1/v_1} - \sqrt{1/v_2}}{\sqrt{1/v_1 + 1/v_2}}, \quad (189)$$

yields a tunneling action between identical transformed fillings  $\tilde{\nu}$ :

$$\tilde{\nu} = \frac{1}{[(\nu^{-1} + 1)/2]} \quad (190)$$

of

$$\begin{aligned}
 S = \frac{1}{4\pi} \int dt dx & \frac{1}{\tilde{\nu}} [(\partial_t \tilde{\phi}_1 - \tilde{\nu} \partial_x \tilde{\phi}_1) \partial_x \tilde{\phi}_1 \\
 & + (\partial_t \tilde{\phi}_2 - \tilde{\nu} \partial_x \tilde{\phi}_2) \partial_x \tilde{\phi}_2 \\
 & + \Gamma \delta(x) e^{i\omega t} e^{-i(1/\tilde{\nu})[\tilde{\phi}_1(0,t) - \tilde{\phi}_2(0,t)] + \text{H.c.}}]. \quad (191)
 \end{aligned}$$

For  $\nu_1=1$  to  $\nu_2=1/3$  tunneling, this results in tunneling between two  $\tilde{\nu}=1/2$  edges! This case therefore corresponds to the exactly soluble case discussed by Fendley, Ludwig, and Saleur, for which the entire scaling function is known.

The final step is to assume that in the cleaved-edge tunneling experiment, electron tunneling takes place under the condition of weak tunneling at multiple contact points, where the tunneling at successive points is incoherent in nature, as depicted in Fig. 8. At each point, the receiving chiral Luttinger edge mode is characterized by a voltage  $V_i$ , while the injecting  $\nu=1$  chiral fermion edge mode always resides at the voltage of the 3D, normal-metal reservoir. In other words, energy relaxation is fast within the 3D,  $n + \text{GaAs}$  normal metal compared to the time between successive tunneling events at the incoherent tunneling points. Whatever voltage the effective chiral fermion channel ends up with after pass-

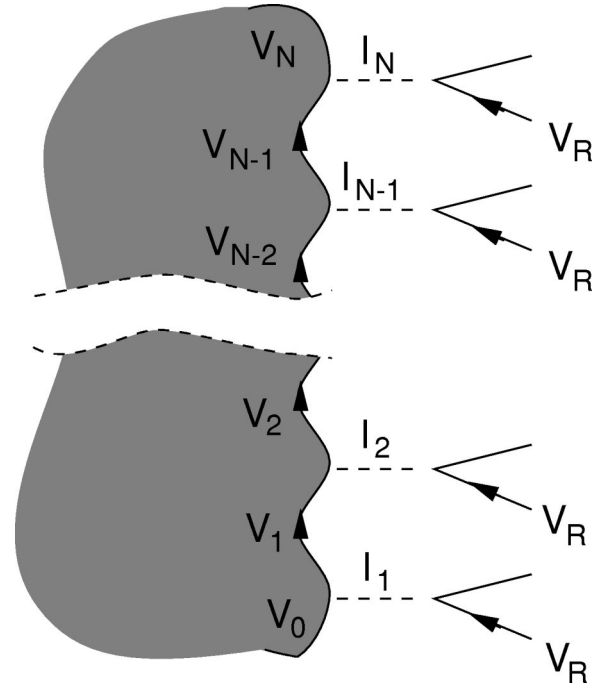


FIG. 8. Multi ( $N$ ) -impurity scattering, assembled from the one-impurity building block. It is crucial that the voltages on the fractional quantum Hall fluid side be maintained in between scattering events, whereas the electrons from the reservoir side should always come into the scattering process at  $V_R$ . From Chamon and Fradkin, 1997.

ing a given point-contact tunneling point is replenished by rapid energy exchange with the rest of the bulk 3D metal. A full scaling curve extending from the weak- to strong-tunneling regime relevant to the experimental situation can now be obtained from two relationships: (1) with the chiral Luttinger edge between two successive tunneling points, we have

$$V_i - V_{i-1} = \frac{I_i}{\nu e^2/h}, \quad (192)$$

where  $I_i$  is the tunneling current at the  $i$ th point. The total tunneling current is then the sum of the currents,  $I_i, I_{\text{tun}} = \sum_i I_i$ ; (2) at each tunneling point, the tunneling is weak and we have, from Eq. (180),

$$\begin{aligned}
 I_i = \nu \frac{e^2}{h} & \frac{T_{K_i}}{2\{\Gamma[(\alpha+1)/2]\}^2} \left( \frac{2\pi T}{T_{K_i}} \right)^\alpha \\
 & \times \{\Gamma[(\alpha+1)/2]\}^2 x + x^\alpha, \quad (193)
 \end{aligned}$$

where  $(\alpha+1)/2 = \alpha_{12}$ . The first equation, Eq. (192), is strictly correct only when the dissipative conductance  $G_{xx}$  is zero, as in the case of a well-developed quantized Hall state. It is still a good approximation as long as  $G_{xx} \ll G_{\text{Hall}}$ , as is the case for the high-quality samples used in the experiments at general fillings. Combining these two equations yields

$$-2\pi T \Delta x_i = \frac{1}{2} T_{K_i} \left( \frac{2\pi T}{T_{K_i}} \right)^\alpha \left[ x_{i-1} + \frac{1}{\left[ \Gamma\left( \frac{\alpha+1}{2} \right) \right]^2} x_{i-1}^\alpha \right]. \quad (194)$$

By fine-graining the successive tunneling points, Chamon and Fradkin obtained a differential equation:

$$-\frac{dx}{di} = \frac{1}{2} \left( \frac{2\pi T}{T_{K_i}} \right)^{\alpha-1} \left[ x_{i-1} + \frac{1}{\left[ \Gamma\left(\frac{\alpha+1}{2}\right) \right]^2 x_{i-1}^\alpha} \right]. \quad (195)$$

Imposing the boundary conditions valid for 1 to  $\nu$  tunneling,

$$x_o = \frac{e(V_R - V_o)}{2\pi T} = \frac{eV}{2\pi T} \quad (196)$$

and

$$I_{tun} = \sum_i I_i = \nu \frac{e^2}{h} \frac{2\pi T}{e} (x_o - x_N), \quad (197)$$

where  $N$  indexes the last tunneling point, one obtains with  $\beta = \alpha - 1$

$$I_{tun} = \nu \frac{e^2}{h} V \left\{ 1 - \frac{e^{-(1/2)(2\pi T/T_s)^\beta}}{\left[ 1 + \frac{1}{\left[ \Gamma\left(\frac{\alpha+1}{2}\right) \right]^2} (1 - e^{-(\beta/2)(2\pi T/T_s)^\beta}) \left( \frac{eV}{2\pi T} \right)^\beta \right]^{1/\beta}} \right\}, \quad (198)$$

yielding

$$G_{tun} = \frac{dI_{tun}}{dV} = \nu \frac{e^2}{h} \left\{ 1 - \frac{e^{-(1/2)(2\pi T/T_s)^\beta}}{\left[ 1 + \frac{1}{\left[ \Gamma\left(\frac{\alpha+1}{2}\right) \right]^2} (1 - e^{-(\beta/2)(2\pi T/T_s)^\beta}) \left( \frac{eV}{2\pi T} \right)^\beta \right]^{\alpha/\beta}} \right\}. \quad (199)$$

Here,  $T_s$  denotes a crossover temperature to the strong-tunneling regime, where

$$\left( \frac{1}{T_s} \right)^\beta = \sum_{i=1}^N \left( \frac{1}{T_{K_i}} \right)^\beta. \quad (200)$$

Strictly speaking this expression is valid only for  $\nu_1 = 1/m_1$ ,  $\nu_2 = 1/m_2$ , and  $m_i$  is an odd integer, so that tunneling occurs between a single edge mode for each fluid. In practice, however, one is able to interpolate to continuous values of  $\nu_i$ . This is the expression used extensively in data analysis to extract the tunneling exponent  $\alpha$ .

## 6. Resonant tunneling

In the discussion above, we focused on tunneling events in which the individual event is in the weak-tunneling regime, and the total tunneling current is the incoherent sum of weakly tunneling events. In fact, it is often possible to observe tunneling resonances as the magnetic field is swept (Milliken *et al.*, 1996; Maasilta and Goldman, 1997; Grayson *et al.*, 2001). In resonant tunneling, the process is presumably mediated by a resonant bound-level or impurity state situated spatially close to the two chiral edges. In fact the tunneling current in resonant tunneling can be computed in a manner similar to that discussed above for both the incoherent, sequential resonant-tunneling case, for which  $I_{tun} \ll \nu(e^2/h)V$  (Chamon and Wen, 1993; Furusaki *et al.*, 1993), and the fully coherent case for which  $I_{tun}$  approaches  $\nu(e^2/h)V$  (Kane and Fisher, 1992c; Moon

*et al.*, 1993; Fendley *et al.*, 1995b). To gain physical insight and to make contact with the experimental results presented below, we address the key features of sequential tunneling treated in first-order perturbation theory.

The coupling between a given edge  $i=R,L$ , and the impurity  $I$  can be written as (Chamon and Wen, 1993; Furusaki *et al.*, 1993)

$$H_{I,i} = \Gamma_i \Psi_I^\dagger \Psi_i|_{x=0} + \text{H.c.}, \quad (201)$$

where the first term contributes to filling the impurity level while the second (H.c.) contributes to the emptying of the level. The field operators can be both electrons and quasiparticles of  $e^*$ . In this sequential tunneling limit and neglecting higher-order virtual processes, the tunneling current will contain contributions from both the filling of the impurity level when empty (off) and emptying when occupied (on). In analogy to the off-resonance case between two chiral edges [Eq. (161)], using standard first-order perturbation theory the current from the  $i$ th chiral edge onto the impurity is given by (Chamon and Wen, 1993)

$$I_i = e^* \frac{|\Gamma_i|^2}{a_I} \int_{-\infty}^{\infty} dt' \Theta(t-t') \exp[-i(e^*V_i - E_I)(t-t')] \times \langle [\Psi_I^\dagger(x=0,t) \Psi_i(x=0,t), \Psi_i^\dagger(x=0,t') \Psi_I(x=0,t')] \rangle, \quad (202)$$

where the energy of the impurity level is denoted by  $E_I$ , and  $a_I$  is a characteristic length. As before, the expectation of the chiral edge operator is given by Eqs. (171) and (172),

$$\begin{aligned} & \langle \Psi_i^\dagger(x=0,t) \Psi_i(x=0,t) \rangle \\ &= \frac{a_i^{\alpha_i-1}}{v_i^{\alpha_i}} \left| \frac{\pi T}{\sinh[\pi T(t-t')]} \right|^{\alpha_i} \exp\left(\pm i \frac{\pi}{2} \alpha_i \operatorname{sgn}(t-t')\right), \end{aligned} \quad (203)$$

and

$$\langle \Psi_i^\dagger(t) \Psi_i(t') \rangle = n_I, \quad (204)$$

$$\langle \Psi_i(t) \Psi_i^\dagger(t') \rangle = 1 - n_I, \quad (205)$$

where  $n_I$  is the average occupation of the impurity level.

In terms of the fill current when the impurity level is entirely empty,  $I_{i,fill}$ , and the removal current when the level is fully occupied,  $I_{i,rem}$ , the  $i$ th current can be written as (see inset to Fig. 9)

$$I_i = [I_{i,fill}(1 - n_I) + I_{i,rem}n_I], \quad (206)$$

where

$$\begin{aligned} I_{i,fill} &= -e^* r_{i,fill} \\ &= e^* |\Gamma_i|^2 \frac{a_i^{\alpha_i-1}}{a_I v_i^{\alpha_i}} (2\pi T)^{\alpha_i-1} \\ &\quad \times B\left(\frac{\alpha_i}{2} - \frac{i\omega}{2\pi T}, \frac{\alpha_i}{2} + \frac{i\omega}{2\pi T}\right) \\ &\quad \times \exp\left(\frac{\omega}{2T}\right) \Bigg|_{\omega = -(e^* V_i - E_I)}, \end{aligned} \quad (207)$$

and

$$\begin{aligned} I_{i,rem} &= e^* r_{i,rem} = e^* |\Gamma_i|^2 \frac{a_i^{\alpha_i-1}}{a_I v_i^{\alpha_i}} (2\pi T)^{\alpha_i-1} \\ &\quad \times B\left(\frac{\alpha_i}{2} - \frac{i\omega}{2\pi T}, \frac{\alpha_i}{2} + \frac{i\omega}{2\pi T}\right) \\ &\quad \times \exp\left(-\frac{\omega}{2T}\right) \Bigg|_{\omega = -(e^* V_i - E_I)}. \end{aligned} \quad (208)$$

Here  $r_{i,fill}$  and  $r_{i,rem}$  denote the rate of filling and removal, respectively. The total combined currents of filling,  $I_{fill}$ , and removal,  $I_{rem}$ , from both the  $R$  and  $L$  channels are

$$I_{fill} = [I_{R,fill} + I_{L,fill}] = -e^* [r_{R,fill} + r_{L,fill}] \quad (209)$$

and

$$I_{rem} = [I_{R,rem} + I_{L,rem}] = e^* [r_{R,rem} + r_{L,rem}]. \quad (210)$$

The times to fill when empty,  $\tau_{off}$ , and to empty when filled,  $\tau_{on}$ , are

$$\tau_{off} = \frac{1}{r_{R,fill} + r_{L,fill}} = \frac{-e^*}{I_{fill}} \quad (211)$$

and

$$\tau_{on} = \frac{1}{r_{R,rem} + r_{L,rem}} = \frac{e^*}{I_{rem}}. \quad (212)$$

The average occupancy  $n_I$  of the impurity level is

$$n_I = \frac{\tau_{on}}{\tau_{on} + \tau_{off}} = \frac{-I_{fill}}{I_{rem} - I_{fill}} \quad (213)$$

and

$$1 - n_I = \frac{\tau_{off}}{\tau_{on} + \tau_{off}} = \frac{I_{rem}}{I_{rem} - I_{fill}}. \quad (214)$$

The final form of the tunnel current is given by

$$I_{tun} = \langle I_R \rangle = \frac{1}{I_{rem} - I_{fill}} [I_{R,fill} I_{L,rem} - I_{R,rem} I_{L,fill}]. \quad (215)$$

Specializing to the  $\nu_R=1$  to  $\nu_L=1/m$  resonant electron-tunneling case for which  $\alpha_R=1$  and  $\alpha_L=3$ , we have

$$\begin{aligned} I_{R,fill} &= \frac{-e |\Gamma_R|^2}{a_I v_R} B\left[\frac{1}{2} - \frac{i\omega}{2\pi T}, \frac{1}{2} + \frac{i\omega}{2\pi T}\right] \\ &\quad \times \exp\left[\frac{\omega}{2T}\right] \Bigg|_{\omega = -(e^* V_R - E_I)}, \end{aligned} \quad (216)$$

$$\begin{aligned} I_{R,rem} &= \frac{e |\Gamma_R|^2}{a_I v_R} B\left[\frac{1}{2} - \frac{i\omega}{2\pi T}, \frac{1}{2} + \frac{i\omega}{2\pi T}\right] \\ &\quad \times \exp\left[-\frac{\omega}{2T}\right] \Bigg|_{\omega = -(e^* V_R - E_I)}, \end{aligned} \quad (217)$$

$$\begin{aligned} I_{L,fill} &= \frac{-e |\Gamma_L|^2 a_L^2}{a_I v_L^3} (2\pi T)^2 B\left[\frac{3}{2} - \frac{i\omega}{2\pi T}, \frac{3}{2} + \frac{i\omega}{2\pi T}\right] \\ &\quad \times \exp\left[\frac{\omega}{2T}\right] \Bigg|_{\omega = -(e^* V_L - E_I)}, \end{aligned} \quad (218)$$

and

$$\begin{aligned} I_{L,rem} &= \frac{e |\Gamma_L|^2 a_L^2}{a_I v_L^3} (2\pi T)^2 B\left[\frac{3}{2} - \frac{i\omega}{2\pi T}, \frac{3}{2} + \frac{i\omega}{2\pi T}\right] \\ &\quad \times \exp\left[-\frac{\omega}{2T}\right] \Bigg|_{\omega = -(e^* V_L - E_I)}. \end{aligned} \quad (219)$$

This expression gives rise to an asymmetry as one sweeps through the resonance, and a power-law integrated area versus  $T$  in the differential conductance  $dI/dV$ , as well as nonpreservation of the integrated area, as shown in Fig. 9. As a result of this first-order perturbation treatment based on sequential tunneling, Eqs. (215)–(219) are valid when the on and off times in the impurity level,  $\tau_{on}$  and  $\tau_{off}$ , satisfy their respective conditions,  $\tau_{on} \gg \min(|e^* V_R - E_I|^{-1}, T^{-1})$  and  $\tau_{off} \gg \min(|e^* V_L - E_I|^{-1}, T^{-1})$ , in the case where  $e^* V_R > e^* V_L$ . Beyond the sequential regime the resonant-tunneling current, including in the case of perfect resonant transmission, can be calculated by renormalization-group and quantum Monte Carlo methods (Moon *et al.*, 1993) and exact Bethe-ansatz calculations (Fendley, Ludwig, and Saleur, 1995b). In the opposite limits of off-resonance tunneling occurring in the tail region of

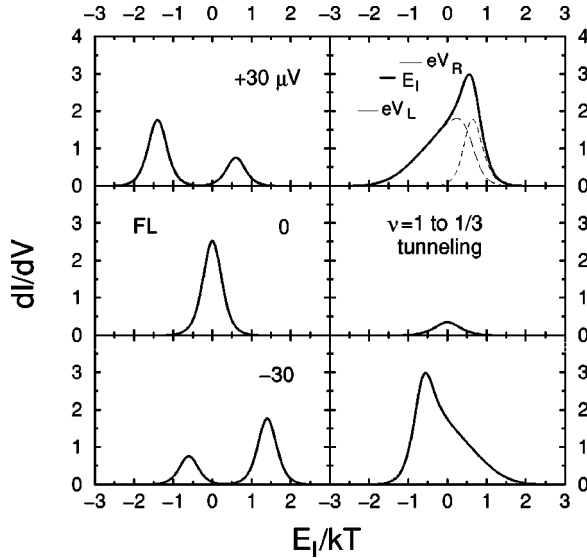


FIG. 9. The differential conductance,  $dI/dV$ , under bias, for the resonant tunneling of electrons (holes): Left panels, tunneling into a Fermi-liquid (FL) edge; right panels, tunneling into a  $\nu=1/3$  chiral Luttinger liquid edge, plotted as a function of the impurity level position referenced to the thermal energy,  $E_I/kT$ . Dashed curves in the upper right panel show the separate contributions for the right and left leads. Here the convention is that the right lead refers to the  $n+\text{GaAs}$  metallic lead, while the left lead refers to either the Fermi-liquid or Luttinger-liquid edge lead. The linear portions of the left dashed peak reflects the energy derivative of the chiral Luttinger-liquid tunneling density of states,  $D_{\text{tun}}(\omega) \sim \omega^2$ . Inset shows the energy positions of the  $n+\text{GaAs}$  normal metal,  $eV_R$ , Fermi liquid or CLL edge,  $eV_L$ , and the impurity level position  $E_I$ .

the tunneling resonance, second-order virtual processes contribute. This leads to off-resonance tunneling with an effective coupling between the  $R$  and  $L$  chiral Luttinger modes of

$$H'_{R,R} = \Gamma' \Psi_R^\dagger \Psi_L + \text{H.c.}, \quad (220)$$

where the coupling,  $\Gamma = \Gamma_L \Gamma_R^\dagger / \Delta E$ , and  $\Delta E = |e^*(V_R + V_L)/2 - E_I|$  when far off resonance and is essentially independent of the bias voltage  $V_R - V_L$  for small voltages  $|V_R - V_L| \ll \max(|\Delta E/e^*|, T)$ . This corresponds to the case treated previously in Sec. II.B.5 on scaling functions.

### 7. Shot noise and fractional charge: quasiparticle tunneling

In addition to the hallmark signatures of the CLL in the tunneling current, remarkable indicators are present in the current and voltage fluctuations, resulting in quantum current shot noise and voltage noise. These noise fluctuations can be measured or computed under equilibrium as well as in nonequilibrium conditions. In fact, generalization of the fluctuation-dissipation theorem to its nonequilibrium analog within the chiral Luttinger liquid model implies that, in the case of weak backscattering and strong coupling for which quasiparticle tunneling dominates, the low-frequency current shot noise

provides a measure of the fractional charge  $e^*$  of the tunneling quasiparticle. Shot-noise fluctuations then reflect the graininess of the charge carriers in units of  $e^*$  (Kane and Fisher, 1994; Chamon *et al.*, 1995; Fendley *et al.*, 1995c). Furthermore, high-frequency noise is predicted to exhibit singularities in its power spectrum at frequencies related to the Josephson frequencies of the quasiparticles (Chamon *et al.*, 1995). Such noise represents fluctuations in the ac current.

In mesoscopic conductors, recent theoretical (Lesovik, 1989; Buttiker, 1990) and experimental work (Li *et al.*, 1990; Dekker *et al.*, 1991; Liefrink *et al.*, 1994) has shown that the zero-frequency quantum shot noise in a one-dimensional conductor scales as

$$S(\omega \rightarrow 0) = \frac{e^2}{h} t(1-t)(eV), \quad (221)$$

where  $t$  is the transmission probability of the electron. In the limit  $t \ll 1$ , the classical, uncorrelated shot-noise result is recovered with  $I \approx (e/h)t(eV)$ . In the opposite limit of  $(1-t) \ll 1$ , one obtains the shot noise associated with “holes.” Similar results can be deduced for the tunneling of electrons and quasiparticles between identical fractional Hall edges. In particular, Kane and Fisher (1994) showed that for tunneling between two Laughlin,  $\nu=1/m$  edges under nonequilibrium conditions, with current flow and voltage bias across the tunnel junction, an analog of the fluctuation-dissipation theorem takes the form

$$c_I(\omega) - \coth\left(\frac{\omega}{2T}\right) R_I(\omega) = \left(\frac{ve^2}{h}\right)^2 \left[ c_V(\omega) - \coth\left(\frac{\omega}{2T}\right) R_V(\omega) \right], \quad (222)$$

where  $c_I$  ( $c_V$ ) and  $R_I$  ( $R_V$ ) are the respective correlation and response functions for  $I$  and  $V$ . Both sides of this expression become identical to 0 only under equilibrium, yielding the fluctuation-dissipation theorem. Remarkably as  $\omega \rightarrow 0$  this expression implies

$$c_I(\omega \rightarrow 0) = \left(\frac{ve^2}{h}\right)^2 c_V(\omega), \quad (223)$$

relating the power of the current and voltage shot noises with the extra factor  $\nu^2$ .

From such expressions one obtains the quantum shot noise for quasiparticle tunneling under weak backscattering:

$$c_I(\omega \rightarrow 0) \approx \frac{(ve^2)^2}{h} eV. \quad (224)$$

The above results were obtained using the lowest-order terms. Inclusion of higher-order terms leads to “interaction effects” and singularities in the noise power spectrum at Josephson frequencies,  $\omega = e^*V$  (Chamon *et al.*, 1995). Due to the integrability of the single-point-contact backscattering model within the effective-field theory, it is possible to derive the exact expression for

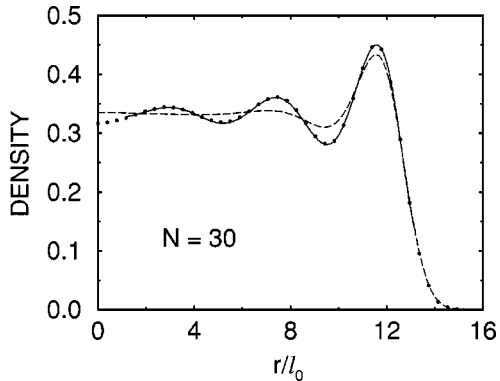


FIG. 10. Density profiles for the  $\nu=1/3$  Laughlin-type wave function (dashed line), and the modified wave function (filled circles) due to intercomposite Landau-level mixing for  $N=30$ . The solid line is a fit according to  $\rho(r)=1/3+0.113/(1-0.415x+0.086x^2)\cos[2\pi x/(4.02-0.029x)]$  with  $x=r/l_o$ ,  $-11.407$ , while  $l_o$  is the magnetic length. From Mandal and Jain, 2001.

any amount of backscattering at  $T=0$  using the Bethe ansatz (Fendley *et al.*, 1995c).

#### 8. Finite-size numerical investigations

The basic prediction of power-law tunneling characteristics has now been unequivocally substantiated in experiment. To gain insight into possible causes for differences between other key predictions of the effective-field theories and experiment (see detailed discussion in Sec. III.D), several groups have recently performed finite-size numerical studies. Encouragingly, the results are in considerably better agreement with experiment than with effective theories. However, as is the usual case, caution must be exercised when extrapolating from finite,  $N=10-60$  systems to the thermodynamic limit of  $N\rightarrow\infty$ . With this in mind we briefly summarize the approaches and main findings in these computations.

Goldman and Tsiper (2001) performed exact diagonalization studies for systems of  $N=3$  to  $N=12$  electrons on a disk, at Landau filling  $\nu=1/3$ . Both short-range interaction favoring the Laughlin wave function from the bulk all the way to the edge, and long-range Coulomb interaction were investigated. Wan, Yang, and Rezayi (2002) investigated the effect of the spacer distance  $d$  between the positively charged dopant layer and the two-dimensional electron gas (2DEG), in a model with Coulomb interaction for six or seven electrons. Mandal and Jain (2001, 2002) considered corrections to the Laughlin-series and Jain-series wave functions by including the lowest-order composite-fermion Landau-level mixing due to long-range Coulomb interaction. Using composite-fermion wave functions as a starting point, they were able to study systems with  $N$  up to 40–60 for  $\nu=1/3$ ,  $2/5$ , and  $3/7$ . In all cases a common feature emerged. When Coulomb interaction was included, excess edge density oscillations, which are absent in a Laughlin-type wave function, become apparent, as shown in Fig. 10. Goldman and Tsiper interpreted

such oscillations as evidence for edge density wave formation. In the work of Wan, Yang, and Rezayi, the oscillations arise as a result of edge reconstruction when  $d$ , the spacer distance, exceeds a critical value,  $d_c\approx 1.6l_o$ , where  $l_o=\sqrt{\hbar c/eB}$ . (Note that in experiment,  $d\geq 7l_o > d_c$ .) The results found by Mandal and Jain, which for  $\nu=1/3$  are similar to those of Goldman and Tsiper, are a consequence of residual composite-fermion interaction and Landau-level mixing. Such density oscillation can in principle lead to additional edge channels, some of which are counterpropagating, and therefore will renormalize the tunneling exponent  $\alpha$ .

Mandal and Jain and Goldman and Tsiper went on to compute the equal-time correlation function  $G_{edge}$ , using the ground-state wave function  $\psi$ . At large distances  $G_{edge}$  is believed to decay with the same exponent as the tunneling exponent  $\alpha$ . Even though strictly speaking the equal-space correlation must be computed, the equal-time correlation is believed to yield an identical exponent value (Lee and Wen, 1991). In other words,

$$G_{edge}(|\mathbf{r}-\mathbf{r}'|)=\frac{\langle\psi|\Psi_e^\dagger(\mathbf{r})\Psi_e(\mathbf{r}')|\psi\rangle}{\langle\psi|\psi\rangle} \\ =N\frac{\int\prod_{j=1}^{N-1}d^2\mathbf{r}_j\psi^*(\mathbf{r},\{\mathbf{r}_j\})\psi(\mathbf{r}',\{\mathbf{r}_j\})}{\int\prod_{k=1}^Nd^2\mathbf{r}_k\psi^*(\{\mathbf{r}_k\})\psi(\{\mathbf{r}_k\})} \\ \rightarrow|\mathbf{r}-\mathbf{r}'|^{-\alpha}, \quad (225)$$

where  $\Psi_e$  is the electron creation field operator,  $\mathbf{r}$  and  $\mathbf{r}'$  are two points along the edge, and  $\Psi_e(\mathbf{r})|\psi\rangle\propto\psi(\mathbf{r},\{\mathbf{r}_j\})$ . As a result of the modification of the wave function from the Laughlin-type wave function, as exemplified by the extra density oscillations near the boundary, the exponent  $\alpha$  is renormalized in a direction consistent with experiment, as will be shown in Sec. III.D following the presentation of data. From Mandal and Jain's calculation, a remarkable result emerges. Without residual composite-fermion interaction and mixing, the exponent for  $\nu=1/3$ ,  $2/5$ , and  $3/7$  is universal and equal to 3, in complete agreement with the predictions of the effective-field theories. The renormalization of the exponent occurs only as a consequence of long-range interaction and the residual composite-fermion mixing it entails. Thus numerical computations support the basic picture put forth by Wen of chiral Luttinger liquid dynamics at the edge of the incompressible fractional quantum Hall fluids. On the other hand, the prediction of universality of the exponents based on the topological characterization of the bulk 2D fluid appears *not* to be robust against the introduction of long-range interactions.

### III. EXPERIMENTS ON CHIRAL LUTTINGER LIQUIDS—TUNNELING INTO THE FRACTIONAL QUANTUM HALL EDGE

The most outstanding physical characteristic that distinguishes a Luttinger liquid, chiral or nonchiral, from a conventional Fermi liquid metal is its low-energy behavior when an external “bare” electron is added or re-

moved at energies near the “Fermi” energy. The associated orthogonality catastrophe, which occurs between the state consisting of a bare particle added to (or removed from) a highly correlated  $N$ -electron ground state and the ground state of the  $N+1$  ( $N-1$ ) electron system, gives rise to a power-law suppression of the tunneling current as the energy from the Fermi surface,  $E - E_F$ , approaches zero. A tunneling transport experiment is a natural way to study this unique low-energy property. Although lacking the ability to resolve momentum due to the fact that in reality most tunneling takes place at pointlike contacts, the distinct advantage of a transport experiment is the precise control of the low-energy scale, set either by an external voltage bias across the tunnel junction down to the  $1\text{-}\mu\text{eV}$  level, or by temperature down to  $25\text{ mK}$ , for which  $kT \approx 2.15\ \mu\text{eV}$ . This enables truly low-energy behavior to be studied in detail. These energies are a factor of  $10^2\text{--}10^3$  smaller than the relevant characteristic energies of either the Fermi energy,  $E_F \sim 4\text{ meV}$ , or the quasiparticle gap,  $\Delta$ , of  $\sim 0.1\text{--}1\text{ meV}$  in the most robust incompressible fractional Hall fluids such as  $\nu=1/3$ . In contrast, a powerful and complementary technique such as angle-resolved photoemission spectroscopy (ARPES), while offering the ability to resolve  $k$  dependences, nevertheless requires the use of energetic photons of energy  $\sim 20\text{ eV}$  to eject surface electrons in an attempt to determine low-energy properties down to the meV level. For example, it is often technically challenging to locate the Fermi level precisely to meV accuracy, as well as to find the position and width of the quasiparticle peak (or the absence of such a peak) in the spectral function. Damage to the specimen can also result from the radiation of energetic photons.

In electron-tunneling transport measurements several key conditions must be met to achieve a successful demonstration of chiral Luttinger liquid behavior. These include:

- (i) the requirement that the observed nonlinearity in the current-voltage ( $I$ - $V$ ) characteristics arise from the tunneling density of states, and not from residual energy dependences in the tunneling matrix element across the tunnel barrier;
- (ii) the existence of a power-law regime in the  $I$ - $V$  relationship with a substantial dynamic range in both the current and the excitation bias voltage to enable a reliable differentiation between a power-law functional form and other competing forms such as exponential, Arrhenius, or variable-range hopping;
- (iii) consistency in the power-law tunneling density of states  $\rho_{\text{TDOS}}$ , deduced independently from measurements of the  $I$ - $V$  relation, temperature dependence of the low-bias linear conductance  $G(T)$ , and the differential conductance under bias  $dI/dV$ ;
- (iv) an exponent  $\alpha$  with  $I \propto V^\alpha$ , in the range  $\sim 1.5\text{--}4$ . This is desirable to ensure good dynamic range in both the current and the excitation energy scale

(either bias voltage or temperature). Below 1.5,  $\alpha$  is readily distorted by other residual nonlinearities, while for  $\alpha > 4$ , the noise floor for the current is reached over a reduced dynamic range in the bias voltage or temperature.

Our approach is to first convincingly establish the presence of a power-law functional dependence in the  $I$ - $V$  characteristics. The clear-cut observation of power-law behavior with unsurpassed quality—the hallmark signature of Luttinger-liquid behavior—unequivocally establishes the fractional quantum Hall edge as a chiral Luttinger liquid system. Subsequently, we provide detailed investigations of the nature of the chiral Luttinger liquid, in particular, its dependence on magnetic field for samples with fixed electron densities. This amounts to a study of the different chiral Luttinger liquids at the edge of fractional Hall fluids at different filling factors.

The first attempts to investigate Luttinger-liquid behavior in semiconductor-based systems were undertaken in one-dimensional quantum-wire systems at zero magnetic field. Two approaches were attempted, lateral (side) gating to form relatively long channel quantum point contacts (Tarucha *et al.*, 1995), and the formation of a cleaved-edge overgrown quantum wire (Yacoby *et al.*, 1996). The results were inconclusive. Although an intriguing suppression of the conductance below the quantized value of  $e^2/h$  was observed, clear signatures of power-law dependences in the deviation were not observable. In the case of a 1D conductor at  $B=0$ , the power-law exponent is determined by the reduced conductance  $g \equiv G/(e^2/h)$ , where  $g < 1$  for repulsive interaction potentials. Since  $g$  is dependent on the exact nature of the interaction, it is not universal. Experiments to observe Luttinger-liquid behavior must deal with the complications of *localization effects*, which tend to obscure the power-law characteristics and which result from the back-scattering of electrons by residual disorder or nonideality in the one-dimensionality. Consequently only indirect hints were initially observed (Tarucha *et al.*, 1995; Yacoby *et al.*, 1996). (Recent notable advances will be described in Sec. IV.) In contrast, as discussed in detail in the theory section, in the fractional quantum Hall effect the edge is expected to behave as a chiral Luttinger liquid, where the chirality arises from the presence of the magnetic field and the formation of skipping orbit states along the two-dimensional electron gas (2DEG) boundary. In this system, the forward- and backward-propagating edge modes are spatially separated, minimizing backscattering and localization effects. Impurities and imperfections only cause the one-dimensional boundary to meander and have negligible effect on the nature of the chiral Luttinger liquid. Furthermore, here  $g$  is well defined and is expected to be simply related to the reduced quantized Hall conductance, at least within the context of the effective theories.

Two distinct geometries have been employed to study chiral Luttinger liquid behavior via tunneling at the fractional quantum Hall edge: the point-contact geometry

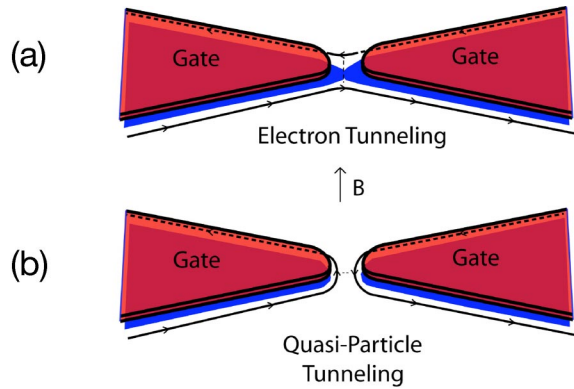


FIG. 11. (Color in online edition) Point-contact geometry: (a) electron tunneling, (b) quasiparticle tunneling.

and the cleaved-edge overgrowth geometry. The point-contact method employs electrostatic gating using “pincher” metallic electrode pairs spaced  $\sim 100$  nm apart on the surface of a conventional GaAs/ $\text{Al}_x\text{Ga}_{1-x}\text{As}$  heterostructure and the application of a negative voltage to these gates relative to the 2D electron sheet below the surface, to bring the edge states propagating on opposite edges of the device into close proximity as shown in Fig. 11. In the cleaved-edge geometry discussed in greater detail below (Sec. III.C.1), a thin  $\text{Al}_x\text{Ga}_{1-x}\text{As}$  tunnel barrier of thickness  $b \sim l_o$  is grown in the (011) crystallographic direction perpendicular to the initial conventional growth of a quantum well in the (100) direction, as depicted in Fig. 12. The presence of this tunnel barrier terminates the 2D electron sheet contained within the quantum well, creating an atomically sharp edge. Subsequent growth of a bulk-doped  $n + \text{GaAs}$  normal metal on the other side of the tunnel barrier enables the tunneling of electrons to take place.

Each method has advantages and disadvantages. In the point-contact geometry, due to the large, vertical spatial separation ( $>100$  nm) between the metal gate (situated on the sample top surface) and the electron

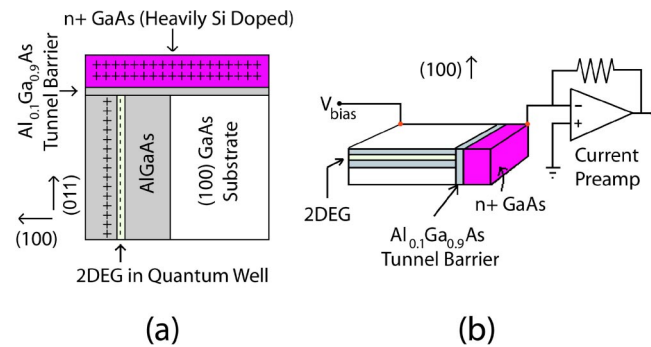


FIG. 12. (Color in online edition) Cleaved-edge-overgrowth device and tunneling current measurement geometries: (a) Device geometry showing the cleaved-edge  $\text{Al}_{0.1}\text{Ga}_{0.9}\text{As}$  tunnel barrier and the heavily doped 3D  $n + \text{GaAs}$  metal; (b) geometry for the tunneling current measurements. (Device is rotated by  $90^\circ$ .)

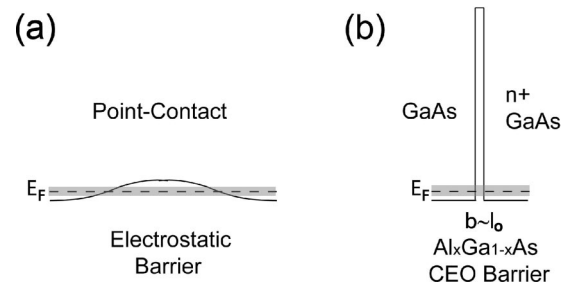


FIG. 13. Tunnel barriers for (a) the point-contact geometry, and (b) the cleaved-edge overgrowth geometry with barrier thickness  $b \sim l_o$ . Here  $l_o$  denotes the magnetic length ( $l_o = \sqrt{\hbar c / eB} = 8.1$  nm at  $B = 10$  T). The gray regions represent thermal smearing.

gas, the boundary of the 2DEG is necessarily smooth. Consequently the point contact is characterized by a shallow and broad tunnel barrier, shown in Fig. 13(a), leading to a narrow window for investigating the energy dependence in the tunneling density of states, as discussed in detail below. On the other hand, this geometry offers the advantage of tunability and versatility. The barrier shape can readily be modified by the adjustment of the gate voltages, enabling both electron and quasi-particle (hole) tunneling to take place (Fig. 11). The cleaved-edge overgrowth (CEO) geometry is characterized by a tall and thin tunnel barrier, depicted in Fig. 13(b). This barrier yields the most notable advantage as it leads to a tunneling matrix that is essentially energy independent in the relevant energy range. This property enables a clean and direct study of the energy dependence in the tunneling density of states. On the other hand, a clear disadvantage is the fixed barrier in a given sample. This means a limited magnetic-field range is accessible, resulting from the sensitivity of the tunneling matrix to  $B$ . Consequently a series of samples with varying barrier thickness must be grown. Moreover, thus far tunneling has been limited to electrons.

To better understand the results to be presented below it is necessary to examine in detail the consequences of the different geometries. In the weak-tunneling limit the tunnel current for an individual process arises as a product of two contributions: the probability for tunneling through the barrier, given by the square modulus of the tunneling matrix element, and the tunneling density of states. The latter is central to establishing a power-law, chiral Luttinger liquid behavior in the tunnel-current dependence on energy, set in experiment by temperature ( $kT$ ) or bias voltage ( $eV$ ). Ideally, the non-linearity arises solely from the density of states, with minimal effect from the matrix element. In this respect, the cleaved-edge geometry offers a real advantage. In the relevant energy regime between  $2.5 \mu\text{eV}$  and  $3$  meV probed in experiment, the tall and thin barrier, typically of height  $\geq 100$  meV and width  $5\text{--}20$  nm, will be minimally distorted, leading to an essentially ideal, energy-independent tunneling matrix. The observed nonlinearity thus directly reflects the tunneling density of states. (For reference the incompressible fractional Hall excitation gap  $\Delta$  is  $\sim 100 \mu\text{eV}$ , and the Fermi energy  $E_F$  is

$\sim 2\text{--}6$  meV.) This contrasts with the point-contact geometry in which the broad and shallow barrier (of height  $\leq 10$  meV and width  $\geq 100$  nm) can readily be distorted by a voltage bias, causing appreciable change in the tunneling matrix, or else when thermal smearing takes place at moderately elevated temperatures ( $> 250$  mK), higher-energy excited edge states can be accessed which have significantly larger tunneling matrix and probability. Moreover, the inherent gradualness of the edge carrier-density profile in the electrostatic gating method accentuates complications from a phase separation of the edge into alternating strips of compressible and incompressible quantum Hall fluids, each of an appreciable spatial extent (Beenakker, 1990; Chang, 1990; Chklovskii *et al.*, 1992). For instance, a 2D electron gas exhibiting a  $\nu=1/3$  effect in the bulk may be bordered by  $\nu=1/4$  and  $1/5$  fluids, etc. (Ando *et al.*, 1998). Electrons tunneling into the  $1/3$  edge must cross the other phases, giving rise to complex tunneling characteristics. The combination of these two effects has yielded a limited energy window accessible to experiment, in the range of  $\sim 2.5\text{--}25$   $\mu\text{eV}$  ( $T \sim 25\text{--}250$  mK).

#### A. Measurement techniques

The tunneling experiment requires the measurement of ultralow currents down to the level of a few femtoamperes ( $10^{-15}$  A), at voltage bias excitations as low as  $1$   $\mu\text{V}$ . To achieve the conditions to enable such measurements, several key features and safeguards must be incorporated into the measurement circuitry and low-temperature dilution refrigerator cryostat. Several similar but complementary ways to perform a high-sensitivity  $I$ - $V$  tunneling measurement are utilized. The most straightforward is a dc measurement. A floating voltage source is used for supplying the dc-bias excitation voltage across the tunnel junction, while a dc current meter with a high-gain preamplifier is used to measure the tunnel current. The entire circuitry is grounded at a single point, typically at the input low of the current amplifier. This arrangement avoids ground loops and the associated noise currents, as well as undesirable shunting of currents through unwanted paths. A typical noise floor of the order of  $30\text{--}50$  fA is achievable with an integration time constant of  $10\text{--}30$  sec/point. To improve beyond the dc noise floor and achieve a few-fA sensitivity, it is necessary to utilize an ac lock-in technique. There are two basic methods: (i) a small ac sinusoidal excitation is superimposed on top of a dc bias to yield a measure of the differential conductance  $dI/dV$ , and (ii) a symmetric, square-wave excitation about zero bias voltage is applied to generate a square-wave output current. This is a viable method when the  $I$ - $V$  relationship is odd-symmetrical (antisymmetrical) under reversal of the bias voltage ( $V \rightarrow -V$ ). For our experiments on tunneling into the fractional quantum Hall edge, this antisymmetry requirement turns out to be satisfied at low excitations, typically for  $|V_{\text{bias}}| \leq 5$  meV.

Our ac lock-in measurements are performed at  $2.3$  Hz frequency. A typical circuitry excitation is shown in Fig.

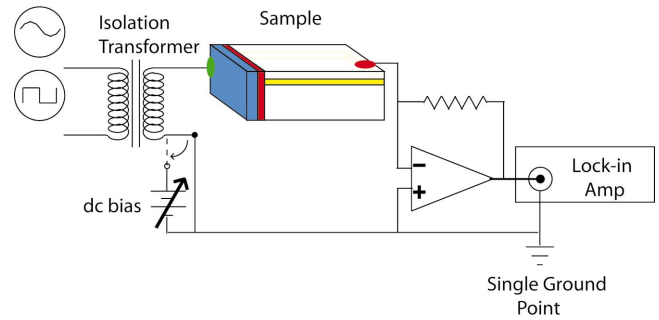


FIG. 14. (Color) ac measurement circuit for both square-wave excitation at zero dc bias and  $dI/dV$  measurements with a finite dc bias plus a small ac sinusoidal excitation superimposed on top. The isolation of this measurement circuit from external electrical circuitry is achieved by the use of an isolation transformer, battery dc supply, and single ground point applied at the input to the lock-in amplifier in order to avoid any ground-loop problem.

14. As in the dc case, it is desirable to float the voltage source and ground at a single point. The floating is achieved with an isolation transformer. The current is fed into the negative input of the operational amplifier, which performs the current-to-voltage conversion (inverting amplifier). Typical feedback resistances are in the megaohm to gigaohm range for current values in the  $\mu\text{A}$ -fA ( $10^{-15}$  A) range. This type of circuitry is relatively insensitive to parasitic capacitance to ground, since one end of the tunnel junction is driven by the source, which ideally would have low source impedance, and the other end is at the negative input of the op-amp and is therefore at virtual ground, being driven by the feedback loop. On the other hand, parasitic capacitance between the leads connected to these two sides of the tunneling junction will end up shunting the current, bypassing the tunnel junction. These leads are brought out of the cryogenic system to room temperature and are therefore  $\sim 1\text{--}2$  m in length and will have capacitances in the  $100\text{-pF}$  range. As a result, at  $2.3$  Hz, the in-phase and out-of-phase components of the current response typically become equal around a tunnel resistance of  $0.3$  G $\Omega$ . By properly setting the phase of the lock-in it is possible to extend the range and measure up to  $1$  G $\Omega$  of tunnel resistance with reliability. A more complete solution would be to use coaxial cables for each lead and to twist the coaxes together. The outer ground shield of the coax will provide shielding to eliminate the mutual capacitance between leads, while by twisting the coaxes, inductive pickup will be minimized. The inner and outer conductors must be separately thermally anchored at some low-temperature point, at which the shielding will be broken. A further consideration is mechanical vibrations. Microphonics must be reduced by proper vibrational isolation. One final and important feature is line filtering. This is absolutely necessary in order both to achieve the lowest electron temperature and to prevent extraneous noise voltages from reaching the device, thereby overwhelming the low voltage bias down at the  $\mu\text{V}$  level. Such noise can either arise from pickup or

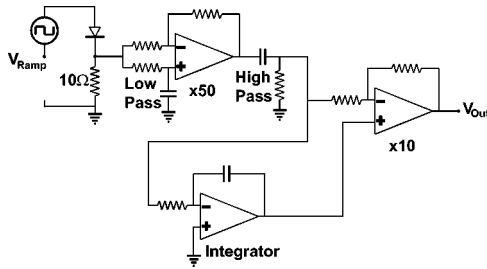


FIG. 15. A continuous-sweep, exponential-amplifier ramp via a linear  $V_{ramp}$  input. The exponential output is used to bias the tunnel junction in a sample. The output spans several decades. To compensate for the poor frequency response of the isolation transformer circuitry (Fig. 14) at the 2.3-Hz lock-in frequency, an integrated signal of the exponentiated output is added on to achieve flatness during each 1/2 cycle of the square wave to better than 5%.

from room-temperature Johnson noise radiated down the lines.

Aside from the basic low-current, low-excitation techniques described above, one additional feature of the measurement warrants discussion. The range of voltage bias typically spans up to five orders of magnitude, from 1 to 100 mV. The first measurements carried out by Chang *et al.* (1996, 1998) were performed using a set of discrete points. This turned out to be inconvenient. Subsequently, a continuous sweep was employed (Grayson *et al.*, 1998; Chang *et al.*, 2001). To span five orders of magnitude, an exponential ramp is necessary. Furthermore a square wave at 2.3 Hz must pass through the isolation transformer without distortion. A nonideal transformer, coupled with a wave-form generator with a finite (nonzero) source impedance, typically has reduced response at low frequencies. To compensate for the 30% dropoff in voltage at the tail end of each square-wave step contained within a half cycle, it was necessary to add a linear ramp of the exponentiated output. Such a circuit is depicted in Fig. 15. Very recently, a new generation of commercial ultralow-noise current preamplifiers with noise figures of  $30 \text{ nA}/\sqrt{\text{Hz}}$  at 0.1 Hz have become available. With such advanced instrumentation, measurements with sub-fA resolution will likely be achievable, further expanding the dynamic range of the tunneling current-voltage measurements.

## B. Point-contact experiments

Milliken *et al.* (1996) pioneered the investigation of tunneling between two  $\nu=1/3$  edges in the conventional, point-contact geometry. They reported several indications of non-Fermi-liquid behavior. In particular, they observed a marked difference in the low-temperature behavior of tunneling resonances for tunneling between two  $\nu=1/3$  edges versus two  $\nu=1$  edges, as shown in Fig. 16. In the two cases, the resonances were observed as the point contact was gradually closed by the application of increasing negative gate voltages, under the condition the filling factor in the quantum Hall fluid was tuned via

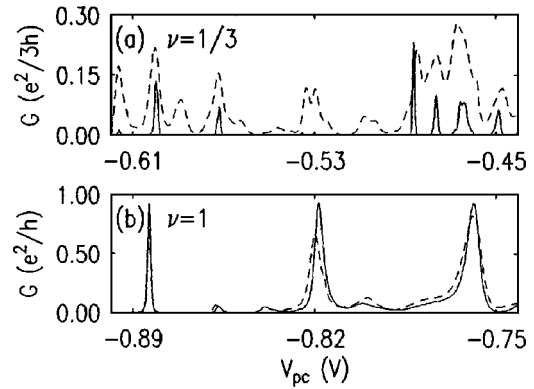


FIG. 16. Conductance vs point-contact voltage: (a) at the  $\nu=1/3$  plateau for  $T=41$  mK (solid line) and 172 mK (dashed line); (b) at the  $\nu=1$  plateau for  $T=42$  mK (solid line) and 101 mK (dashed line). From Milliken *et al.*, 1996.

the magnetic field to 1/3 or 1, respectively. Whereas in the  $\nu=1$  case, the resonances became virtually temperature independent below 101 mK, in the  $\nu=1/3$  case the resonances exhibited substantial sensitivity to a decrease in temperature from 172 to 41 mK. Notably, the width of the resonances narrowed appreciably, exhibiting a variation consistent with the functional form of  $T^{2/3}$  predicted by the effective chiral Luttinger liquid theory. Furthermore, clear nonlinear behavior in the off-resonance tunneling characteristics measurable in the tail of resonance peaks was observed. These observations are qualitatively consistent with theoretical predictions. Subsequent work by Turley *et al.* (1998) provided confirmation of several qualitative features, although resonances in the  $\nu=1/3$  region were not investigated, while Ando *et al.* (1998) presented evidence for resonant tunneling between multiple-edge channels, which may be interpreted as supportive of either Luttinger-liquid or Fermi-liquid behavior.

Beyond the qualitative aspects, it is less straightforward to extract quantitative information from this type of experiment. Because of the low and broad tunnel barrier achievable in this point-contact geometry, a limited energy range is accessible before significant distortion of the barrier tunneling characteristics complicates the extraction of the tunneling density of states. Consequently, within the limited temperature range of a factor of 2–3, in the case of off-resonance tunneling, the differentiation of a power-law temperature dependence ( $T^4$  from conventional variable-range hopping forms ( $e^{-(T_o/T)^{1/2}}$  or  $e^{-(T_o'/T)^{1/3}}$ ), based on least-squares analysis, for example, is not clear cut. Similarly, the establishment of the precise functional dependence of the linewidth in the tunneling resonances poses a challenge (Maasilta and Goldman, 1998). Furthermore, some aspects of these results have also proven difficult to reproduce to date (Alphenaar *et al.*, 1995; Kouwenhoven and McEuen, 1995). Nevertheless, these experiments provided a glimpse of the novel non-Fermi-liquid character of the  $\nu=1/3$  fractional Hall edges.

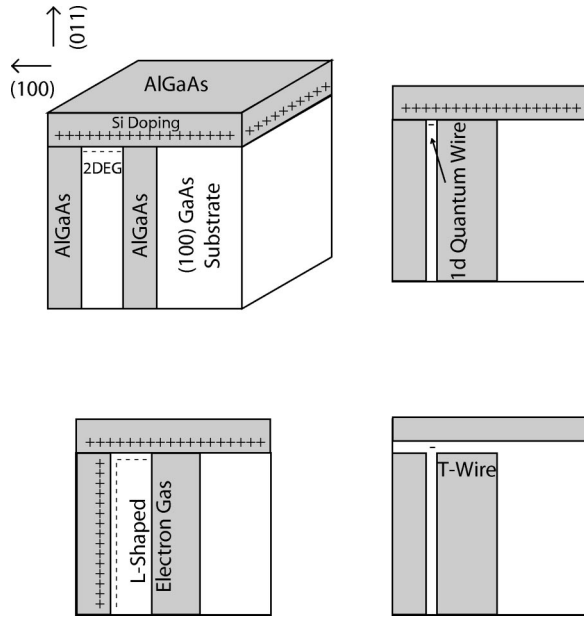


FIG. 17. Several unusual electron-gas geometries made available by the cleaved-edge overgrowth (CEO) technique. Clockwise from upper left: two-dimensional electron gas (2DEG) on the (011) plane, 1D quantum wire,  $T$  wire, and  $L$ -shaped electron gas.

### C. Cleaved-edge experiments

The author and co-workers achieved a breakthrough in observing clear power-law characteristics in both the  $I$ - $V$  relation and the temperature dependence of the tunneling conductance (Chang *et al.*, 1996; Levi, 1996), by use of the novel CEO geometry (Pfeiffer *et al.*, 1990; Grayson *et al.*, 1996). In this geometry tunneling takes place from a 3D, bulk  $n+$  doped GaAs metal overgrown on the (011) plane into the edge of a fractional quantum Hall fluid within a quantum well in the (100) plane. Devices of this geometry are fabricated via a two-step growth process discussed below. (See Figs. 12, 17, and 18.) Here the ability to create well controlled, sharp boundaries, and a tall and thin barrier has opened up new possibilities for studying the chiral Luttinger liquid.

#### 1. Crystal and sample preparation

Pfeiffer *et al.* (1990) pioneered the cleaved-edge overgrowth (CEO) technique for the molecular-beam epitaxy (MBE) growth of GaAs/ $\text{Al}_x\text{Ga}_{1-x}\text{As}$  on the unconventional (011) cleavage plane. The overgrowth takes place after an initial growth in the conventional (100) direction and subsequent *in situ* cleaving along the (011) direction. Since the (100) and (011) planes are perpendicular to each other, the overgrowth achieves structures that contain an element of three dimensionality, going beyond the two-dimensional layered growth in the (100) direction alone. In Fig. 17 we show some of the unusual structures that can be obtained using this CEO technique. By the combination of growths in the two directions and suitable modulation doping, it has been possible to fabricate 1D wires in which the walls of

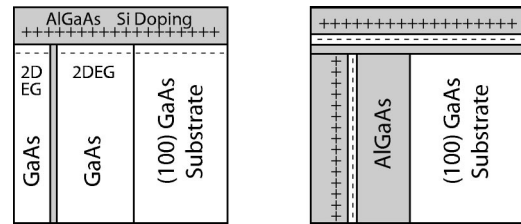


FIG. 18. Cleaved-edge overgrowth structure for 2D-to-2D tunneling: left, in the (011) plane; right, from the (011) plane to the (100) plane.

confinement are nominally uniform to one monolayer of atoms (Zaslavsky *et al.*, 1991; Kurdak *et al.*, 1994; Wegscheider, Kang, *et al.*, 1994; Wegscheider, Pfeiffer, *et al.*, 1994; Someya *et al.*, 1995; Yacoby *et al.*, 1996; Depicciotto *et al.*, 2001). Such uniformity is nearly impossible by any state-of-the-art lithographic techniques. To date the most successful application of CEO to technology is the invention of the  $T$ -wire laser based on electronic transitions between 1D subbands in the 1D quantum wires (Wegscheider, Kang, *et al.*, 1994; Wegscheider, Pfeiffer, *et al.*, 1994; Someya *et al.*, 1995). Here, the 1D quantum wire is formed at the  $T$  junction of quantum wells grown separately in the (100) and (011) directions. Going one step further by successive cleaved-edge overgrowth in two orthogonal directions, a cleaved-edge quantum dot has now been invented as well (Wegscheider *et al.*, 1997). In addition, a novel surface resonant-tunneling diode structure has been demonstrated on the (011) direction, where tunneling occurs through a 1D quantum wire (Zaslavsky *et al.*, 1991; Kurdak *et al.*, 1994).

By virtue of the same process which makes it possible to grow quantum wires with minimal width fluctuations, one can interchange the GaAs and  $\text{Al}_x\text{Ga}_{1-x}\text{As}$  to form energy barriers of unparalleled uniformity, as shown in Fig. 18 left. Not only can one design structures in which tunneling takes place between different electron gases within the (011) plane, it is also possible to achieve tunneling between electron gases residing separately in the (100) and (011) planes, through a barrier grown in the (011) plane (Fig. 18 right). A variation of these types of structures has proven to be extremely useful for edge tunneling in the fractional quantum Hall regime.

In the devices used in the edge-tunneling experiments, the aluminum content in the thin  $\text{Al}_x\text{Ga}_{1-x}\text{As}$  barrier,  $x$ , is varied between 0.1 and 0.3 (Chang *et al.*, 1996, 1998, 2001; Grayson *et al.*, 1996, 1998, 2001, 2002; Hilke *et al.*, 2001). The sharp edge is formed by *in situ* cleaving along the (011) direction, overgrowth of the thin barrier, followed by a 15-nm region of undoped GaAs and the heavily doped  $n+$  GaAs metal. The barrier potential, which results from a band-gap discontinuity between the  $\text{Al}_x\text{Ga}_{1-x}\text{As}$  and GaAs, imposes a nearly atomically sharp potential of 100 meV in height on the electrons relative to the band bottom at  $x=0.1$ , while an even higher barrier occurs when  $x>0.1$ . The high-mobility 2DEG in the (100) plane is terminated in the (011) direction by this abrupt barrier, giving rise to a structurally

TABLE I. Sample parameters.

Sample	$n$ ( $10^{11} \text{ cm}^{-2}$ )	$\mu$ ( $\text{cm}^2/\text{V s}$ )	$E_F$ (meV)	$E_o^a$ (meV)	$QW$ (nm)	Barrier (nm)	$n+$ Doping ( $10^{18} \text{ cm}^{-3}$ )	$\mu_{n+}$ (meV)	$\nu\Delta$ ( $\mu\text{eV}$ )	Figures
1.1	1.08	$2.9 \times 10^6$	3.9	23	25	9.0	$2.1 \times 10^{18}$	90	1/3: 450	1, 20–24, 30 31, 32, 34, 35
1.2	1.16	$3.3 \times 10^6$	4.1	23	25	22.5	$2.1 \times 10^{18}$	90	1: 1450	25, 30
1.3	1.13	$3.2 \times 10^6$	4.0	23	25	12.5	$2.1 \times 10^{18}$	90		26–28, 30 31, 32
1.4	1.27	$2.9 \times 10^6$	4.5	24	25	24.5	$2.1 \times 10^{18}$	90		30
2	0.87	$1.4 \times 10^6$	3.2	23	25	9.0	$2.1 \times 10^{18}$	90	1/3: 320	1, 23, 29 30, 34
3.1	2.06	$1.6 \times 10^6$	7.3	31	25	12.5	$2.1 \times 10^{18}$	90	1: 2600	25, 30
3.2	1.94	$1.5 \times 10^6$	6.9	31	25	9.0	$2.1 \times 10^{18}$	90	2/3: 220	25, 30
4	1.80	$2.0 \times 10^6$	6.4	30	25	9.0	$2.1 \times 10^{18}$	90	2/3: 140	25, 30
5.1	1.24	$0.5 \times 10^6$	4.4	24	25	16.0	$2.1 \times 10^{18}$	90		30
5.2	1.09	$0.5 \times 10^6$	3.9	24	25	9.0	$2.1 \times 10^{18}$	90	1/3: 380	30
6	0.61	$1.0 \times 10^6$	2.2	8	25	5.0	$2.1 \times 10^{18}$	90		32

<sup>a</sup>Estimates based on Stern and Das Sarma (1994).

sharp 2DEG edge structure, in direct contrast to the situation in a gated, smooth boundary. The barrier thickness is of order 5–25 nm, while its height rises  $\sim 75$  meV above the 2DEG chemical potential, far exceeding the 2DEG Fermi energy of  $\sim 4$  meV. Note that in a quantum well the lowest subband energy is  $\sim 10$ –25 meV above band bottom.

A typical, complete structure consists of a delta-doped quantum well on a GaAs (100) substrate situated 600 nm below the surface, followed by the cleaved-edge overgrowth of the barrier on the (011) plane, the 15 nm of undoped GaAs, and a 485-nm layer of highly doped  $n+$  GaAs (see Fig. 12). The  $n+$  doping density is in the  $0.5$ – $2.2 \times 10^{18}$ - $\text{cm}^{-3}$  range. It is essential to use a quantum well to confine the 2DEG rather than a single heterojunction, to prevent leakage through a second channel. In the undesirable case when a single heterojunction is used in place of the quantum well in the initial (100) growth, this second channel will form at a second heterojunction on the (011) plane between the GaAs of the first growth and the cleaved-edge overgrowth  $\text{Al}_{0.1}\text{Ga}_{0.9}\text{As}$  barrier. Although in principle this second heterojunction is undoped and devoid of carriers, under even a small voltage bias carriers can readily tunnel across the  $\text{Al}_{0.1}\text{Ga}_{0.9}\text{As}$  barrier from the 3D  $n+$  GaAs layer into the (011) 2D layer and subsequently trickle down into the 2DEG in the (100) heterojunction,

thereby shorting out the highly suppressed tunneling path into the chiral Luttinger liquid at the 2DEG edge.

Because the bare tunneling matrix element across the barrier is strongly dependent on magnetic field (Sec. III.C.2), to obtain data spanning a sizable range of Landau-level filling factor  $\nu$ , corresponding to different fractional quantum Hall fluids, it is necessary to perform measurements on a set of samples with varying 2DEG densities and barrier thicknesses. In Table I we summarize the device characteristics, while the substrate growth parameters are summarized in Table II. For example the set of samples 1.1, 1.2, 1.3, and 1.4 were all grown from the same high-quality quantum-well substrate, but with different tunnel barrier thicknesses. For these samples, the 2DEG is of density  $\sim 1.08 \times 10^{11} \text{ cm}^{-2}$  and mobility  $\sim 3 \times 10^6 \text{ cm}^2/\text{V s}$ . Sample 2 has a 2DEG density of  $0.87 \times 10^{11} \text{ cm}^{-2}$  and a mobility of  $1.8 \times 10^6 \text{ cm}^2/\text{V s}$ , etc. The  $\text{Al}_{0.1}\text{Ga}_{0.9}\text{As}$  barrier thicknesses for samples 1.1, 1.2, 1.3, and 1.4, are 9, 22.5, 12.5, and 24.5 nm, respectively. The  $n+$  GaAs is doped to  $0.5$ – $2 \times 10^{18} \text{ cm}^{-3}$  carrier density, yielding a chemical potential of 29–85 meV from the GaAs band bottom (34–90 meV from the impurity band bottom), while the chemical potential of the 2DEG is approximately 27 meV ( $E_o + E_F$ ) above band bottom for samples 1.1, etc. Charge redistribution can take place across the barrier due to the difference chemical potential. The actual den-

TABLE II. Substrates.

Sample	$n$ ( $10^{11} \text{ cm}^{-2}$ )	$d$ , spacer distance (nm)	$s$ , surface distance (nm)
1	1.08–1.27	60	600
2	0.87	39	600
3	1.94–2.06	40	450
4	1.80	40	580
5	1.09–1.24	40	590
6 <sup>a</sup>	0.61		

<sup>a</sup>Symmetrically doped on both sides of the quantum well.

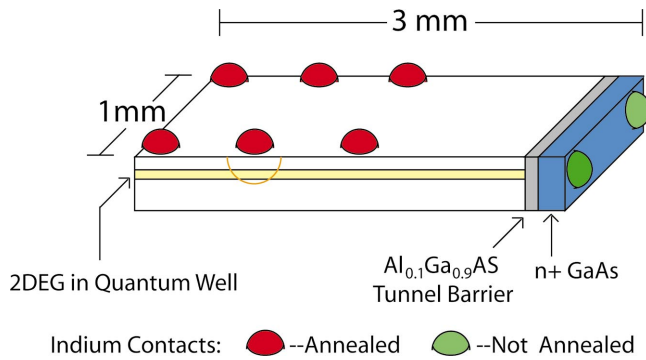


FIG. 19. (Color) Sample with indium contacts. The dark contacts are first annealed to enable diffusion into the GaAs quantum well, where the 2DEG resides. Subsequently the light-colored contacts were cold-soldered onto the  $n+$  GaAs metal at  $200^\circ\text{C}$  to prevent any diffusion or shorting of the tunnel barrier.

sity profile will also depend on whether residual silicon dopants penetrate into the 15-nm undoped GaAs buffer layer during the regrowth process (see Levitov *et al.*, 2001 and Chang, 2002 for a full discussion). Most of the available data were taken in devices grown with aluminum content  $x=0.1$ , with the exception of the work of Hilke *et al.* (2001), for which  $x=0.2$ .

A typical device used in measurement is of physical dimensions  $1 \times 3 \times 0.15 \text{ mm}^3$  (width  $\times$  length  $\times$  thickness) where the length of the  $\text{Al}_{0.1}\text{Ga}_{0.9}\text{As}$  tunnel barrier spans the sample width of 1 mm. Because of this long barrier, in off-resonance tunneling processes electrons are most likely injected and removed at many pointlike contacts along the 1 mm length. Moreover, the tunneling events at different points are believed to be largely incoherent. This is to be contrasted to the case of resonant tunneling discussed in Secs. II.B.6 and III.C.5. To make ohmic contact to the 2DEG in the (100) quantum well and to the 3D bulk  $n+$  GaAs on the cleaved (011) edge, indium metal is used in two separate steps. These two steps are necessary to avoid unwanted shorting of the tunnel barrier due to uncontrolled indium diffusion. The contact arrangements are shown in Fig. 19. In the first step, indium is diffused into the quantum well at various contact positions located away ( $>0.5 \text{ mm}$ ) from the tunnel junction. This enables ohmic contacts to be made to the 2DEG while avoiding degradation of the tunnel barrier due to the penetration of residual amounts of indium. These 2DEG contacts are utilized for *in situ* measurements of the transport coefficients, the longitudinal ( $R_{xx}$ ) and Hall resistances ( $R_{xy}$ ), enabling the characterization of the electron density and mobility. The second step involves contacting the 3D  $n+$  GaAs layer on the cleaved edge. To accomplish this, indium is applied to the  $n+$  GaAs using a soldering iron at  $\sim 200^\circ\text{C}$ . Note that the melting point of indium is  $156^\circ\text{C}$ . Typically, the  $n+$  GaAs is sufficiently highly doped ( $0.5\text{--}2.2 \times 10^{18} \text{ cm}^{-3}$ ) that an ohmic contact is routinely made. This ohmic behavior of the  $n+$  GaAs contact persists down to mK temperatures. It has turned out to be absolutely necessary that the indium on the  $n+$  GaAs not be

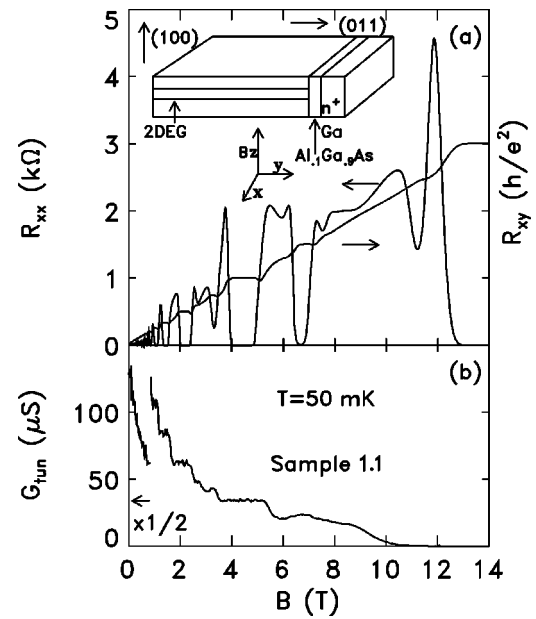


FIG. 20. Magnetic-field traces of (a) longitudinal resistance ( $R_{xx}$ ) and Hall resistance ( $R_{xy}$ ); (b) tunneling conductance ( $G_{tun}$ ), at low bias for sample 1.1. The temperature is 50 mK. From Chang *et al.*, 1996.

annealed at temperatures exceeding  $\sim 350^\circ\text{C}$  to avoid accidental diffusion into the tunnel barrier. Even trace amounts of indium will short out the power-law tunneling behavior! With careful, consistent preparation, high-quality electron-tunneling data are readily obtainable.

## 2. Tunneling conductances at $\nu=1/3$

We begin the data presentation with the first clear evidence of power-law characteristics for electron tunneling into a fractional quantum Hall edge. Making use of the cleaved-edge overgrowth devices, we studied the tunneling conductance [ $G(T)$ ], current-voltage ( $I$ - $V$ ) relationship, and differential conductance ( $dI/dV$ ), for electron tunneling between the bulk-doped  $n+$  GaAs metal and the edge of various incompressible fractional quantum Hall fluids. For tunneling into the  $\nu=1/3$  edge we found that  $I \propto V^{2.7 \pm 0.06}$  and  $G \propto T^{1.75 \pm 0.08}$ , where the two dependences yielded nearly identical values for the exponent  $\alpha$  of  $\approx 2.7$ . In contrast, tunneling into a  $\nu=1$  edge was essentially linear in the  $I$ - $V$ , while  $G$  was temperature independent. These results strongly indicated that the  $1/3$  fractional edge behaves like a chiral Luttinger liquid, while the  $\nu=1$  edge behaves as a one-dimensional Fermi liquid.

In Fig. 20(a), we show the longitudinal resistance ( $R_{xx}$ ) and Hall resistance ( $R_{xy}$ ), and in (b) the tunneling conductance ( $G_{tun}$ ), for sample 1.1 versus magnetic field at a temperature of 50 mK. The  $\nu=1/3$  fractional quantum Hall effect occurred at 13.4 T. The conductance  $G_{tun}$  exhibited an abrupt drop above a magnetic field of 9.5 T. This reduction arises from two contributions. The first is the chiral Luttinger liquid nature of the edge states, as will be shown in subsequent figures. The

second is the tunneling matrix element across the  $\text{Al}_{0.1}\text{Ga}_{0.9}\text{As}$  barrier. In the Landau gauge where the vector potential  $\mathbf{A} = -By\hat{x}$ , for a perfect, infinitely long barrier, the matrix element is separable into a product of three components associated with the vertical ( $\mathbf{B}$ ) direction  $z$  and the directions along the barrier  $x$  and normal to the barrier  $y$ . The  $z$  matrix element couples the 3D  $n+\text{GaAs}$  electrons into the 2D quantum-well ( $x$ - $y$ ) plane and is insensitive to  $B$ . At low and intermediate  $B$ , the  $y$  matrix element is dominated by the 9-nm-thick barrier and is also insensitive. The  $x$  component, however, can exhibit substantial  $B$  dependence. The  $x$  eigenfunction  $e^{ikx}$  is indexed by the momentum  $k$ , which is proportional to the  $y$  center of coordinate  $y_o$ ; i.e.,  $k \sim y_o l_o^2$ . Tunneling through the barrier involves a displacement in  $y$  of  $\Delta y_o \sim 9$  nm, accompanied by a change in  $k$  of  $\Delta k \sim \Delta y_o l_o^2 \propto B$ . Since the barrier potential is translationally invariant in  $x$ , it cannot couple states of different  $k$ ; the  $x$  matrix vanishes and tunneling is forbidden. However, the presence of imperfections and disorder in a real sample, as well as its finite extent, breaks the  $x$  translational invariance and tunneling becomes possible. Nevertheless,  $\Delta k$  is proportional to  $B$ . At higher magnetic fields, a larger momentum change is required. The  $x$  matrix element which measures the  $x$  Fourier transform of the total potential,  $V(\Delta k, y, z)$ , is expected to fall off with  $B \propto \Delta k$ . Clearly, for the case of ionized impurities or interface roughness mediating the tunneling process, this falloff does occur. Moreover, at high  $B$  the tunneling matrix may become limited by the tunneling barrier. The tunneling probability  $P_{\text{tunn}}$  drops exponentially with  $B$  due to its dependence on the magnetic length,  $l_B = (\hbar/eB)^{1/2}$ :  $P_{\text{tunn}} \sim e^{-(x_o/l_B)^2} \sim e^{-B/l_B o}$ .

To demonstrate the tunneling density-of-states contribution to the reduction of the tunnel current, in Fig. 1 we show the  $I$ - $V$  characteristics in a log-log plot for samples 1.1 and 2 at the filling factor  $\nu=1/3$ . The respective magnetic fields were 13.4 T and 10.8 T, and the temperature was 25 mK. At voltages below  $\sim 12 \mu\text{V}$ , the tunneling was thermally dominated ( $kT/e = 2.15 \mu\text{V}$ ) and  $I$ - $V$  exhibited a linear relationship. The respective tunneling resistances were 100 and 300 M $\Omega$ . Above a crossover voltage of  $\sim 6 \text{ kT}/e \sim 12 \mu\text{V}$ , the  $I$ - $V$  followed a nonlinear power law given by  $I \propto V^\alpha$  where  $\alpha = 2.7 \pm 0.06$  and  $2.65 \pm 0.06$ , respectively. The power law persisted over 1 decade in  $V$  and 2.7 decades in  $I$ , beyond which  $I$  was observed to fall below the power law. This power-law behavior was a main prediction of the chiral Luttinger effective-field theory due to Wen (1992, 1995), Kane and Fisher (1992b, 1995), Moon *et al.* (1993), and Fendley *et al.* (1995a, 1995b) and arises from the power-law tunneling density of states. However, the observed exponent was smaller than the prediction of exactly 3 from effective theories. This discrepancy will be addressed in detail in the ensuing sections. Beyond the prediction of a simple power law, the data could be fitted to the Kane and Fisher universal scaling form, which holds in the limit  $G_{\text{tun}} \ll G_{\text{Hall}} = e^2/3h$ . For tunneling

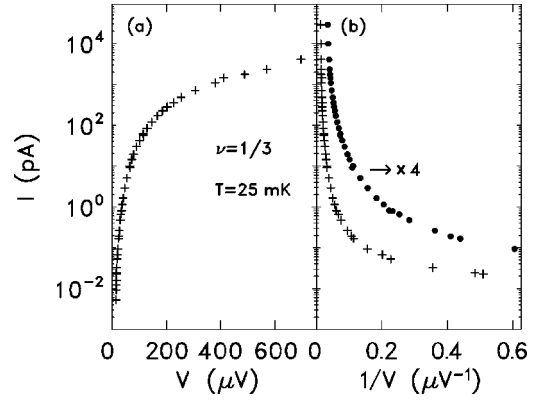


FIG. 21. The data in Fig. 1 for sample 1.1 plotted in different functional forms: (a)  $\log_{10} I$  vs  $V$ ; (b)  $\log_{10} I$  vs  $1/V$ . In (b), the solid dots represent the same data plotted with the  $x$  axis expanded by a factor of 4. The lack of any straight portion demonstrates the poor fit of these functional forms to the data. The corresponding functional forms are  $I \propto e^{-V/V_o}$  and  $I \propto e^{-V_o/V}$ .

into the  $1/3$  edge from a normal metal, it is approximately given by (Kane and Fisher, 1992b, 1992c)

$$I \propto T^\alpha [x + x^\alpha], \quad (226)$$

where

$$x \equiv \frac{eV}{2\pi kT}; \alpha = 3. \quad (227)$$

Note that this expression is an approximation to Eq. (178), since for  $\alpha$  between 2 and 3, the extra factor  $\Gamma[(\alpha+1/2)^2] \approx 1$  and actually falls between the values 0.78 and 1. Because our exponent was different from 3, we replaced  $\alpha$  by 2.7 and 2.65, respectively, and plotted the results as the solid curves. The two fitting parameters were the exponent  $\alpha$  and the proportionality constant between the  $I$  and  $V$ . The fits appear to be excellent. In other words, the predicted  $1/2\pi$  scaling factor between the bias voltage and the temperature was borne out by experiment. The power-law region exceeded

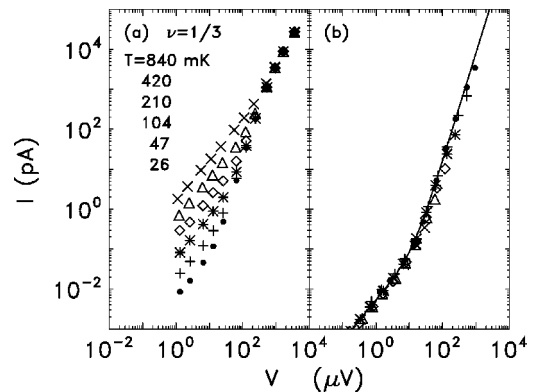


FIG. 22. Temperature evolution of the current-voltage ( $I$ - $V$ ) characteristics at  $\nu=1/3$ : (a) log-log plot of  $I$ - $V$  characteristics for sample 1.1 at  $\nu=1/3$  at six different temperatures; (b) collapsed curves for the data in (a) where  $I_{\text{coll}}(V') = I(V)[G(T_o)/G(T)]_{V=0}$ ,  $T_o = 26$  mK and  $V' = VT/T_o$ . From Chang *et al.*, 1996.

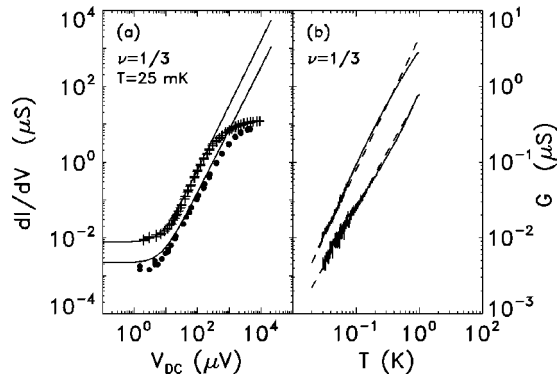


FIG. 23. Bias-voltage dependence of the differential tunneling conductance,  $dI/dV$ , and its temperature evolution at low bias: (a) Log-log plot of  $dI/dV$  for samples 1.1 (crosses) and 2 (solid circles) at  $\nu=1/3$ , at a temperature of 25 mK. The solid curves represent the theoretical  $dI/dV$  obtained from Fig. 1. (b) Log-log plot of the temperature dependence at low voltage bias for samples 1.1 (upper curve) and 2 (lower curve) at  $\nu=1/3$ . The respective voltage biases are 4.97 and 2.64  $\mu\text{V}$ . The solid straight lines represent power laws with the respective exponents,  $\alpha-1$ , of 1.75 and 1.5. From Chang *et al.*, 1996.

three decades in current and 1.4 decades in bias. The large dynamic range enabled us to rule out other competing functional forms, such as  $\exp[-V/V_o]$ , or  $\exp[-V'/V]$ , which gave substantially poorer fits, as shown in Fig. 21. Next we demonstrate that the crossover voltage from linear to power-law behavior scales with temperature by plotting the  $I$ - $V$  characteristics between 26 and 840 mK in Fig. 22(a) and the collapsed

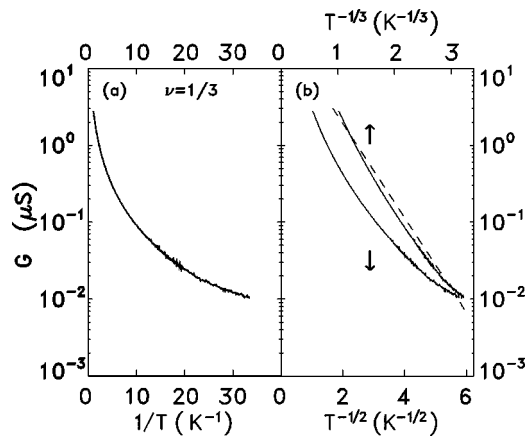


FIG. 24. The data in Fig. 23(b) replotted (a) in an Arrhenius plot, and (b) in variable hopping forms of  $G \propto e^{-(T_o/T)^{1/2}} [\log_{10} G/G_o \propto -(T_o/T)^{1/2}]$  and  $G \propto e^{-(T_o/T)^{1/3}} [\log_{10} G/G_o \propto -(T_o/T)^{1/3}]$ . The clear absence of a straight portion in any of the three plots demonstrates that these functional forms do not adequately describe the data. The dashed line in (b) is included for the purpose of comparison. As the variable-range hopping exponent becomes smaller, from 1 to  $1/2$  and  $1/3$ , the fit improves. This is to be expected since a power law that corresponds to the functional dependence  $\log_{10} G/G_o \propto \log_{10} T/T_o$  is obtained in the limit where this exponent approaches zero.

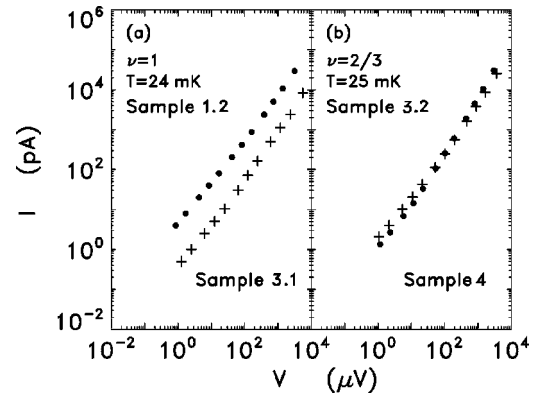


FIG. 25.  $I$ - $V$  tunneling characteristics for  $\nu=1$  and  $\nu=2/3$ : (a) Log-log plot of the  $I$ - $V$  characteristics for tunneling into the  $\nu=1$  quantum Hall edge for samples 1.2 at  $B=4.8$  T (crosses) and 3.1 at  $B=8.5$  T (solid circles). The temperature is 24 mK. (b) Log-log plot of  $I$ - $V$  for tunneling into the  $\nu=2/3$  edge for sample 3.2 at 12.0 T (crosses) and sample 4 at 11.1 T (solid circles) at a temperature of 25 mK. A slightly nonlinear behavior is observed above  $\sim 12$   $\mu\text{V}$  of voltage bias. The respective exponents  $\alpha$  are 1.2 and 1.42. From Chang *et al.*, 1996.

curves normalized to the 26-mK curve in Fig. 22(b). In Fig. 22(b), data points beyond the breakoff voltage of  $\sim 1$  mV were removed for clarity; all other data points fell on a universal curve as required.

In Fig. 23(a) we plotted the differential conductance  $dI/dV$ , measured independently. The agreement with theory is also quite good. Here, the solid curves represent the  $dI/dV$  of the corresponding theoretical curves in Fig. 1. In Fig. 23(b), we plot  $G_{\text{tun}}$  for samples 1.1 and 2 at low voltage bias versus temperature in a log-log plot. Power-law behavior was again observed with an exponent of  $1.75 \pm 0.08$  and  $1.5 \pm 0.08$ , respectively, although the data exhibited a slight meander about ideal behavior. The dynamic range was roughly 1 decade in temperature and 1.7 (1.5) in  $G_{\text{tun}}$ . These exponents yielded values for  $\alpha$  close to those obtained from  $I$ - $V$  and  $dI/dV$ , as required by theory. As a check, we attempted an Arrhenius plot of  $\log_{10} G_{\text{tun}}$  versus  $1/T$  as well as various variable-range-hopping functional forms for sample 1.1, which yielded a large curvature (Fig. 24), clearly indicating that neither a simple activated process over an energy barrier nor standard variable-range hopping is appropriate.

In Fig. 25, we plotted the  $I$ - $V$  characteristics for the  $\nu=1$  edge for samples 1.2 and 3.1, and for the  $\nu=2/3$  edge for samples 3.2 and 4. In direct contrast to tunneling into the  $\nu=1/3$  edge, the  $I$ - $V$  characteristics were nearly linear for the  $\nu=1$  case, and were slightly nonlinear for  $\nu=2/3$ , for voltage bias beyond the temperature-dominated regime. The corresponding values of  $\alpha$  were 1.2 and 1.14 for  $\nu=1$ , and 1.2 and 1.42 for  $\nu=2/3$ . Note that for tunneling into the  $\nu=1$  edge, the experiment indicated that the edge behaves as a *chiral Fermi liquid*. This is a rare example of a strongly interacting 1D system with Fermi-liquid rather than Luttinger-liquid behavior. In the case of tunneling into the  $2/3$  edge, the power-law exponent  $\alpha$  is nonuniversal, ranging from 1.2 to 1.42 where  $I \propto V^\alpha$ . The  $\nu=2/3$  result will be discussed in the context of edge tunneling at general filling factors.

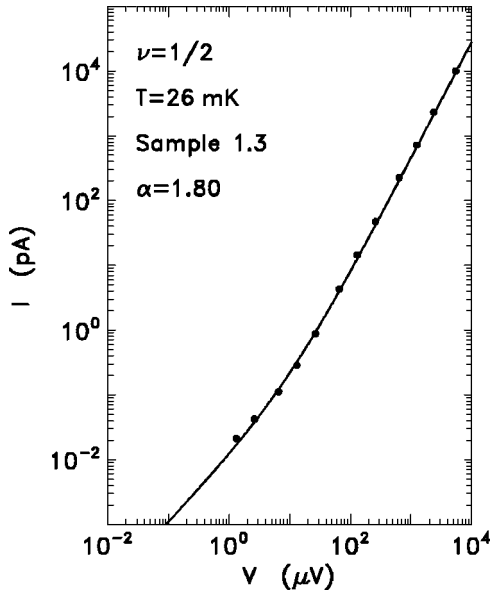


FIG. 26. Current-voltage ( $I$ - $V$ ) characteristics for tunneling from the bulk-doped  $n$ +GaAs into the edge of a  $\nu=1/2$  composite fermion liquid for sample 1.3 at  $B=9.28$  T in a log-log plot. The solid curve represent a fit to Eq. (178) for  $\alpha=1.80$ . From Chang *et al.*, 1998.

3. Tunneling conductances at  $\nu=1/2$

The evidence in the previous section and its overall, reasonably good agreement with theory shed considerable light on the physics of the edge of *incompressible* fractional quantum Hall fluids. On the other hand, the physical properties at the edge of a *compressible* fluid were yet to be explored, for instance, the edge of the  $\nu=1/2$  composite-fermion quantum Hall liquid and its tunneling properties. A composite fermion, initially proposed by Jain, is composed of a real electron (fermion) and an integral number of flux tubes (Jain, 1989a; Willett *et al.*, 1990, 1993; Du *et al.*, 1993, 1994; Halperin *et al.*, 1993; Kang *et al.*, 1993). Due to these attached fluxes, the tunneling of electrons into the bulk can be substantially different from that into the edge. For bulk tunneling, the difficulty in bringing in extra fluxes to attach to the added electrons gives rise to a pseudogap in the tunneling density of states and an exponential suppression of tunneling current with bias (Eisenstein *et al.*, 1992; He *et al.*, 1993). Tunneling into the edge, however, was often surmised to be linear in its  $I$ - $V$  characteristics, since extra flux lines can readily enter from the boundary. In the 2D bulk region of the incompressible  $\nu=1/3$  fractional Hall fluid, the excitation spectrum contains a gap above the ground state and there are no zero-energy excitations. In the  $\nu=1/2$  fluid, no gap exists in the bulk.

Here we show that for electron tunneling into the edge of a  $\nu=1/2$  fractional quantum Hall fluid, nonlinear  $I$ - $V$  characteristics as well as a temperature-dependent low bias tunneling conductance  $G$  can be obtained. In three different samples, 1.3, 1.4, and 5.1, the  $I$ - $V$  exhibited a power-law behavior reminiscent of a chiral Luttinger liquid, with an exponent  $\alpha$  of  $1.80 \pm 0.05$ ,  $2.10 \pm 0.10$ , and  $1.83 \pm 0.05$ , respectively. The exponent de-

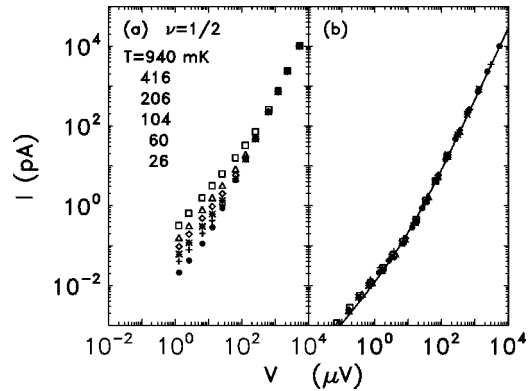


FIG. 27. Temperature evolution of the current-voltage ( $I$ - $V$ ) characteristics at  $\nu=1/2$ : (a) log-log plot of  $I$ - $V$  characteristics for sample 1.3 at at six different temperatures; (b) collapsed curves for the data in (a) where  $I_{coll}(V') = I(V)[G(T_o)/G(T)]_{V \rightarrow 0}$ ,  $T_o=26$  mK and  $V' = VT/T_o$ . From Chang *et al.*, 1998.

duced from  $G(T)$  for the first sample yielded  $\alpha=1.77 \pm 0.07$ , which is consistent with the value of 1.80 deduced from the  $I$ - $V$  curve. In essence,  $\alpha$  was roughly given by  $\alpha=1/g=1/\nu=2$ . These results indicated that the edge of the compressible  $\nu=1/2$  fluid behaves almost like a one-dimensional chiral Luttinger liquid and provided the first compelling evidence that Luttinger-liquid behavior can exist at the edge of a compressible fractional Hall fluid.

Figure 26 shows our main result of a nonlinear tunneling characteristic for sample 1.3 at 26 mK of  $0.023 \mu S$  corresponding to a tunneling resistance of  $43 M\Omega$ . Above  $\sim 15 \mu V$ , power-law behavior with an exponent  $\sim 1.80$  was observed up to an excitation of 5.6 mV. This large excitation exceeded the voltage scale of 3.9 mV set by the Fermi energy. We again fitted the data to the

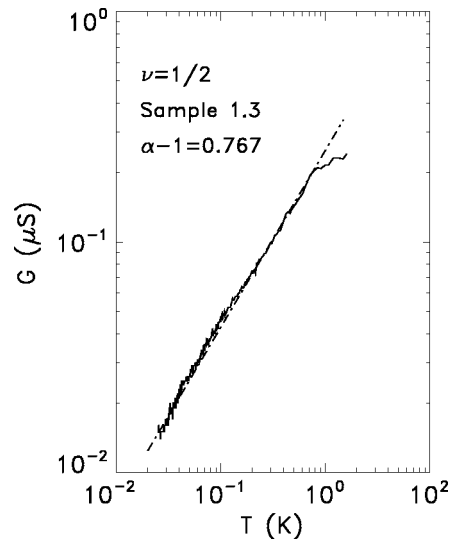


FIG. 28. Log-log plot of the temperature dependence at low voltage bias for sample 1.3 at  $\nu=1/2$ . The dash-dotted straight line represents a power law with an exponent,  $\alpha-1$ , of 0.77. From Chang *et al.*, 1998.

Kane/Fisher functional form appropriate for a chiral Luttinger liquid with a dimensionless conductance  $g$  of  $1/\alpha(e^2/h)$  [Eq. (178)] (Kane and Fisher, 1992c; Chamon and Fradkin, 1997):

$$I = \gamma T^\alpha \left\{ \left[ \Gamma \left( \frac{\alpha+1}{2} \right) \right]^2 x + x^\alpha \right\}, \quad (228)$$

where  $x = eV/2\pi kT$ ,  $\Gamma$  is the gamma function, and  $\gamma$  is a proportionality constant. A best fit was achieved with  $\alpha = 1.80$  and is shown as the solid curve in Fig. 26. In Fig. 27(a) we show the temperature evolution of the  $I$ - $V$  curve. Rescaling the voltage by  $V(T_o/T)$  and the current by  $I(V)[G(T_o)/G(T)]_{V \rightarrow 0}$ , data at all temperatures can be collapsed onto a universal curve, as depicted in Fig. 27(b).

In Fig. 28 we plotted the temperature dependence of the small-bias linear conductance  $G$  in a log-log plot. A power law with  $G \propto T^{0.77 \pm 0.07}$  was observable between 26 and 900 mK. The exponent of  $\alpha - 1 = 0.77$  is consistent with the value of  $\alpha = 1.80 \pm 0.05$  deduced from the  $I$ - $V$  curve in Fig. 26 and satisfies the requirement of Eq. (228), provided Eq. (228) is relevant and appropriate to tunneling into the  $\nu = 1/2$  edge.

#### 4. Power-law exponents and universality

The observation of power-law electron tunneling characteristics at  $\nu = 1/2$  led us naturally to inquire about the behavior at general filling factors. For the best traces, power-law behavior with a dynamic range exceeding 4 1/2 decades in current and 1 1/2 decades in voltage was observed. Two major results emerged: (1) there is a continuum of power-law  $I$ - $V$  behavior, and (2) the  $I$ - $V$  exponent is approximately given by  $1/\nu$ , with the edge appearing to behave as a single-mode Luttinger liquid with reduced conductance parameter  $g \sim \nu$ . Our results came as a major surprise, first because the observation of Luttinger-liquid behavior at all fillings was not fully anticipated (Chang *et al.*, 1998), as incompressibility of the bulk fluid (gapped behavior) was considered crucial to the existence of a Luttinger liquid; and second because the power-law exponent lacked clear-cut plateau features, in direct contrast to theoretical analyses within the effective-field theories based on the intermixing of copropagating versus counterpropagating edge modes (Wen, 1992; Kane and Fisher, 1995; Shytov *et al.*, 1998).

The tunneling exponent  $\alpha$  was extracted from the  $I$ - $V$  data utilizing the theory of Chamon and Fradkin (1993) for a single-mode CLL with  $g = \nu$ , which models the wide tunnel junction as a sequence of incoherent, point-like tunnel junctions, while treating the 3D metal as a chiral Fermi liquid. Although the justification for a single-mode CLL at arbitrary  $\nu$  is still lacking, this model was successful in fitting our data. Ideally, an  $I$ - $V$  curve consists of three regimes:

(a) a low voltage bias regime with a linear  $I$ - $V$  relationship in which the thermal energy  $kT$  dominates over the voltage-bias energy  $eV$  ( $eV \ll 2\pi kT$ ),

- (b) an intermediate voltage-bias regime ( $2\pi kT \leq eV \leq T_S$ ) exhibiting the important power-law  $I$ - $V$  behavior, and
- (c) a high-bias saturation regime ( $eV > kT_S$ ) in which  $I$ - $V$  approaches linearity again and where the tunneling conductance saturates to the two-terminal conductance of the 2DEG as the tunnel barrier becomes transparent.

Here  $T_S$  represents a crossover temperature with  $kT_S$  the crossover energy above which saturation takes place. Since  $T$  is determined by experimental conditions and  $\nu$  from the Hall measurement, the only adjustable parameters are  $\alpha$  and  $T_S$  ( $\beta = \alpha - 1$ ,  $r = 2\pi T/T_S$ ):

$$I = \int \nu \frac{e^2}{h} \times \left( 1 - \frac{e^{-(1/2)r^\beta}}{\left[ \frac{\left( \frac{V}{rT_S} \right)^\beta}{\Gamma^2 \left( \frac{\alpha+1}{2} \right) (1 - e^{-(\beta/2)r^\beta}) + 1} \right]^{\alpha/\beta}} \right) dV. \quad (229)$$

Equation (229) [Eq. (198)] is expected to be appropriate for a single-mode Luttinger liquid with reduced conductance  $g = 1/\alpha$ . At  $B = 11.0$  T ( $\nu = 1/3$ ), it fit the data with remarkable precision (Fig. 29 top, dotted line). For comparison we also plotted the series resistance model used to guide our intuition (Fig. 29 top, dashed line) and noted that the knee of the crossover region at high bias was too soft.

Next we examined the series of log-log  $I$ - $V$  curves over the whole range of the  $B$  field for sample 2 (see bottom of Fig. 29). At the higher  $B$  fields (13.0 T) we observed power-law behavior up to 6 decades in current, whereas at the lowest field (7.0 T) the curve was approximately linear over the entire range. At lower  $B < 10.0$  T (corresponding to high  $\nu > 2/5$ ), the fit of the Chamon-Fradkin theory to each trace was still good, and we were able to extract  $\alpha$  and  $T_S$ . Nonetheless the fit was not as exact in this range, as indicated by the larger error bars in Fig. 30.

Similar  $I$ - $V$  measurements were performed on the three samples 1.1, 5.2, and 1.2 (Table I); we summarize the full result of the exponent  $\alpha$  versus  $1/\nu$  in Fig. 30. Samples 1.1 and 5.2 yielded sufficient decades of power-law behavior to fit to the Chamon-Fradkin theory, whereas sample 1.2 exhibited a strong power law only at the highest magnetic fields, settling to a weak power law with  $\alpha \sim 1.1$  over the  $1/\nu$  range of 1–1.4. Error bars for representative data points are provided at various fillings. For samples 2 and 1.1 above  $1/\nu > 2.8$ , and sample 5.2 above  $1/\nu > 2.4$ , the error is negligible.

Based on our results we make the following observations. First, the plot shows a remarkable continuum of power-law exponent values spanning the entire range 1

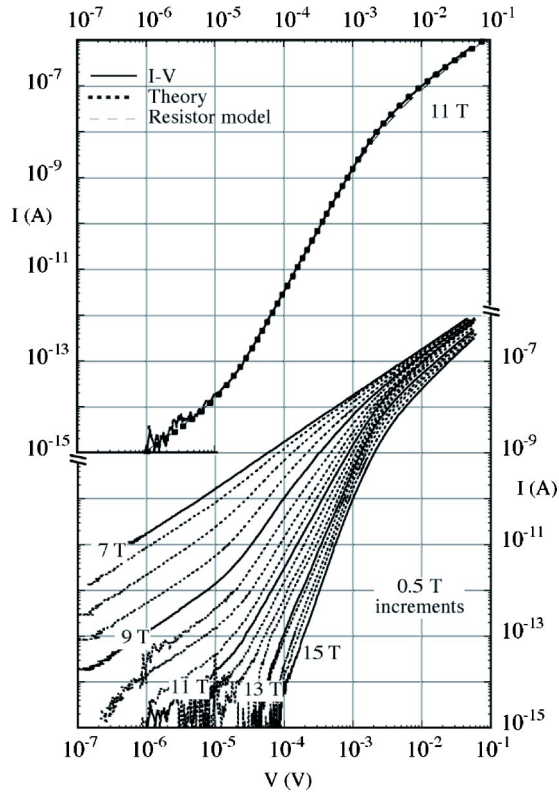


FIG. 29. (Color in online edition)  $I$ - $V$  tunneling characteristics at different magnetic fields: Upper curve, log-log  $I$ - $V$  for sample 2 at 11.0 T,  $\nu=1/3$ . Theory of Chamon and Fradkin (1997), Eq. (229), (dotted line) and simple series resistance model (dashed line) are overlaid for comparison. Lower curves, log-log  $I$ - $V$  for sample 2 at different values of  $B$  from 7.0 to 15.0 T in 0.5-T steps. Solid lines correspond to the labeled magnetic fields. Dotted lines correspond to magnetic fields between those of the solid lines in 0.5-T increments. From Grayson *et al.*, 1998.

$<\alpha < 4$ . This was the first experimental evidence that the characteristic CLL coupling constant  $g$  might in fact assume a whole continuum of values. Second, the trend in  $\alpha$  versus  $1/\nu$  is linear for  $1/\nu > 1.4$  with  $\alpha \approx 1.16/\nu - 0.58$ . This linear behavior appeared to roughly characterize all four samples studied, regardless of electron mobility, carrier density, or tunneling barrier thickness. It is in striking contrast to theoretical expectations that  $\alpha$  would reflect the bulk transport and therefore exhibit plateaus whenever the Hall conductance is quantized. Finally, for  $1/\nu < 1.4$ , the exponent saturated at a lower limit,  $\alpha = 1.1$ , indicating an approach to Fermi-liquid behavior. For certain samples, e.g., 1.1 and 5.2, hints of a possible plateau feature in the exponent near  $1/\nu = 1/3$  do appear. However, the limited range in  $1/\nu$  (or  $B$ ) for the feature precludes a definitive conclusion. This important issue is addressed in a subsequent experiment.

The observation that power-law behavior is not restricted to incompressible quantum Hall fluid edges and is in fact present for general filling factors, with the exponent  $\alpha$  varying in a continuous manner roughly as  $1/\nu$  for  $1/\nu > 1.4$  (Chang *et al.*, 1996; Grayson *et al.*, 1998) presented a puzzle. On the one hand, the effective

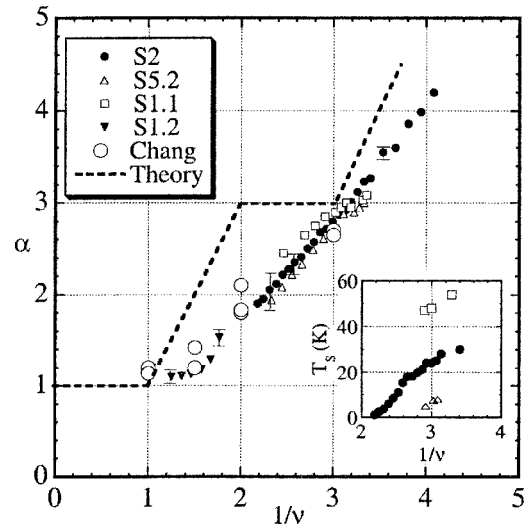


FIG. 30. Power-law exponent  $\alpha$  vs  $1/\nu$ , the reciprocal of the filling factor, for four samples. The data from Chang *et al.* (1996, 1998), plotted as open circles, are included for reference—samples 1.1 and 2 at  $\nu=1/3$ , samples 1.3, 1.4, and 5.1 at  $\nu=1/2$ ; samples 3.2 and 4 at  $\nu=2/3$ ; samples 1.2 and 3.1 at  $\nu=1$ . Inset,  $T_S$  vs  $1/\nu$  for three samples whose traces spanned high excitations. From Grayson *et al.*, 1998.

theory is able to produce power-law behavior at rational filling fractions for the Jain series of incompressible fluids (Kane and Fisher, 1995), and the theory of Shytov, Levitov, and Halperin (1998) based on the composite-fermion effective-field theory predicts power laws at continuous values of inverse filling,  $1/\nu$  (more precisely, Hall resistivity,  $\rho_{xy}$ ). On the other hand, the predicted steplike plateau features in  $\alpha$  (contained in the dashed line in Fig. 30) stand in contrast to the featureless linear behavior of the experiment. These predictions rely directly on our understanding of the relation between the edge-mode structure and the topological characterization of fractional Hall states, as well as the intermixing of co-propagating and counterpropagating edge modes into charged and neutral varieties. The disagreement between theory and experiment involved two important issues. First, the absence of plateaus for  $1/\nu > 1.4$  was difficult to reconcile with the theoretical expectation even without accounting for the finite widths of quantized Hall plateaus. Second, the lack of a plateau near bulk filling,  $\nu=1/3$  ( $1/\nu=3$ ) despite the appearance of a Hall plateau in  $\rho_{xy}$ , indicated that edge tunneling characteristics must not be solely dictated by the bulk Hall resistivity, again in contradiction to expectation. This absence of structure was even invoked by some workers as evidence that Luttinger-liquid behavior had not been conclusively demonstrated (Altland *et al.*, 1999; Bockrath *et al.*, 1999; Egger, 1999). Because the  $\nu=1/3$  fractional quantum Hall fluid possesses the largest gap and is robust, evidence for plateauing in the exponent was of critical importance. Here we demonstrate a clear observation of a plateau feature for the  $\alpha$  versus  $1/\nu$  dependence, with an  $\alpha$  value close to 3. The conclusion of the existence of a plateau feature (Chang *et al.*, 2001) was obtained from careful analysis of  $I$ - $V$  tunneling data

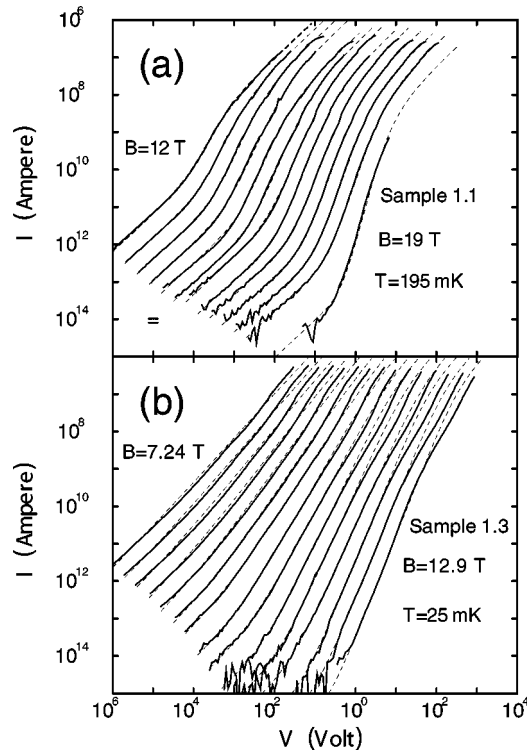


FIG. 31. Log-log plot of the  $I$ - $V$  characteristics (solid lines) for electron tunneling from the bulk doped  $n$ +GaAs into the fractional quantum Hall edge: (a) sample 1.1 at various magnetic fields from 12 T to 19 T in steps of 0.5 T; 18 and 18.5 T are excluded. Corresponding filling factors vary from 2.69 to 4.26. Dashed lines represent best fits to the Chamon-Fradkin expression, Eq. (229). (b) Sample 1.3 at  $B=7.24, 7.5, 7.76, 8.02, 8.28, 8.53, 8.79, 9.31, 9.83, 10.34, 10.86, 11.38, 11.9, 12.4,$  and  $12.9$  T, with  $1.611 < 1/\nu < 3$ . Dashed lines represent best fits. Successive curves are displaced by 0.3 units ( $\ln 2$ ) in the horizontal direction for clarity. From Chang *et al.*, 2001.

with precise fitting to the Chamon and Fradkin (1997) expression, followed by a statistical  $F$  test for the  $\chi^2$  of the  $\alpha$  vs  $1/\nu$  fits. However, the  $1/\nu$  position where this plateau occurs was observed to be sample dependent.

In Fig. 31 we present log-log plots of the tunneling  $I$ - $V$  characteristics (solid curves) for samples 1.1, and 1.3, over a wide range of magnetic fields/filling factors in order to deduce the behavior of the power-law exponent  $\alpha$  as a function of  $1/\nu$ . Successive curves are shifted in the positive direction on the horizontal axis by 0.3 units (a factor of 2) for clarity. The dashed curves represent best fits to the data. Essentially all traces for sample 1.1 exhibited the expected behavior with a low-bias linear region, an intermediate power-law region, and a large-bias saturation regime. Sample 1.3 exhibited a nonideal saturation regime, which may result from the opaqueness of the thicker tunnel barrier of 12.5 nm.

$\alpha$  was again extracted in a systematic way by fitting the entire  $I$ - $V$  range containing the three bias regimes to the Chamon-Fradkin expression for the tunnel current, with the added constraint that  $V_a = V + IR_s$  where  $V_a$  is the voltage applied on the device across contacts and  $R_s$  a 2DEG series resistance. Since the temperature was

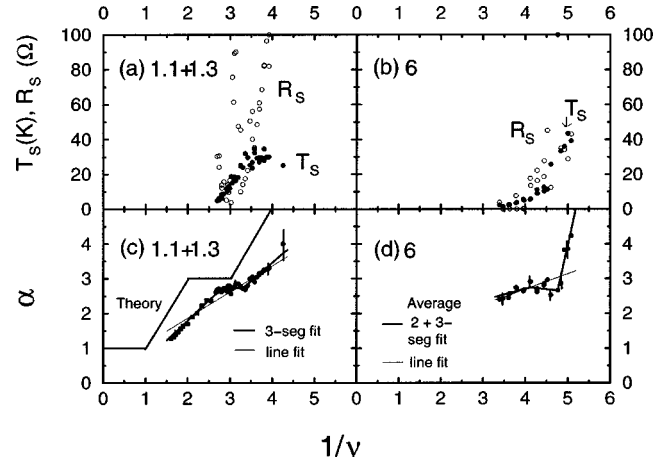


FIG. 32. The chiral Luttinger-liquid exponent  $\alpha$  vs  $1/\nu$ : (c) for samples 1.1 and 1.3; (d) for sample 6. Representative error bars are as shown and solid curves are as labeled. The parameters  $T_S$  and  $R_S$  vs  $1/\nu$ : (a) for sample 1.1; (b) for sample 6. From Chang *et al.*, 2001.

known, three parameters were needed:  $\alpha$ ,  $T_S$ , and the 2DEG series resistance  $R_s$ . Inclusion of the parameter  $R_s$  was necessary to properly fit the saturation regime, since at small filling factors (large  $1/\nu$ ) the background from the longitudinal resistance of the 2DEG ( $\rho_{xx}$ ) could be substantial (of order 100 k $\Omega$ ), and since the edge and bulk densities can differ (Levitov *et al.*, 2001; Chang, 2002).

Figure 32 summarizes the fitting parameters  $\alpha$ ,  $T_S$ , and  $R_s$  deduced for two sets of samples versus  $1/\nu$ . Results for samples 1.1 and 1.3 are presented together, since they contain an identical 2DEG. Focusing our attention on  $\alpha$  in panels (c) and (d). The presence of a plateau was established by fitting our  $\alpha$  vs  $1/\nu$  data to curves containing (i) three line segments, where the middle exhibited a reduced slope, (ii) two line segments, and (iii) a single straight line, indexed by 3, 2, and 1, respectively. Application of the statistical  $F$  test (Chang *et al.*, 2001), conclusively demonstrated that the fits containing a plateau feature were superior. In both data sets the plateau region was found to occur at  $\alpha \sim 2.7$  with corresponding reduced slopes of  $0.15 \pm 0.15$  and  $-0.14 \pm 0.18$ . In terms of  $1/\nu$  the plateau region occurred at  $2.76 < 1/\nu < 3.33$  and  $4.12 < 1/\nu < 4.76$ , respectively. These positions were shifted to higher values compared to the theoretical prediction of  $2 < 1/\nu < 3.3$  (Kane and Fisher, 1995; Shytov *et al.*, 1998) with the finite Hall plateau width taken into account. In the first sample set, the position corresponded well with the bulk  $\nu=1/3$  quantum Hall plateau. In the second set it was shifted substantially beyond the position of the  $\nu=1/3$  Hall plateau. At present it is not fully understood how this shift occurs, although one possibility might be edge reconstruction due to density gradients (Lee and Wen, 1998).

More recently, Hilke *et al.* studied edge tunneling in a cleaved-edge device with a relatively high 2D electron density, but very low  $n$ + doping ( $3 \times 10^{17} \text{ cm}^{-3}$ ) and found a transition between Fermi-liquid and Luttinger-

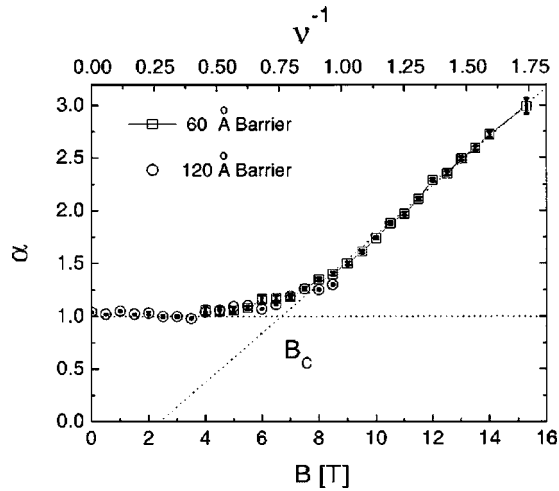


FIG. 33. The chiral Luttinger liquid exponent  $\alpha$  vs the bulk inverse filling,  $1/\nu_{\text{bulk}}$  (top axis), and vs the magnetic field,  $B$  (bottom axis): circular data points, a 12-nm-wide barrier; square data points, a 6-nm-wide barrier. From Hilke *et al.*, 2001.

liquid behavior, qualitatively confirming the above results. The extracted exponents are shown in Fig. 33.

They estimated the edge density that is reduced by 24% from the bulk value and pointed out that with this reduction their data are consistent with an  $\alpha$  reaching  $\sim 3$  at  $1/\nu_{\text{edge}} \approx 2.25$ , close to the value of 2 predicted by the effective-field theories. However, it appears that their estimate, deduced from identifying the position where  $\alpha$  began increasing beyond the Fermi-liquid value of  $\sim 1$  as the  $\nu_{\text{edge}} = 1$  position, did not include the contribution of the finite  $\nu = 1$  Hall plateau width. Inclusion of this width yields a result consistent with Figs. 30 and 32 above.

#### 5. Resonant tunneling into a biased fractional quantum Hall edge

Aside from excellent power-law behavior in the off-resonance tunneling characteristics detailed above, it was mentioned in Sec. II.B.6 that manifestations of CLL behavior should be observable in resonance tunneling as well. Here we briefly discuss resonant tunneling into a *voltage-biased* fractional quantum Hall edge, made possible only by the atomically sharp tunneling barriers unique to cleaved-edge overgrown devices. In the resonances observed on the  $\nu = 1/3$  Hall plateau region, we were able to identify different tunnel coupling strengths to the metallic lead and to the fractional quantum Hall edge. The discovery and characterization of the resonances described in this section represents a new direction for studies of the physics of the fractional quantum Hall edge.

Samples 1.1 and 2 were studied (see Table I for sample parameters). In particular, sample 1.1 was studied in two cooldowns labeled, respectively, as 1.1A and 1.1B, and different resonances were identified by appending an additional suffix (1.1Ba, 1.1Bb, etc.). In our presentation, all filling factors refer to the bulk values.

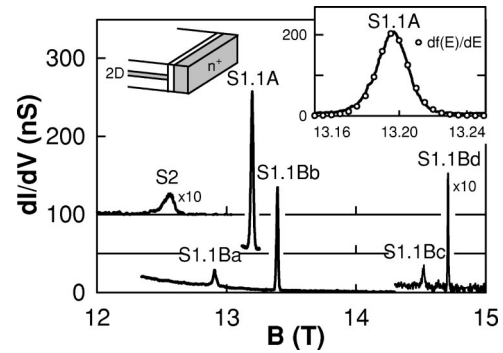


FIG. 34. Conductance resonance for samples 2, 1.1A, and 1.1B (S2, S1.1A, and S1.1B, respectively). Inset, right: 1.1A plotted with expanded scale against a derivative Fermi function. Inset, left: device. From Grayson *et al.*, 2001.

Figure 34 shows that in sample 2 the zero-bias differential conductance  $dI/dV$  at  $V=0$ , exhibited a resonance at  $\nu_{\text{bulk}} = 0.294$  ( $B = 12.6$  T); sample 1.1A showed the strongest resonance at  $\nu_{\text{bulk}} = 0.338 \sim 1/3$  ( $B = 13.2$  T). For the second cooldown 1.1B, four resonances, 1.1Ba, 1.1Bb, 1.1Bc, and 1.1Bd, were obtained, with the first two, 1.1Ba and 1.1Bb, located at  $\nu_{\text{bulk}} = 0.346$  and  $0.333$  ( $B = 12.9$  and  $13.4$  T), respectively, within the  $1/3$  Hall plateau region. We focus on resonances 1.1A and 1.1Ba, labeled S1.1A and S1.1Ba.

To compare S1.1A and S1.1Ba, we measured the bias dependence of the differential conductance as a function of  $B$ , by adding a fixed dc bias to the ac square wave (Fig. 35), with a convention that applied the signed voltage to the  $n^+$  electrode while the 2DEG was held at ground. Under bias the background conductance increased due to the power-law density of states. For S1.1A (Fig. 35 right), the peak split into two peaks of different height, with a separation in  $B$  proportional to the applied voltage. The excess area subtended by the

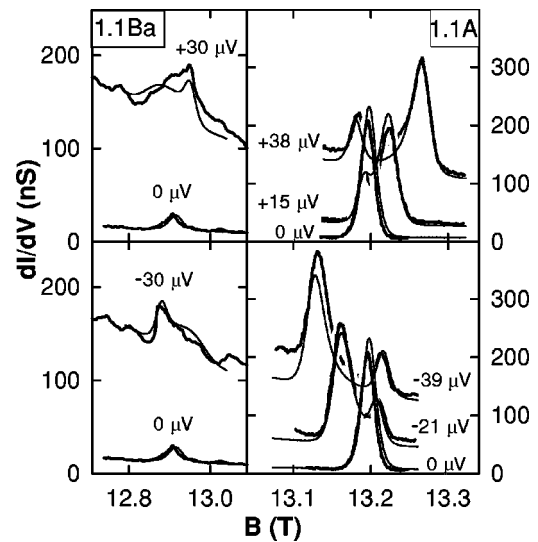


FIG. 35.  $dI/dV$  vs  $B$  at fixed dc bias for resonances 1.1Ba and 1.1A: fine lines, data; heavy lines, fit. From Grayson *et al.*, 2001.

TABLE III. Parameters for lever-arm model.

	1.1A (Fermi liquid)	1.1Ba (CLL)	1.1Bb (Fermi liquid)	
$\lambda'$	0.20	0.30	0.20	Lever arm
$\beta$	+0.43 meV/T	-0.26 meV/T	+0.59 meV/T	$dE_r/dB$
$\Gamma_{\text{FL}}$	1.3	1.0	1.0	Coupling to $n^+$
$\Gamma_{\text{CLL}}$	19.7	3.5	14.0	Coupling to quantum Hall edge
	$\times 1.5 \pm .1$	$\times 6 \pm 1$	$\times 1.7 \pm .1$	Area increase—data
	( $\times 1.54$ )	( $\times 5.9$ )	( $\times 1.58$ )	(Area increase—fit)
	39 $\mu\text{eV}$	30 $\mu\text{eV}$	30 $\mu\text{eV}$	at bias voltage

two peaks above the background increased slightly. In contrast, resonance S1.1Ba (Fig. 35, left), instead of splitting, broadened into an asymmetric single peak that leaned to the right (left) for positive (negative) bias. Notably, at a dc bias of 30  $\mu\text{V}$  the area subtended by the resonance above background increased dramatically, by a factor of  $\sim 6$ , an altogether different qualitative behavior from that of S1.1A.

The differing Fermi-liquid-like and chiral Luttinger-liquid (CLL)-like behaviors for resonances S1.1A and S1.1Ba, respectively, arose from the different *relative coupling strengths* of the resonance to the two leads, where we employ the notation  $\Gamma_{\text{FL}}$  for the tunnel coupling from the resonant state to the  $n^+$  lead, and  $\Gamma_{\text{CLL}}$  to the quantum Hall edge. The strongest peak is a factor of 100 smaller than the perfect resonant conductance,  $e^2/3h$ , indicating that overall the resonance is in the weakly coupled limit. We utilize a simple model in which the real-space position of the resonance in the tunnel junction causes the resonance energy  $E_r$  to depend on bias. Assuming the resonance is bound to the local band structure inside the barrier with energy  $E_0$ , and defining the lever-arm parameter  $\lambda$  as the fraction of the applied bias that falls to the weakly coupled side of the resonance yields (Grayson *et al.*, 2001)

$$E_r(V, B) = \lambda eV + \beta B + E_0. \quad (230)$$

In addition, the magnetic field can be related to an energy scale:

$$|\beta_T| = \left| \frac{dE}{dB} \right| = \frac{\Delta E}{\Delta B} = 0.42 \text{ meV/T}. \quad (231)$$

A reasonable quantitative fit of the data was achieved by adopting the resonance formalism of Chamon and Wen (1993) for sequential tunneling between biased chiral Luttinger liquids to the present situation where tunneling takes place from  $\text{ann}+\text{GaAs}$  metal into the  $\nu = 1/3$  edge (Sec. II.B.6). The simulated resonance curves are plotted with heavy lines against the data in Fig. 35. The resulting fitting parameters are shown in Table III. Here, the fit was not sufficiently precise to distinguish between an exponent of  $\alpha=3$  or 2.7, however. The device-specific lever-arm parameter  $\lambda'$  denotes the fraction of voltage bias on the  $n^+$  side of the resonant state.

#### D. Discussion: Is the chiral Luttinger liquid exponent universal?

The cumulative evidence from electron-tunneling measurements presented in the previous sections indicates that the chiral Luttinger liquid power-law exponent  $\alpha$ , for tunneling into the fractional quantum Hall edge, deviates substantially from the universal behavior predicted by the effective field theories. Let us summarize, again, the experimental findings to date. The results which we have established are

- (1) a power-law behavior for electron tunneling into the fractional quantum Hall edge observed in the  $I$ - $V$  characteristics at all filling factors from  $\nu=1$  to  $\nu \approx 5$ , indicative of chiral Luttinger behavior for the fractional Hall edge;
- (2) the power-law exponent  $\alpha$  defined by  $I \propto V^\alpha$ , when plotted versus  $1/\nu$ , exhibits a plateau for exponent values near  $\alpha \approx 2.7$  for the highest-quality samples, and otherwise behaves roughly as  $1/\nu$ ; and
- (3) in some samples the  $1/\nu$  position where the plateauing in  $\alpha$  occurs can be shifted to higher  $1/\nu$ , where  $\nu$  refers the filling deduced from the bulk 2DEG carrier density, when compared to the expected position center about  $1/\nu=3$  corresponding to the  $\nu = 1/3$  fractional quantum Hall effect.

For comparison, we summarize the predictions of the 1D, edge effective-field theories, which strictly speaking are appropriate for the short-ranged,  $\delta''(\mathbf{r})$  type of interaction (Sec. II.B). Findings from numerical studies will be discussed below.

- (1) Power-law tunneling characteristics. This is the most fundamental chiral Luttinger liquid behavior for incompressible fluids.
- (2) Universality in the tunneling exponent. This is directly tied to the topological characterization of the incompressible fluids. In particular, for the  $1/m$  Laughlin fluids  $\alpha=m$  exactly, while for all Jain-sequence incompressible fluids related to the  $1/m$  fluid containing co-propagating edge modes only (i.e., the  $\nu=|n|/|pn|+1$  series with  $p$  even), the exponent takes the identical value of  $\alpha=|p|+1=m$ . This universality holds regardless of disorder or

edge imperfections, as long as the Hall conductance is quantized. For the Jain series containing counter-propagating modes where  $\nu = -|n|/|pn| - 1$ , the exponents will differ. However, residual disorder drives these to universal values given by  $\alpha = 1 + |p| - 2/|n|$ .

- (3) Luttinger-liquid-like edge dynamics for compressible fluids under the condition of small longitudinal resistivity ( $\rho_{xx} \ll \rho_{xy}$ ). Here the exponent is driven by disorder to nearly universal values approximated by an interpolation between the Jain series values.

Aside from the basic power-law dependence, the experimental results stand in stark contrast to the predictions of the effective-field theories. The key differences are as follows:

- (1) The exponent for tunneling into the  $\nu = 1/3$  edge is always observed to be less than 3. This is a first indication of nonuniversal behavior. The systematic error for the quoted plateau value in  $\alpha$  of  $\approx 2.7$  is unlikely to exceed 0.15, while the uncertainty based on random noise is smaller, of order 0.05. The measured exponent therefore falls below the value of exactly 3 as required by the topological nature of the exponent. Note that the long-range Coulomb interaction can lead to a logarithmic correction to the power-law dependence, yielding an effective, energy-dependent exponent that exceeds 3 (Imura and Nagaosa, 1997; Zheng and Yu, 1997; Zülicke and MacDonald, 1997; Levitov *et al.*, 2001).
- (2) The occurrence of the plateau feature in  $\alpha$  is sample dependent and very sensitive to the sample quality.
- (3) Accounting for the quantized Hall plateau width at  $\rho_{xy}/(h/e^2) = 3$ , and the difference between edge and bulk densities (and hence filling factors), the  $\alpha$  versus  $\rho_{xy}/(h/e^2)$  plot (as opposed to versus  $1/\nu$ ) behaves roughly as  $1/[\rho_{xy}/(h/e^2)]$ , or as  $1/\nu$  in the absence of a plateau feature in  $\alpha$ , in contrast to the steplike dependence shown in Fig. 7. In any event, even generously allowing for experimental error in the determination of the edge filling factor  $\nu_{edge}$  and of  $\alpha$ ,  $\alpha$  shows no evidence of reaching the predicted value of 3 (Shytov *et al.*, 1998; Levitov *et al.*, 2001) at  $1/\nu = 2$  ( $\nu = 1/2$ ).
- (4) The edge-tunneling exponent  $\alpha$  is *not* directly tied to the bulk filling factor, as evidenced by the large shifts in  $1/\nu$  position in some samples (Chang *et al.*, 2001; Hilke *et al.*, 2001). Such indications of nonuniversality are found in all existing work in the cleaved-edge geometry (Chang *et al.*, 1996, 1998, 2001; Grayson *et al.*, 1998; Hilke *et al.*, 2001).

First we need to address the issue of the difference in the edge versus bulk 2DEG density (Levitov *et al.*, 2001; Chang, 2002). Due to the chemical potential imbalance between the 2DEG and the 3D  $n +$  doped GaAs, charge transfer can occur across the tunnel barrier, leading to an inhomogeneous density profile near the tunneling edge. It is therefore not surprising to have an edge density different from the bulk. The tunneling experiment

probes a spatial region within a few magnetic lengths  $l_o$  of the boundary and is therefore sensitive to the edge density, which may differ from the bulk 2DEG density. The Hall resistance (conductance), on the other hand, directly reflects the bulk density and should be insensitive to the edge density so long as the sample boundary is sufficiently long to allow for a full equilibrium of the edge modes. These edge modes may include, in addition to the boundary modes at the outermost edge of the sample, those which exist in the transition region between the edge and bulk density regions.

In the absence of a direct method for independently determining the edge density, we propose the following method to produce an estimate which we argue should be accurate to 5–10%. We would reasonably expect the tunneling exponent to remain nearly constant when the Hall resistance  $\rho_{xy}$  is quantized at  $3(h/e^2)$  (note  $\rho_{xx} \ll \rho_{xy}$  always), and, at the same time, we would expect  $\alpha$  to be able to exceed 3 only when  $\rho_{xy}/(h/e^2)$  exceeds 3. We can therefore determine the  $1/\nu_{edge} = 3$  ( $\nu_{edge} = 1/3$ ) position by the  $1/\nu_{bulk}$  value where  $\alpha$  first exceeds 3, or more accurately, where it exceeds the experimental plateau value of 2.7. This position value must be reduced by roughly 5%, equaling one-half of a typical  $1/3$  Hall plateau width. In samples that do not exhibit a plateau in  $\alpha$ , the corresponding  $1/\nu_{edge} = 3$  position is simply given by the  $1/\nu_{bulk}$  value where  $\alpha = 2.7$ . For example, in samples 1.1 and 2, this yields an edge density roughly equal to 1.05 of the bulk density. Based on this type of estimate, it would appear that the plateau feature in  $\alpha$  is more likely ascribable to the finite width of the Hall plateau than to a step of the type predicted by the effective-field theories. In any event, the exponent at  $\nu_{edge} = 1/2$  is highly unlikely to reach the value 3, as noted above. While there might be legitimate concern that the edge density profile could be highly inhomogeneous, i.e., not constant on the scale of a few magnetic lengths, the prediction that the exponent must remain unchanged within a rather large range from  $1/\nu_{edge} = 2$  to 3 [more precisely  $2 \leq \rho_{xy}/(h/e^2) \leq 3$ ] means that even if some type of weighted averaging over density is necessary, the exponent will most likely still take on the topological value of 3, albeit over a reduced range.  $\nu_{edge}$  may be estimated from other  $\alpha$  plateau positions as well. Estimates from  $\alpha \sim 1$  (Hilke *et al.*, 2001) tend to be less accurate, however. Near 1,  $\alpha$  can readily be distorted by other residual nonlinearities such as those arising from slight changes in barrier shape with bias, and there is greater difficulty in estimating the edge  $\nu = 1$  Hall plateau width.

At this point it is imperative to examine all the non-idealities that could lead to the discrepancy between experiment and theory. Two major issues come to mind: (i) the long-range nature of the Coulomb interaction, and (ii) a nonconstant density profile near the tunneling edge, leading to edge reconstruction. Based on the effective-field theories, long-range Coulomb interactions will lead to a  $\log_{10}(V)$  correction in the power-law relation, with an increase in the effective exponent at low energies (Wen, 1992; Zülicke and MacDonald, 1996, 1997; Shytov *et al.*, 1998; Levitov *et al.*, 2001). However,

interestingly enough, no evidence of this type is observable in the tunneling data despite the large dynamic range in the  $I$ - $V$ , as evidenced by a nearly perfect straight line in the power-law region of the data. Furthermore, the observation of  $\alpha \sim 1/\nu$ , in one interpretation, is an indication that only the charged mode is observable in tunneling, while the neutral modes (see Sec. II.B.3) become effectively decoupled from the tunneling process. On the other hand, based on the large dynamic range spanned by the data, a  $\log_{10}(V)$  increase in the propagation velocity of the charged mode relative to the neutral modes appears insufficient to separate out the respective energy scales and lead to the apparent absence of a contribution from the neutral modes (Lee and Wen, 1998). Edge reconstruction, however, can lead to the formation of extra edge modes, which can renormalize the exponent when counterpropagating varieties are present.

A number of works have attempted to explain the discrepancy between experiment and the effective-field theories. The following approaches have been explored:

- (i) finding sensible mechanisms to ensure that only the charged mode (see Sec. II.B.3) contributes to the tunneling exponent, yielding  $\alpha \approx 1/\nu$ , while the neutral modes are undetectable. These mechanisms include a separation of energy scales for the different types of modes (Zülicke and MacDonald, 1996, 1997, 1999; Lee and Wen, 1998; Zülicke *et al.*, 1998), and topological constructions (Lopez and Fradkin, 1999);
- (ii) the introduction of extra edge modes, which result from edge reconstruction (Chamon and Wen, 1994; Lee and Wen, 1998) or smooth disorder, which can produce local pockets of differing filling values (Pruisken *et al.*, 1999; Skoric and Pruisken, 1999);
- (iii) coupling to additional impurity levels located near the chiral edge (Aleksiev *et al.*, 2000);
- (iv) continuum elasticity theory (Conti and Vignale, 1996, 1997, 1998; Han, 1997; Han and Thouless, 1997a, 1997b),
- (v) various other scenarios and possibilities (Yu *et al.*, 1997; Imura, 1999; Khveshchenko, 1999, 2000; Yang *et al.*, 2000; Yu, 2000).

Thus far, no clear consensus has emerged as to what the correct picture should be. In view of the lack of a coherent picture it is necessary to consider scenarios that go beyond mere extensions of the existing effective-field-theory analyses. The key pieces of physics which may be missing from the idealized model of the fractional quantum Hall fluid edge include extra edge modes from edge reconstruction, and the renormalization of the exponent due to the long-range potential  $V(r)$ , or due even to any type of interaction potential that differs from the idealized  $\delta''(r)$  potential.

Several recent and independent numerical, finite-systems studies are beginning to yield evidence indicating that, indeed, a renormalization of the edge tunneling exponent is possible. These include exact numerical di-

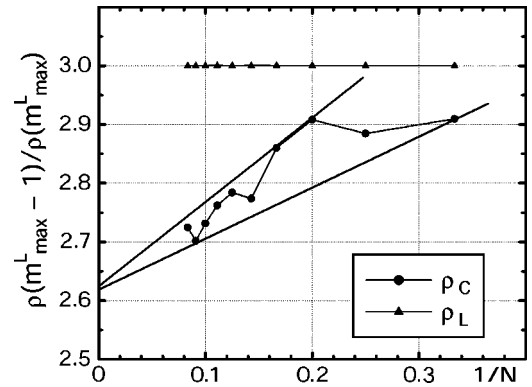


FIG. 36. The ratio of the angular momentum occupation number  $\rho(m)$ , for  $N$  interacting electrons on the disk. This ratio measures the power-law decay exponent of the equal-time correlation function, which is believed to be identical to the equal-space exponent measured in experiment. Shown are the Laughlin state  $\rho_L$  for a short-range interaction and the exact ground state for the Coulomb interaction  $\rho_C$ . Solid lines indicate the bounds for  $\rho(m)$ . From Goldman and Tsiper, 2001.

agonalization in a disk geometry (Goldman and Tsiper, 2001) as well as calculations based on the mixing of composite-fermion Landau-level wave functions at the sample edge (Mandal and Jain, 2001). It was found that for a 3D Coulomb interaction the exponent  $\nu = 1/3$  is no longer universal and instead takes on a value in the 2.5–2.75 range. In the exact diagonalization calculation by Goldman and Tsiper (2001), the exponent value for up to 12 particles is shown in Fig. 36. Extrapolating to an infinite system yields a value of  $\alpha$  which falls between 2.58 and 2.75. In a separate and related work, Mandal and Jain (2001) studied a system of up to 40 particles using composite-fermion wave functions and found a similar renormalization of the exponent at  $\nu = 1/3$ . Another study investigating the effect of the edge confinement potential (Wan *et al.*, 2000) has found evidence for reconstruction of the edge leading to extra counterpropagating modes and a possible renormalization of the exponent. In all such numerical calculations, it was found that extra oscillations in the density which are absent in a Laughlin-type edge wave function occur near the edge. Although the largest system studied was on the order of a few tens of electrons and cannot be taken as rigorous proof for the thermodynamic limit, it is nevertheless clear that in all situations where the interacting potential or edge confinement favors the Laughlin-type edge function, the “universal” exponent value of 3 is recovered for the  $\nu = 1/3$  fractional Hall edge. Deviation from this universal value arises only when the Laughlin-type edge wave function is no longer exact and is modified. These new developments suggest that the edge dynamics in the fractional quantum Hall regime may be more complex than previously thought and could well lead to further discoveries of novel and interesting physics.

Taken as a whole, our experimental results in conjunction with the recent numerical work suggest that the existing analyses based on effective 2D Chern-Simon field

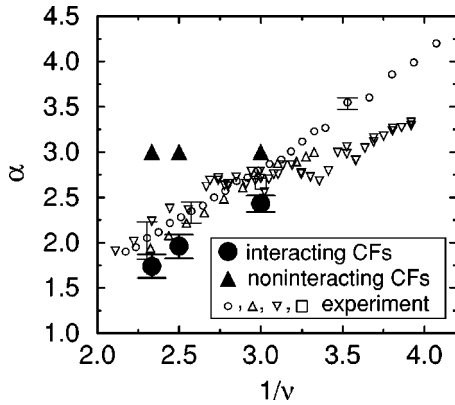


FIG. 37. Tomonaga-Luttinger exponent  $\alpha$ , for the fractional quantum Hall edge fluid as a function of the inverse filling factor  $1/\nu$ . ●, theoretical values for interacting composite fermions (CF) at  $\nu=1/3$ ,  $2/5$ , and  $3/7$ ; ▲, theoretical values for noninteracting composite fermions at the same  $\nu$ . The experimental results (open symbols) are taken from the following sources: □, Chang *et al.* (1996; sample 2); ○, △, from Grayson *et al.* (1998; samples 1.1 and 2 in this review); ▽, Chang *et al.* (2001; samples 1.1 and 1.3 in this review). From Mandal and Jain, 2002.

theories (Girvin and MacDonald, 1987; Read, 1989; Zhang *et al.*, 1989; Wen and Niu, 1990; Frohlich and Zee, 1991; Wen, 1995) deserve careful reexamination when applied to the dynamics at the Hall fluid edge. These results raise questions regarding our fundamental understanding of the connection between edge dynamics and the topological characterization of bulk fluids, even though the hallmark feature of the Luttinger liquid, i.e., power-law tunneling, is unequivocally established. Despite the fact that finite-size calculations cannot be taken as definitive proofs, the combined experimental and computational evidence should stimulate a reexamination of the detailed properties of the rich and novel physics at the edge of the fractional quantum Hall fluids. Very recently, Mandal and Jain (2002) have extended their work on the mixing of composite-fermion Landau levels to the  $\nu=2/5$  and  $3/7$  fractional Hall fluid edge. They found that in the absence of composite-fermion Landau-level interaction, the exponent is quantized at exactly 3, in agreement with existing effective-field theories (Sec. II.B). However, as soon as interaction is introduced, the exponent is renormalized downward from 3. In Fig. 37 we show their results plotted alongside experimental data taken from Sec. III.C.4. The good quantitative agreement is striking. Mandal and Jain went on to point out that the appearance of nonuniversality may be a sign that in an effective 1D theory of the edge, the electron operator (see Sec. II.B.1) has become nonlocal in character. If proven correct, this is a major and significant new development in our understanding of the chiral Luttinger liquid and of 1D Tomonaga-Luttinger liquids in general.

### E. Shot-noise characteristics and fractional charges

Aside from a determination of the power-law tunneling density of states discussed in detail in the above sec-

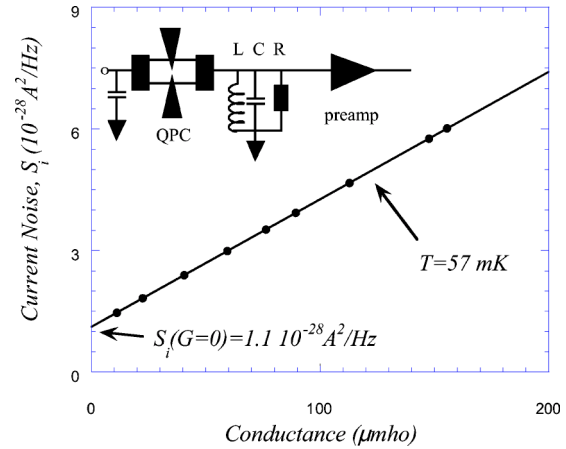


FIG. 38. (Color in online edition) The total current noise inferred to the input of the preamplifier as a function of the input conductance at equilibrium (circles). The measured noise is a sum of thermal noise and the (conductance-independent) noise of the amplifier (intercept of the vertical axis at zero conductance). Inset, the quantum point contact (QPC) embedded in the 2D electron gas is shown to be connected to an LCR tank circuit at the input of a cryogenic preamplifier. From De-Picciotto *et al.*, 1997.

tions, there are other consequences of a chiral Luttinger liquid description of edge dynamics. Particularly intriguing is the possibility of a direct measurement of the quasiparticle fractional charge predicted for the Laughlin incompressible states (Laughlin, 1983). There have been two approaches to the detection of fractional charge, (i) transport through antidots in which the edge states encircling an antidot can mediate backscattering between counterpropagating edge modes on opposing boundaries, at opposite sides of a device, and (ii) a direct measurement of the quantum shot noise in the regime of quasiparticle tunneling between counterpropagating edge modes at opposing boundaries when the boundaries are brought into close contact.

Simmons *et al.* (1989) first attempted to determine the fractional charge of the Laughlin quasiparticles in the  $\nu=1/3$  fractional quantum Hall fluid by studying the Aharonov-Bohm quantum interference effect in narrow wires. They observed a suggestive tripling of the magnetic-field period in the Aharonov-Bohm oscillations when going from the  $\nu=1$  integer Hall effect to the  $\nu=1/3$  fractional Hall effect. Such oscillations were a result of the presence of edge states encircling an accidental impurity site mediating the tunneling between edges. Although suggestive, it was argued that the period tripling was more likely associated with a difference in energy scales, rather than a direct manifestation of the quasiparticle charge (Lee, 1990; Thouless and Gefen, 1991). Subsequently, Goldman and Su (1995) reported an extremely interesting result from introducing a submicron-size antidot (potential hill) between counterpropagating fractional Hall edges to mediate tunneling, implemented in a conventional planar geometry. By combining the Aharonov-Bohm period in the tunneling conductance and the backgate voltage period, which

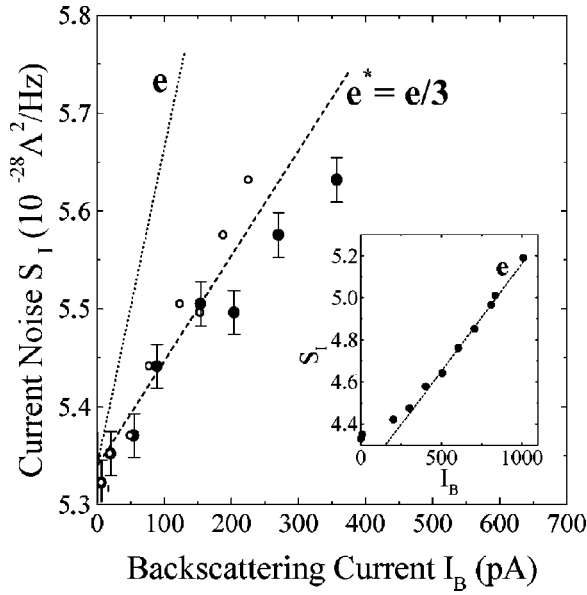


FIG. 39. Tunneling noise at  $\nu=1/3$  as a function of the backscattering current,  $I_B = (e^2/3h)V_{ds} - I$  (filled circles), and as a function of  $I_B(1 - I_B 3h/e^2 V_{ds})$ : dashed line, slope for  $e/3$  quasiparticles; dotted line, slope for electrons. The temperature is 25 mK. Inset, data showing electron tunneling but in the integer quantum Hall regime at  $\nu=4$ . The data follow the expected slope for charge  $e$ . Adapted from Saminadayar *et al.*, 1997.

modulates the carrier density, and relating the area of the antidot determined in the two measurements, they were able to determine the quasiparticle charge for the  $\nu=1/3, 2/5$ , and higher-order states. An alternative interpretation of this type of experiment, however, has been advanced by Franklin *et al.* (1996).

Two groups have independently accomplished the technically impressive feat of measuring tunneling-

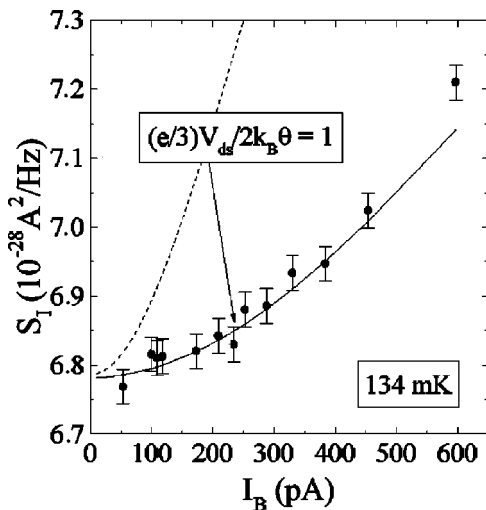


FIG. 40. Crossover from Johnson-Nyquist to shot noise. The arrow indicates the data for which  $e^*V_{ds} = 2k_B T$ . Solid curve, comparison with Eq. (232); dotted curve, comparison with a similar expression for electrons. Adapted from Saminadayar *et al.*, 1997.

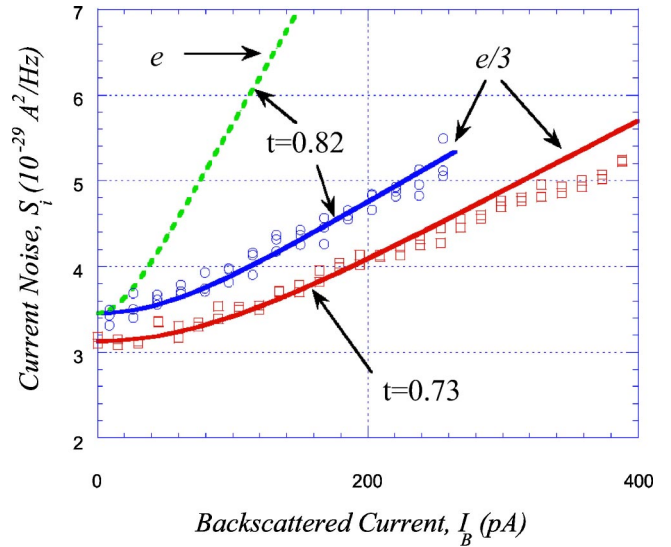


FIG. 41. (Color in online edition) Quantum shot noise as a function of the backscatter current  $I_B$  in the fractional quantum Hall regime at  $\nu=1/3$  for two different transmission coefficients through the quantum point contact (circles and squares): solid lines, Eq. (232) with a charge  $Q=e/3$  and the appropriate transmission probability,  $t$ ; dotted line, the expected behavior of the noise for  $Q=e$ . From De-Picciotto *et al.*, 1997.

current shot noise in the fractional Hall regime discussed in Sec. II.B.7 of the theory section. These experiments probed quasiparticle tunneling and were performed in the versatile, point-contact geometry. By alternatively using a tank circuitry at 4 MHz coupled to a low-noise GaAs preamp operated at low temperatures (Fig. 38) or using noise-correlation techniques, De-Picciotto *et al.* (1997) and Saminadayar *et al.* (1997) independently measured the “low” frequency noise down to the  $10^{-14}$  A/ $\sqrt{\text{Hz}}$  level and below. The resultant noise curves for tunneling between two counterpropagating  $\nu=1/3$  edges are shown in Figs. 39–41. In the fractional Hall regime where  $e/3$  charged quasiparticles are expected to dominate the tunneling between counterpropagating  $\nu=1/3$  edge modes, the noise characteristics as a function of backscattered current could no longer be accounted for by the conventional shot-noise expression involving  $e$  charge carriers. Instead, the data were successfully fitted by extending the conventional expression via a replacement of the electron charge  $e$  by the fractional charge  $e^*$  (Fendley *et al.*, 1995c; De-Picciotto *et al.*, 1997; Saminadayar *et al.*, 1997; see also Reznikov *et al.*, 1999):

$$S_I = 2g_o t(1-t) \left[ e^* V \coth\left(\frac{e^* V}{2kT}\right) - 2kT \right] + 4kT g_o t, \tag{232}$$

where  $g_o t(1-t)V = I_{Bt} \approx I_B$  at low temperatures. Note that, to be more precise, the second and third terms in the above formula are sometimes expressed in terms of  $dI_B/dV$ , which accounts for the nonlinearity of the tunneling characteristics of chiral Luttinger liquids (Sami-

nadayar *et al.*, 1997). This expression closely approximates the exact solution computed numerically from the Bethe ansatz solution (Fendley *et al.*, 1995c). The data shown in Figs. 39–41 indicate that, remarkably, the quantum shot noise follows the expressions with  $e^* = e/3$  rather than  $e$ . This is a striking and significant result. More recently, additional measurements on other fractional fluids yielding the  $e/5$  fractional charge have also been reported (Reznikov *et al.*, 1999; Comforti *et al.*, 2002).

Associated with these experiments (Saminardayar *et al.*, 1997; De-Picciotto *et al.*, 1998; Glatli *et al.*, 2000; Griffiths *et al.*, 2000; Comforti *et al.*, 2002; Chung *et al.*, 2003a, 2003b; Roddaro *et al.*, 2003), the smooth edge issue within the point-contact must be carefully accounted for. Fortunately in these noise measurements the voltage excitations were often low,  $< 30 \mu\text{V}$ . As a result the distortion of the broad and smooth edge potential defined by electrostatic top gating is likely small. Nevertheless, several complications can arise. For instance, the tunneling  $I$ - $V$  characteristics often do not fully display the expected power-law exponent (Glatli *et al.*, 2000; Glatli, 2002). There is also an often observed and rather substantial shift in the filling factor at which  $e$  charge shot-noise signatures can be recovered, often taking place not at  $\nu=1$  but rather at significantly higher filling factors  $\nu$ . Anomalous charge values (nonstandard fractions) can also be observed in various regimes.

More recent experiments have focused on detailed investigations of the behavior of  $e^*$  as a function of backscattering in the point contact, characterized by  $t$ , the transmission probability through the point contact, from transparency to opaqueness. Remarkably, when  $t$  is very nearly 1, *no excess noise* was found on the Hall plateaus. This is a nontrivial indication of a strong-interaction effect. In the absence of interaction, at these fractional Landau fillings measurable shot noise should be present, reflecting the graininess of the electron charge  $e$ . Other results qualitatively supportive of the CLL picture have also emerged, as well as surprising and as yet unexplained behaviors. It has been found that a point contact tuned to relative transparency at high temperatures or when probed at high source-drain bias voltages will become opaque at low temperatures or source-drain bias. This remarkable feature is in agreement with the effective-field theories. On the other hand, the shot-noise characteristics have exhibited surprising tendencies to agree better with theory at intermediate and higher temperatures (50–150 mK), than at the lowest temperatures ( $< 50$  mK), where the quasiparticles appear to bunch together, leading to larger values of  $e^*$ . This unusual behavior was uncovered both for opaque (Glatli *et al.*, 2000) and transparent (Chung *et al.*, 2003a) settings. Specifically, at  $\nu=1/3$  Glatli *et al.* observed that  $e/3$  quasiparticles could not penetrate opaque point contacts, and above 48 mK the shot noise became Poissonian, with an effective charge of  $e^*=e$ , in good agreement with theory. At lower temperatures, e.g.,  $T=20$  mK, however, the shot noise exceeded that expected for carriers of charge  $e$ . Similarly, in a recent

study Chung *et al.* (2003b) found that at very low temperatures ( $\sim 9$  mK) and for a very transparent setting, the shot noise yielded charges of  $e^*=e/3$ ,  $2e/5$ , and  $< 3e/7$  for  $\nu=1/3$ ,  $2/5$ , and  $3/7$ . At slightly higher temperatures, charges  $e^*=e/3$ ,  $e/5$ , and  $e/7$  were recovered. Although this type of crossover behavior is anticipated by theory (Kane and Fisher, 1995), the observed temperature dependence of the backscattered current is completely at variance with expectations. Other surprises include reports by Griffiths *et al.* (2000) and Comforti *et al.* that  $e/5$  and  $e/3$  quasiparticles can traverse opaque barriers. At this point the cause of these intriguing observations (Chung *et al.*, 2003a; Kane and Fisher, 2003) is not clear. One possibility is complications from the influence of additional low-energy modes, e.g., phonons, as discussed by Rosenow and Halperin (2002), who made a first attempt at explaining why it has been possible to observe novel shot-noise behavior in the point contacts but not yet possible to find the predicted power-law  $I$ - $V$  characteristics.

#### IV. OTHER LUTTINGER LIQUID SYSTEMS

Evidence for one-dimensional physics has been observed not only at the edge of the fractional quantum Hall fluid, but also in several other interesting systems. These systems are emerging as fertile grounds for the investigation of the unique properties associated with an interacting 1D electron system. In this final section we present a brief summary of the most promising examples. These include ballistic 1D wires, carbon nanotubes, 1D atom chains, and the venerable quasi-1D system of Bechgaard and Fabre organic salts and blue-bronze conductors.

We have seen that, for the fractional quantum Hall edge, the chiral Luttinger liquid tunneling exponent in an idealized model is given by universal values determined by the topological characterization of the bulk 2D fluid, as discussed in Sec. II.B. Moreover in the case of a single edge branch, e.g., the  $\nu=1/3$  or  $1/5$  edges, the electron-tunneling exponent is related to the Hall conductance:  $\alpha=1/g$ , where  $g$  is the dimensionless Hall conductance,  $g=\nu$ . In the case of the Luttinger liquid in quantum wires, the exponent is again related to the conductance  $g$ . However, in general the exponent is not universal, since  $g$  is interaction dependent [Eq. (5), Sec. II.A]. Moreover, depending on the tunneling geometry, the exponent value takes different forms whether tunneling into the end of a Luttinger liquid or into the side from a normal-metal electrode (Kane and Fisher, 1992a; Egger and Gogolin, 1997; Kane *et al.*, 1997):

$$\alpha=1+[g^{-1}-1]/n_{ch}, \quad \alpha-1=[g^{-1}-1]/n_{ch}, \quad (233)$$

$$\alpha=1+[g+g^{-1}-2]/2n_{ch}, \quad \alpha-1=[g+g^{-1}-2]/2n_{ch}, \quad (234)$$

where  $n_{ch}$  is the number of conducting channels (modes), including spin. As will be seen below in the case of carbon nanotubes, both types of tunneling are realizable.

### A. Ballistic single-channel wires

Tarucha *et al.* (1995) pioneered the study of single-channel ballistic nanowires in top-gated devices implemented in the planar geometry. By using very-high-quality GaAs/Al<sub>x</sub>Ga<sub>1-x</sub>As crystals, they were able to observe a suppression in the quantized conductance below  $e^2/h$  for a single-channel ballistic point contact with a channel length as long as 10  $\mu\text{m}$ . To date the best evidence for Luttinger-liquid behavior in semiconductor ballistic nanowires is provided by cleaved-edge overgrowth nanowires (Yacoby *et al.*, 1996; Auslaender *et al.*, 2000). When the carrier density of the single-channel cleaved-edge wire is reduced, accidental imperfections along the wire lead to the formation of double tunnel barriers. Yacoby and colleagues were able to study the resultant resonances in the tunnel conductance. Although a non-Fermi-liquid line shape was not observable, the resonance linewidth  $\Gamma_i$  exhibited the nonlinear dependence on temperature expected for a Luttinger liquid, as shown in Fig. 42 (Furusaki, 1998; Auslaender *et al.*, 2000). This is an interesting and promising result. We need to improve dynamic range and consistency between independently measured power-law exponent values from the resonance linewidth,  $\alpha_{LW}=[g^{-1}-1]$ , and from 1D-wire tunneling conductance, where  $\alpha-1=2[g^{-1}-1]$  for end-to-end tunneling between two Luttinger-liquid segments, as well as the dimensionless conductance  $g$ . If these improvements can be met, then this system has the potential for fruitful investigations of momentum-resolved Luttinger-liquid properties (Altland *et al.*, 1999; Auslaender *et al.*, 2002).

### B. Carbon nanotubes

An extremely promising system for the investigation of conventional, nonchiral Luttinger liquids in a different realization of ballistic nanowires is the single-walled carbon nanotube/multiwalled carbon nanotube system. In the single-walled nanotube, due to the fact that the electronic wave function is spread over several atoms, the characteristic energy scale for Peierls distortion and the associated formation of an energy gap is exponentially suppressed and below accessible temperatures. Therefore the system is a nearly ideal 1D conductor albeit with a fourfold degeneracy due to the presence of two metallic bands and the spin degree of freedom (Egger and Gogolin, 1997; Kane *et al.*, 1997). Since typical nanotubes are a few microns in length, this finite length sets a lower cutoff energy, given by the Coulomb charging energy,  $E_C=e^2/2C\sim 2$  meV, below which the zero-dimensional Coulomb-blockade phenomenon dominates the transport. Note that here  $C$  is the nanotube capacitance to the environment. There are two relevant tunneling geometries readily achievable by clever fabrication methods and manipulation of the nanotubes on the surface of a substrate: (i) tunneling into the side wall, and (ii) tunneling into the end of a nanotube. In Figs. 43 and 44 we show the data obtained for single-walled nanotube bundles by Bockrath *et al.* (1999) for tunneling

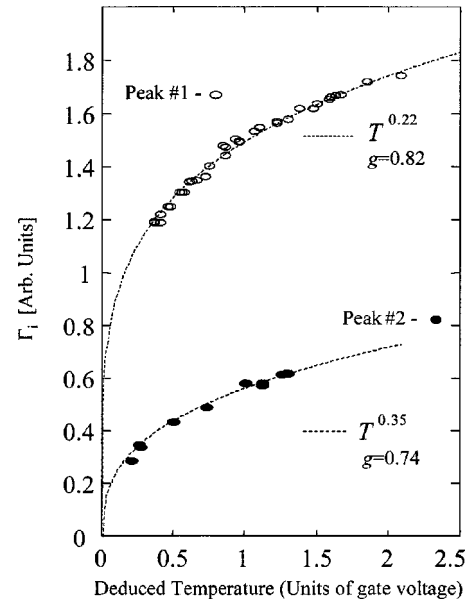


FIG. 42. The intrinsic linewidth of the resonance  $\Gamma_i$  vs temperature (in units of gate voltage). A power-law behavior is observed, indicating Luttinger-liquid behavior. Open and filled circles correspond to resonance peaks 1 and 2, respectively. Dashed lines are fits to the data. From Auslaender *et al.*, 2000.

from a metallic, gold contact. Above the Coulomb charging energy scale, behavior suggestive of power-law  $I$ - $V$ , and power-law tunneling conductance was observed (see Fig. 43). In a log-log plot, after accounting for contact resistance, power-law behavior was observed in the two contact geometries of side wall and end tunneling. In addition, Yao *et al.* (1999) have demonstrated that it is possible to achieve nanotube-to-nanotube tunneling in these geometries of side-wall-to-side-wall and end-to-end tunneling. The tunneling data exhibiting power-law signatures are shown in Figs. 45 and 46. In either case of metal-to-nanotube or nanotube-to-nanotube tunneling it is possible to deduce a consistent

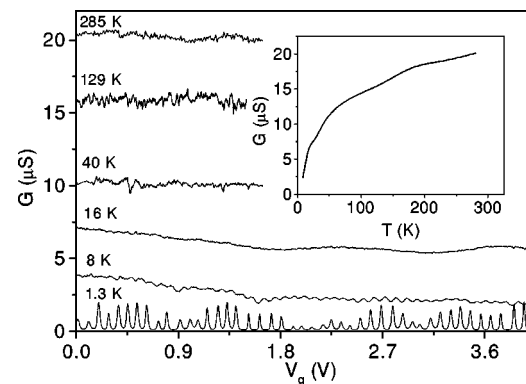


FIG. 43. The two-terminal linear-response conductance  $G$  vs gate voltage  $V_g$  for a sidewall-contacted metallic nanotube rope at different temperatures. The data show significant temperature dependence for energy scales above the Coulomb charging energy  $E_C$ . Inset, average conductance as a function of temperature. From Bockrath *et al.*, 1999.

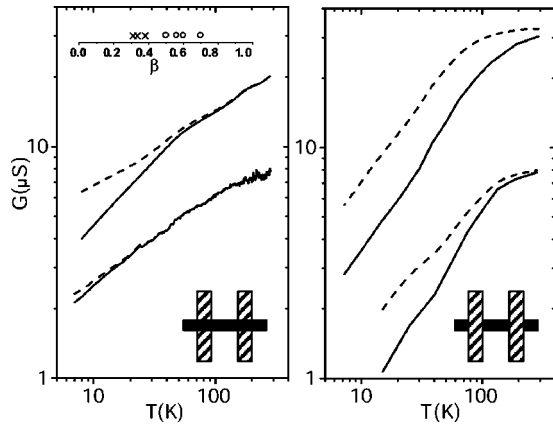


FIG. 44. Log-log plots of the conductance  $G$  vs temperature  $T$  for individual nanotube ropes: (a) data for ropes that are deposited over predefined leads (sidewall-contacted); (b) data for ropes that are contacted by evaporating the leads on top of the ropes (end-contacted). Insets show the respective geometries; solid lines, the raw data; dashed lines, the data corrected for the temperature dependence of the Coulomb-blockade contribution. After correction, the dependences follow a power-law form with a different exponent for the two geometries. The upper inset to (a) shows the power-law exponent  $\beta$  inferred for a variety of samples. Open circles denote end-contacted samples, and crosses denote bulk-contacted ones. Adapted from Bockrath *et al.*, 1999.

value of the conductance, based on the expressions given above for the tunneling exponent, Eqs. (233) and (234). The deduced value of  $g \sim 0.22$  is also consistent with theoretical estimates (Egger and Gogolin, 1997; Kane *et al.*, 1997). These initial findings bode well for future studies. Particularly noteworthy is the current trend towards the growth of extremely long single-

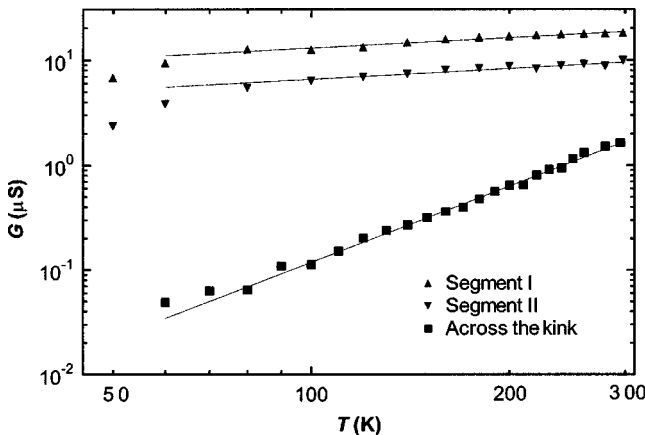


FIG. 45. Linear-response two-probe conductances  $G$  for tunneling into an individual single-walled carbon nanotube plotted against temperature  $T$ , on a log-log scale. The data are fitted (solid lines) by the power law  $G(T) \propto T^\beta$ . The exponent  $\beta$  for the two straight segments (I and II) is roughly 0.34, corresponding to sidewall tunneling. Across the kink where tunneling occurs between the ends of two single-walled nanotube segments an exponent  $\beta$  of 2.2 is obtained. From Yao *et al.*, 1999.

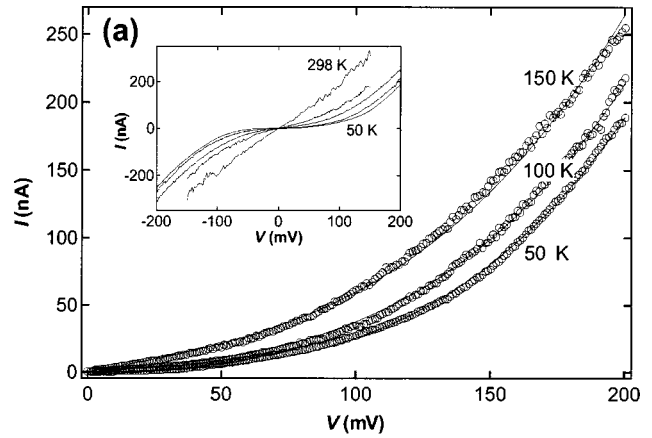


FIG. 46. Large-voltage-bias transport characteristics: (a) non-linear  $I$ - $V$  characteristics; the inset shows  $I$ - $V$  curves at temperatures of 298, 200, 150, 100, and 50 K; (b) scaled differential conductance plotted against the dimensionless voltage bias,  $eV/k_B T$ , for tunneling across the kink (end-to-end tunneling). The data for different temperatures collapse onto a single universal curve. The dashed line represents the theoretical expectation corresponding to the exponent  $\beta=2.2$ . Adapted from Yao *et al.*, 1999.

walled nanotubes—up to mm in length. These long tubes, once proven to be ballistic, should greatly expand the available low-energy range for Luttinger-liquid behavior by reducing the limitation set by the lower energy cutoff resulting from finite size.

C. One-dimensional gold atom chains

Another unique and promising 1D system has recently been created, that of single-atom-wide, 1D Au chains on the vicinal silicon [111] surface ( $9.45^\circ$  mis-cut in the  $[\bar{1}\bar{1}2]$  direction) (Bertel and Lehmann, 1988; Segovia *et al.*, 1999; see also Hill and McLean, 1997 for indium atoms). In an intriguing experiment, Segovia *et al.* (1999) reported angle-resolved photoemission measurements at low temperatures ( $\sim 10$  K) which probed the spectral density of the 1D chains as a function of momentum. They observed the absence of a qua-

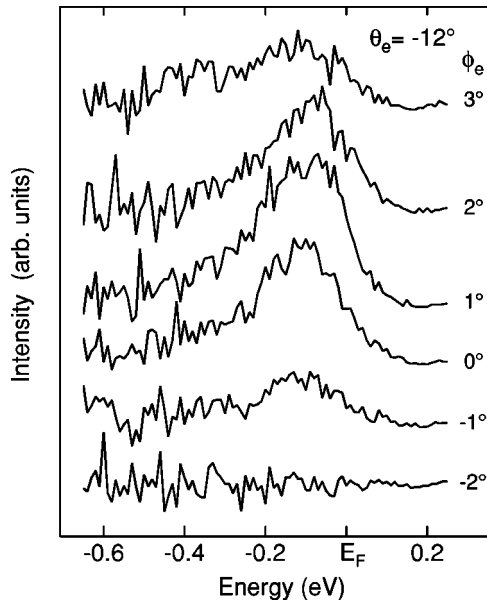


FIG. 47. Angle-resolved photoemission spectra with varying surface wave vector  $k_{\parallel}$  perpendicular to the chains. The polar angle  $\theta_e$  in the emission plane was fixed at  $-12^\circ$ , and the angle  $\phi_e$  in the perpendicular plane was varied. The lack of dispersion in this direction appears to confirm the one-dimensional nature of the system. From Segovia *et al.*, 1999.

si-particle peak as shown in Fig. 47, where in all traces, no sharp peak is apparent in the spectral density. They attempted to probe further the spin-charge separation of spinon and holon excitations. Although two distinct, separately dispersing peaks were observed, the interpretation that these represent evidence for spin-charge separation into spinon and holon modes needs further substantiation since band hybridization effects with the underlying silicon substrate may well account for the two distinct peaks. Nevertheless, this work points to a new avenue for research. Future work on suitable substrates inert to band hybridization may well lead to new and significant advances.

#### D. Quasi-one-dimensional conductors

The final system or set of systems we shall mention arguably represents the first experimental system for which 1D interaction physics was evident. This includes the organic salts of the TTF-TCNQ,  $(\text{TMTSF})_2X$  (tetrathiafulvalene-tetracyanoquinodimethane; tetramethyl-tetraselenafulvalene) series, where  $X = \text{PF}_6$ ,  $\text{AsF}_6$ , etc. (Bechgaard Salts), as well as the  $(\text{TMTTF})_2X$  salts (Emery, 1979; Solyom, 1979; Basista *et al.*, 1990; Jerome and Schulz, 1990; Voit, 1995), the blue-bronze metals  $\text{K}_{0.3}\text{MoO}_3$  and  $(\text{TaSe}_4)_2\text{I}$ ,  $\text{NbSe}_3$  (Dardel *et al.*, 1991; Sing *et al.*, 1999), and the non-charge-density-wave 1D metal  $\text{Li}_{0.9}\text{Mo}_6\text{O}_{17}$  (Denlinger *et al.*, 1999). The organic salts have chain structures that naturally lead to large anisotropy in transport and other properties (Emery, 1979; Jerome and Schulz, 1990; Voit, 1995). The bulk of these highly anisotropic, quasi-1D conductors, both the organic salt and blue-bronze variety, by and large un-

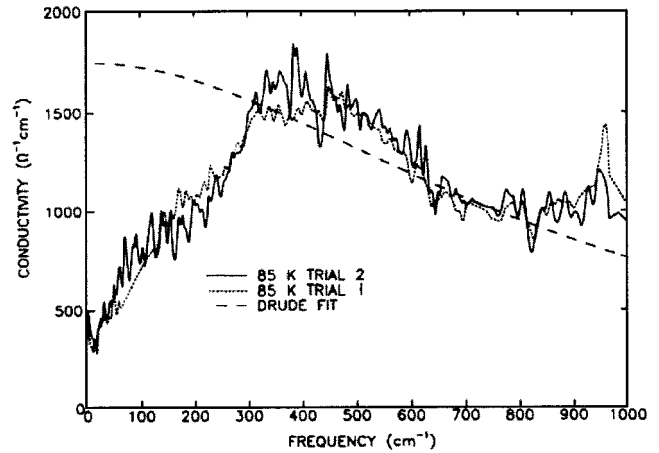


FIG. 48. Real part of the optical conductivity of TTF-TCNF at a temperature of 85 K contrasted with the expected conventional Drude curve (dashed line). These data represent one of the first indications that 1D interaction physics may be relevant in this type of system. Trials 1 and 2 correspond to samples from different sources. From Basista *et al.*, 1990.

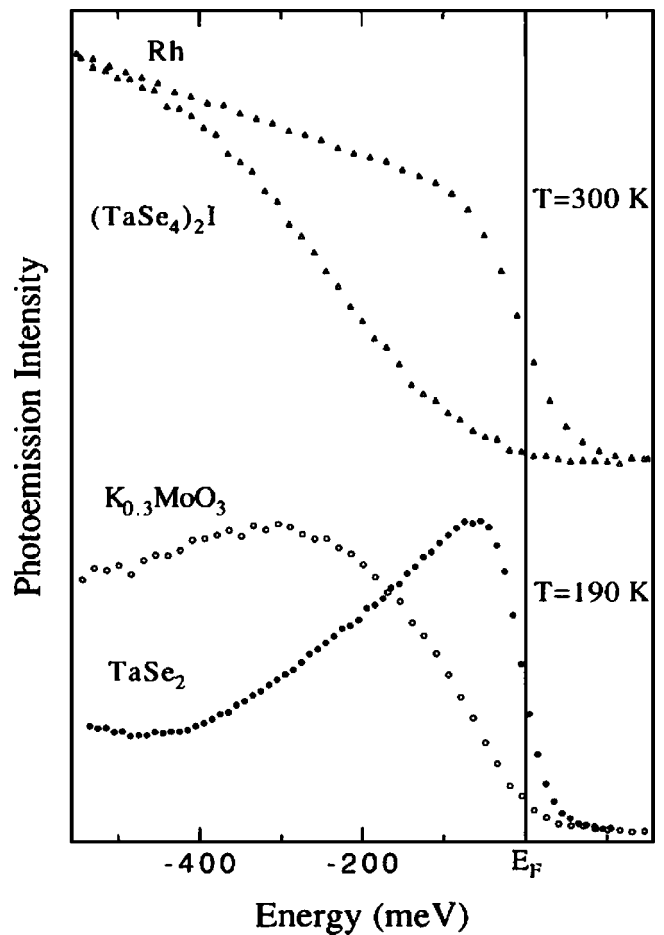


FIG. 49. Angle-integrated photoemission spectra of the  $\text{K}_{0.3}\text{MoO}_3$  and  $(\text{TaSe}_4)_2\text{I}$  quasi-1D conductors measured just above the Peierls charge-density-wave transition temperature. The absence of a sharp Fermi edge is apparent. For comparison, the spectra of 2D ( $\text{TaSe}_2$ ) and 3D (Rh) metals are also shown. From Dardel *et al.*, 1991.

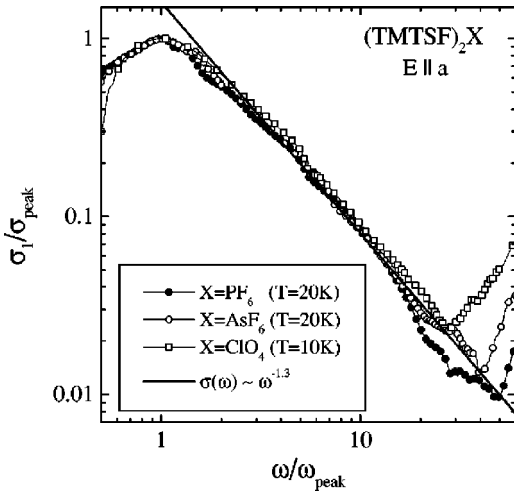


FIG. 50. The normalized frequency-dependent conductivities for 1D organic conductors  $(\text{TMTSF})_2X$ , where  $X = \text{PF}_6$ ,  $\text{AsF}_6$ , and  $\text{ClO}_4$ , in a log-log plot to demonstrate the power-law frequency dependence. The solid line shows a fit of the form  $\sigma(\omega) \sim \omega^\delta$ . From Schwartz *et al.*, 1998.

dergo charge-density-wave or spin-density-wave transitions at sufficiently low temperatures. Some salts also undergo a superconducting transition, e.g.,  $(\text{TMTSF})_2\text{ClO}_4$ . An exception is the non-charge-density-wave blue-bronze metal  $\text{Li}_{0.9}\text{Mo}_6\text{O}_{17}$ . Evidence that 1D interaction physics is relevant comes from a variety of sources, including transport measurements, frequency-dependent conductivity measurements from the microwave to optical and uv range, NMR, and photoemission. Evidence from all of these measurements points to strong deviations from conventional 3D behavior. See Voit (1995) for a recent comprehensive review of this exciting field. Particularly noteworthy is evidence for optical absorption where substantial deviation from simple Drude behavior is observable (Basista *et al.*, 1990; Dardel *et al.*, 1991; Schwartz *et al.*, 1998), anomalous NMR relaxation (Behnia, 1995; Bourbonnais and Jerome, 1998), and photoemission data in which the quasiparticle peak is absent (Dardel *et al.*, 1993; Zwicky *et al.*, 1997; Denlinger *et al.*, 1999) in a manner reminiscent of the normal state in high- $T_c$  superconductor materials (Ding *et al.*, 1997; Shen and Schrieffer, 1997). Some of these examples are presented below.

This field has a long and venerable history. Perhaps the very first system in which 1D physics was thought to be relevant is the TTF-TCNQ system. Figure 48, reproduced from a seminal work by Basista *et al.* (1990), shows the optical conductivity (solid curves), which is suppressed below the Drude conductivity (dashed line). This suppression likely arises from the formation of a pseudogap due to umklapp processes in a 1D electron gas (Lee *et al.*, 1973).

This important finding was followed closely by the discovery of unusual photoemission spectra at temperatures just above the Peierls charge-density-wave transition in the inorganic quasi-1D conductors  $\text{K}_{0.3}\text{MoO}_3$  and  $(\text{TaSe}_4)_2\text{I}$ , where the absence of a Fermi-liquid quasiparticle peak was observed (Dardel *et al.*, 1991), as

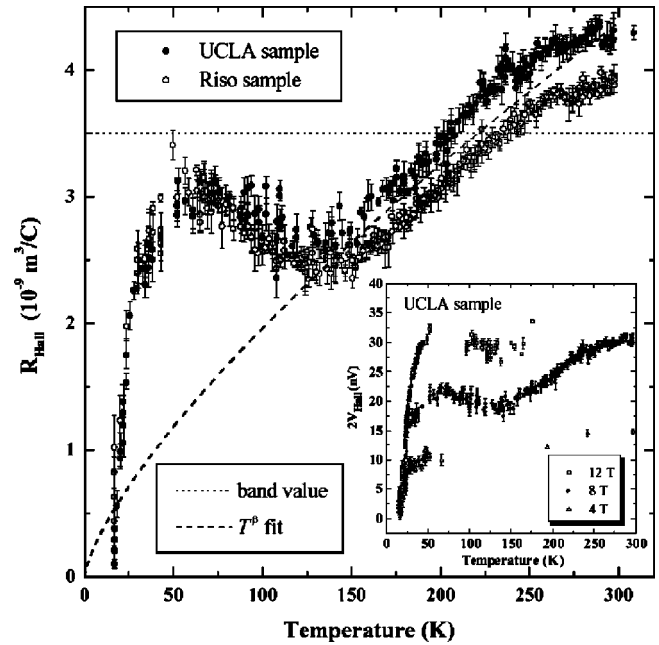


FIG. 51. Hall constant of  $(\text{TMTSF})_2\text{PF}_6$  samples vs temperature:  $\bullet$ , UCLA-Gruner group;  $\circ$ , Riso-Bechgaard group; dotted line, the Hall constant derived in a band model; dashed line, a  $T^\beta$  power-law fit with  $\beta=0.73$ . Inset, magnetic-field data for the UCLA sample. Adapted from Moser *et al.*, 2000.

shown in Fig. 49. More recently, in a non-charge-density-wave organic conductor,  $(\text{TMTSF})_2\text{ClO}_4$ , which undergoes a spin-density-wave transition at 12 K, a nondispersive feature was found along the 1D direction at 150 K (Zwick *et al.*, 1997). In addition electrodynamic response measurements from microwave to uv frequencies in the  $(\text{TMTSF})_2X$  Bechgaard salts were found to be consistent with Luttinger-liquid behavior, with a power-law conductivity as a function of photon energy  $\omega$ , as shown in Fig. 50 (Schwartz *et al.*, 1998). The discovery of a strongly temperature-dependent Hall coefficient down to 12 K in  $(\text{TMTSF})_2\text{PF}_6$ , again with power-law behav-

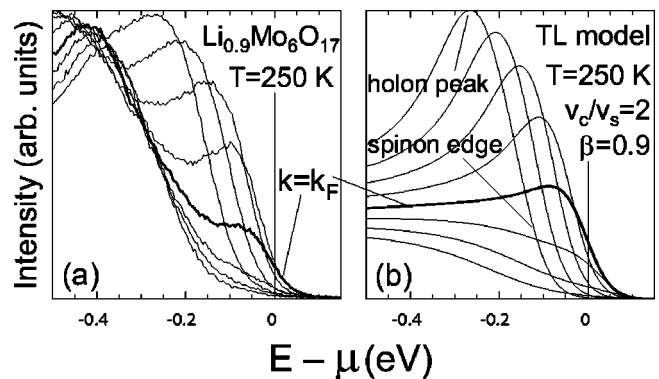


FIG. 52. High-resolution angle-resolved photoemission spectroscopy (ARPES) data for the Li purple bronze taken at  $T = 250$  K, with photon energy 30 eV, energy resolution 49 meV, and angle resolution  $0.36^\circ$ . (a) Points along the  $\Gamma$ -Y line within the Brillouin zone; (b) Tomonaga-Luttinger model simulation. Adapted from Gweon *et al.*, 2002.

ior (Fig. 51), lent further support to the relevance of 1D physics (Moser *et al.*, 2000).

The last example is the non-charge-density-wave inorganic, quasi-1D blue-bronze conductor (Sing *et al.*, 1999). In this system, extensive ARPES studies clearly demonstrated the absence of a quasiparticle pole in the spectral function, consistent with Luttinger-liquid behavior, as shown in Fig. 52 (Denlinger *et al.*, 1999; Gweon *et al.*, 2001, 2002).

Although many of these systems are complex, exhibiting a variety of phases as the temperature or pressure is varied, as well as different signatures arising from Coulomb interaction, it is undoubtedly the case that conventional 3D scenarios are not adequate to describe the essential features of the diverse observations, whereas 1D physics, and particularly Tomonaga-Luttinger-liquid physics, is relevant in the appropriate regime. All these examples show that the unique physics associated with interaction in the 1D world is not limited to the realm of purely theoretical and mathematical discourse, but is relevant in a diverse variety of physically realized systems.

#### ACKNOWLEDGMENTS

I am truly grateful to Virginia Pang-Ying Yeh Chang for her many contributions. I gratefully acknowledge the contributions of my collaborators C. C. Chi, M. Grayson, L. N. Pfeiffer, D. C. Tsui, K. W. West, and M. K. Wu. I would also like to thank the many colleagues with whom I have had stimulating conversations: C. Chamon, M. P. A. Fisher, E. Fradkin, S. M. Girvin, V. J. Goldman, B. I. Halperin, Song He, J. K. Jain, C. L. Kane, Yong-Baek Kim, L. Levitov, A. H. MacDonald, and X.-G. Wen. In addition, I thank K. Matveev for a careful reading of Sec. II.A. Work at Purdue was supported in part by NSF Grant Nos. DMR-9801760 and DMR-0135931.

#### REFERENCES

- Abrikosov, A. A., L. P. Gorkov, and I. E. Dzyaloshinskii, 1963, *Methods of Quantum Field Theory in Statistical Physics* (Prentice-Hall, Englewood Cliffs, NJ), Chaps. 1 and 4.
- Alekseev, A., V. Cheianov, A. P. Dmitriev, and V. Yu. Kachorovskii, 2000, "Tunneling spectroscopy of localized states near the quantum Hall edge," JETP Lett. **72**, 333–336.
- Alphenaar, B. W., *et al.*, 1995, unpublished.
- Altland, A., C. H. W. Barnes, F. W. J. Hekking, and A. J. Schofield, 1999, "Magnetotunneling as a probe of Luttinger-liquid behavior," Phys. Rev. Lett. **83**, 1203–1206.
- Anderson, P. W., 1987, "The resonating valence bond state in  $\text{La}_2\text{CuO}_4$  and superconductivity," Science **235**, 1197–1198.
- Anderson, P. W., 1990, "'Luttinger-liquid' behavior of the normal metallic state of the 2D Hubbard model," Phys. Rev. Lett. **64**, 1839–1841.
- Anderson, P. W., 1992, "Experimental constraints on the theory of high  $T_c$  superconductivity," Science **256**, 1526–1531.
- Ando, M., A. Endo, S. Katsumoto, and Y. Iye, 1998, "Conduction through point contacts in fractional quantum Hall fluid," Physica B **249-251**, 426–429.
- Ando, Y., G. S. Boebinger, A. Passner, T. Kimura, and K. Kishio, 1995, "Divergence of both in-plane and out-of-plane normal-state resistivities of superconducting  $\text{La}_{2-x}\text{Sr}_x\text{CuO}_4$  in the zero-temperature limit," Phys. Rev. Lett. **75**, 4662–4665.
- Auslaender, O. M., A. Yacoby, R. de Picciotto, K. W. Baldwin, L. N. Pfeiffer, and K. W. West, 2000, "Experimental evidence for resonant tunneling in a Luttinger liquid," Phys. Rev. Lett. **84**, 1764–1767.
- Auslaender, O. M., A. Yacoby, R. de Picciotto, K. W. Baldwin, L. N. Pfeiffer, and K. W. West, 2002, "Tunneling spectroscopy of the elementary excitations in a one-dimensional wire," Science **295**, 825–828.
- Bachtold, A., M. de Jonge, K. Grove-Rasmussen, P. L. McEuen, M. Buitelaar, and C. Schonenberger, 2001, "Suppression of tunneling into multiwall carbon nanotubes," Phys. Rev. Lett. **87**, 166801.
- Basista, H., D. A. Bohn, T. Timusk, J. Voit, D. Jerome, and K. Bechgaard, 1990, "Far-infrared optical properties of tetrathiofulvalene-tetracyanoquinodimethane (TTF-TCNQ)," Phys. Rev. B **42**, 4088–4099.
- Baskaran, G., and P. W. Anderson, 1988, "Gauge-theory of high-temperature superconductors and strongly correlated Fermi systems," Phys. Rev. B **37**, 580–583.
- Bednorz, J. G., and K. A. Muller, 1986, "Possible high  $T_c$  superconductivity in the Ba-La-Cu-O System," Z. Phys. B: Condens. Matter **64**, 189–193.
- Beenakker, C. W. J., 1990, "Edge channels for the fractional quantum Hall effect," Phys. Rev. Lett. **64**, 216–219.
- Behnia, K., L. Balicas, W. Kang, D. Jerome, P. Carretta, Y. Fagotrevurat, C. Berthier, M. Horvatic, P. Segransan, L. Hubert, and C. Bourbonnais, 1995, "Confinement in Bechgaard salts—Anomalous magnetoresistance and nuclear-relaxation," Phys. Rev. Lett. **74**, 5272–5275.
- Bertel, E., and L. Lehmann, 1998, "Electronic structure of self-organized lateral superlattices on a metal surface: O/Cu (110)," Phys. Rev. Lett. **80**, 1497–1500.
- Blok, B., and X. G. Wen, 1990a, "Effective theories of the fractional quantum Hall effects for generic filling fractions," Phys. Rev. B **42**, 8133–8144.
- Blok, B., and X. G. Wen, 1990b, "Effective theories of the fractional quantum Hall effects: Hierarchy construction," Phys. Rev. B **42**, 8145–8156.
- Bockrath, M., D. H. Cobden, J. Lu, A. G. Rinzler, R. E. Smalley, T. Balents, and P. L. McEuen, 1999, "Luttinger-liquid behaviour in carbon nanotubes," Nature (London) **397**, 598–601.
- Bourbonnais, C., and D. Jerome, 1998, "One-dimensional conductors," Phys. World **11** (9), 41–45.
- Buttiker, M., 1990, "Scattering theory of thermal and excess noise in open conductors," Phys. Rev. Lett. **65**, 2901–2904.
- Carlson, E. W., D. Orgad, S. A. Kivelson, and V. J. Emery, 2000, "Dimensional crossover in quasi-one-dimensional and high- $T_c$  superconductors," Phys. Rev. B **62**, 3422–3437.
- Carmelo, J. M. P., and A. H. Castro Neto, 1996, "Electrons, pseudoparticles, and quasiparticles in the one-dimensional many-electron problem," Phys. Rev. B **54**, 11 230–11 244.
- Castellani, C., and C. Di Castro, 1999, "Breakdown of Fermi liquid in correlated electron systems," Physica A **263**, 127–207.
- Castellani, C., C. Di Castro, and W. Metzner, 1994, "Dimensional crossover from Fermi to Luttinger liquid," Phys. Rev. Lett. **72**, 316–319.

- Chamon, C. de C., and E. Fradkin, 1997, “Distinct universal conductances in tunneling to quantum Hall states: The role of contacts,” *Phys. Rev. B* **56**, 2012–2025.
- Chamon, C. de C., D. E. Freed, and X. G. Wen, 1995, “Tunneling and quantum noise in one-dimensional Luttinger liquids,” *Phys. Rev. B* **51**, 2363–2379.
- Chamon, C. de C., and X. G. Wen, 1993, “Resonant tunneling in the fractional quantum Hall regime,” *Phys. Rev. Lett.* **70**, 2605–2608.
- Chamon, C. de C., and X. G. Wen, 1994, “Sharp and smooth boundaries of fractional Hall liquids,” *Phys. Rev. B* **49**, 8227–8241.
- Chang, A. M., 1990, “A unified transport-theory for the integral and fractional quantum Hall effects—Phase boundaries, edge currents, and transmission reflection probabilities,” *Solid State Commun.* **74**, 871–876.
- Chang, A. M., 2002, unpublished, <http://www.phy.duke.edu/~yingshe>. See EPAPS Document No. E-RMPHAT-75-002304 for supplemental material. In particular, sections summarizing the Landau Fermi liquid and the justification of the Fermi liquid using many-body techniques are presented. In addition, a discussion of the issue of non-uniform edge electron density in cleaved-edge overgrown devices, which are used in electron tunneling experiments, is contained in the Appendix.
- Chang, A. M., L. N. Pfeiffer, and K. W. West, 1996, “Observation of chiral Luttinger behavior in electron tunneling into fractional quantum Hall edges,” *Phys. Rev. Lett.* **77**, 2538–2541.
- Chang, A. M., L. N. Pfeiffer, and K. W. West, 1998, “An apparent  $g=1/2$  chiral Luttinger liquid at the edge of the  $\nu=1/2$  compressible fractional quantum Hall liquid,” in *Proceedings of the 12th International Conference on the Electronic Properties of Two-Dimensional Systems*, Tokyo, *Physica B* **249-251**, 383–387.
- Chang, A. M., M. K. Wu, J. C. C. Chi, L. N. Pfeiffer, and K. W. West, 2001, “Plateau behavior in the chiral Luttinger liquid exponent,” *Phys. Rev. Lett.* **86**, 143–146.
- Chklovskii, D. B., and B. I. Halperin, 1998, “Consequences of a possible adiabatic transition between  $\nu=1/3$  and  $\nu=1$  quantum Hall states in a narrow wire,” *Phys. Rev. B* **57**, 3781–3784.
- Chklovskii, D. B., B. I. Shklovskii, and L. I. Glazman, 1992, “Electrostatics of edge channels,” *Phys. Rev. B* **46**, 4026–4034.
- Chung, Y. C., M. Heiblum, Y. Oreg, V. Umansky, and D. Mahalu, 2003a, “Anomalous chiral Luttinger liquid behavior of diluted fractionally charged quasiparticles,” *Phys. Rev. B* **67**, 201104.
- Chung, Y. C., M. Heiblum, and V. Umansky, 2003b, “Scattering of bunched fractionally charged quasiparticles,” e-print cond-mat/0305325.
- Comforti, E., Y. C. Chung, M. Heiblum, V. Umansky, and D. Mahalu, 2002, “Bunching of fractionally charged quasiparticles tunneling through high-potential barriers,” *Nature (London)* **416**, 515–518.
- Conti, S., and G. Vignale, 1996, “Collective modes and electronic spectral function in smooth edges of quantum Hall systems,” *Phys. Rev. B* **54**, 14 309–14 312.
- Conti, S., and G. Vignale, 1997, “Bosonization theory for tunneling spectra in smooth edges of quantum Hall systems,” *Physica E* **1**, 101–104.
- Conti, S., and G. Vignale, 1998, “Dynamics of the two-dimensional electron gas in the lowest Landau level: A continuum elasticity approach,” *J. Phys. C* **10**, L779–L786.
- Dardel, B., D. Malterre, M. Grioni, P. Weibel, Y. Baer, and F. Levy, 1991, “Unusual photoemission spectral function of quasi-one-dimensional metals,” *Phys. Rev. Lett.* **67**, 3144–3147.
- Dardel, B., D. Malterre, M. Grioni, P. Weibel, Y. Baer, J. Voit, and D. Jerome, 1993, “Possible observation of a Luttinger-liquid behavior from photoemission spectroscopy of one-dimensional organic conductors,” *Europhys. Lett.* **24**, 687–692.
- De-Picciotto, R., M. Reznikov, M. Heiblum, V. Umansky, G. Bunin, and D. Mahalu, 1997, “Direct observation of a fractional charge,” *Nature (London)* **389**, 162–164.
- De-Picciotto, R., H. L. Stormer, L. N. Pfeiffer, K. W. Baldwin, and K. W. West, 2001, “Four-terminal resistance of a ballistic quantum wire,” *Nature (London)* **411**, 51–54.
- Dekker, C., A. J. Scholten, F. Liefink, R. Eppenga, H. van Houten, and C. T. Foxon, 1991, “Spontaneous resistance switching and low-frequency noise in quantum point contacts,” *Phys. Rev. Lett.* **66**, 2148–2151.
- Denlinger, J. D., G.-H. Gweon, J. W. Allen, C. G. Olson, J. Marcus, C. Schlenker, and L.-S. Hsu, 1999, “Non-Fermi-liquid single-particle line shape of the quasi-one-dimensional non-CDW metal  $\text{Li}_{0.9}\text{Mo}_6\text{O}_{17}$ : Comparison to the Luttinger liquid,” *Phys. Rev. Lett.* **82**, 2540–2543.
- Ding, H., M. R. Norman, T. Yokoya, T. Takeuchi, M. Randeria, J. C. Campuzano, T. Takahashi, T. Mochiku, and K. Kadowaki, 1997, “Evolution of the Fermi surface with carrier concentration in  $\text{Bi}_2\text{Sr}_2\text{CaCu}_2\text{O}_{8+\delta}$ ,” *Phys. Rev. Lett.* **78**, 2628–2631.
- Dover, C. B., 1968, “Properties of the Luttinger model,” *Ann. Phys. (N.Y.)* **50**, 500–533.
- Du, R. R., H. L. Stormer, D. C. Tsui, L. N. Pfeiffer, and K. W. West, 1993, “Evidence for new particles in the fractional quantum Hall effect,” *Phys. Rev. Lett.* **70**, 2944–2947.
- Du, R. R., H. L. Stormer, D. C. Tsui, L. N. Pfeiffer, and K. W. West, 1994, “Shubnikov-DeHaas oscillations around  $\nu=1/2$  Landau-level filling factor,” *Solid State Commun.* **90**, 71–75.
- Dzyaloshinskii, I. E., and A. I. Larkin, 1973, “Correlation functions for a one-dimensional Fermi system with long-range interaction (Tomonaga model),” *Zh. Eksp. Teor. Fiz.* **65**, 411–426 [*Sov. Phys. JETP* **38**, 202–208 (1974)].
- Efetov, K., and A. I. Larkin, 1975, “Correlation functions in one-dimensional systems with a strong interaction,” *Zh. Eksp. Teor. Fiz.* **69**, 764–776 [*Sov. Phys. JETP* **42**, 390–396 (1976)].
- Egger, R., 1999, “Luttinger liquid behavior in multiwall carbon nanotubes,” *Phys. Rev. Lett.* **83**, 5547–5550.
- Egger, R., and A. O. Gogolin, 1997, “Effective low-energy theory for correlated carbon nanotubes,” *Phys. Rev. Lett.* **79**, 5082–5085.
- Eisenstein, J. P., L. N. Pfeiffer, and K. W. West, 1992, “Coulomb barrier to tunneling between parallel two-dimensional electron-systems,” *Phys. Rev. Lett.* **69**, 3804–3807.
- Emery, V. J., 1979, in *Highly Conducting One-Dimensional Solids*, edited by J. T. Devreese, R. E. Evrard, and V. E. van Doren (Plenum, New York), pp. 247–303.
- Emery, V. J., S. A. Kivelson, and J. M. Tranquada, 1999, “Stripe phases in high-temperature superconductors,” *Proc. Natl. Acad. Sci. U.S.A.* **96**, 8814–8817.

- Everts, H. U., and H. Schulz, 1974, “Application of conventional equation of motion methods to the Tomonaga model,” *Solid State Commun.* **15**, 1413–1416.
- Fendley, P., A. W. W. Ludwig, and H. Saleur, 1995a, “Exact conductance through point contacts in the  $\nu=1/3$  fractional quantum Hall effect,” *Phys. Rev. Lett.* **74**, 3005–3008.
- Fendley, P., A. W. W. Ludwig, and H. Saleur, 1995b, “Exact nonequilibrium transport through point contacts in quantum wires and fractional quantum Hall devices,” *Phys. Rev. B* **52**, 8934–8950.
- Fendley, P., A. W. W. Ludwig, and H. Saleur, 1995c, “Exact nonequilibrium dc shot noise in Luttinger liquids and fractional quantum Hall devices,” *Phys. Rev. Lett.* **75**, 2196–2199.
- Fetter, A., and J. D. Walecka, 1971, *Quantum Theory of Many-Particle Systems* (McGraw-Hill, New York).
- Finkelstein, A. M., 1977, “Correlation functions in the one-dimensional Hubbard model,” *Pis'ma Zh. Eksp. Teor. Fiz.* **25**, 83–86 [JETP Lett. **25**, 73–76 (1977)].
- Fradkin, E., 2000, “Exploring the fractional quantum Hall effect with electron tunneling,” in *Proceedings of the XXXIVth Recontres de Moriond, January 23–30, 1999*, edited by G. Glattli, M. Sanquer, and J. Tran Thanh Van (Editions Frontières, Gif sur Yvette), pp. 197–218.
- Franklin, J. D. F., I. Zailer, C. J. B. Ford, P. J. Simpson, J. E. F. Frost, D. A. Ritchie, M. Y. Simmons, and M. Pepper, 1996, “The Aharonov-Bohm effect in the fractional quantum Hall regime,” *Surf. Sci.* **362**, 17–21.
- Frohlich, J., and A. Zee, 1991, “Large-scale physics of the quantum Hall fluid,” *Nucl. Phys. B* **364**, 517–540.
- Furusaki, A., 1998, “Resonant tunneling through a quantum dot weakly coupled to quantum wires or quantum Hall edge states,” *Phys. Rev. B* **57**, 7141–7148.
- Furusaki, A., and N. Nagaosa, 1993, “Resonant tunneling in a Luttinger liquid,” *Phys. Rev. B* **47**, 3827–3831.
- Geller, M. R., D. Loss, and G. Kirczenow, 1996, “Mesoscopic effects in the fractional quantum Hall regime: Chiral Luttinger liquid versus Fermi liquid,” *Phys. Rev. Lett.* **77**, 5110–5113.
- Ghoshal, S., and A. Zamolodchikov, 1994, *Int. J. Mod. Phys. A* **9**, 3841–3885.
- Girvin, S. M., and A. H. MacDonald, 1987, “Off-diagonal long-range order, oblique confinement, and the fractional quantum Hall effect,” *Phys. Rev. Lett.* **58**, 1252–1255.
- Glattli, D. C., 2002, unpublished.
- Glattli, D. C., V. Rodriguez, H. Perrin, P. Roche, Y. Jin, and B. Etienne, 2000, “Shot noise and the Luttinger liquid-like properties of the FQHE,” *Physica E* **6**, 22–28.
- Goldman, V. J., and B. Su, 1995, “Resonant-tunneling in the quantum Hall regime—Measurement of fractional charge,” *Science* **267**, 1010–1012.
- Goldman, V. J., and E. V. Tsiper, 2001, “Dependence of the fractional quantum Hall edge critical exponent on the range of interaction,” *Phys. Rev. Lett.* **86**, 5841.
- Grayson, M., C. Kurdak, D. C. Tsui, S. Parihar, S. Lyon, and M. Shayegan, 1996, “Novel cleaved edge overgrowth structures for tunneling into one- and two-dimensional electron systems,” *Solid-State Electron.* **40**, 233–236.
- Grayson, M., D. C. Tsui, L. N. Pfeiffer, K. W. West, and A. M. Chang, 1998, “Continuum of chiral Luttinger liquids at the fractional quantum Hall edge,” *Phys. Rev. Lett.* **80**, 1062–1065.
- Grayson, M., D. C. Tsui, L. N. Pfeiffer, K. W. West, and A. M. Chang, 2001, “Resonant tunneling into a biased fractional quantum Hall edge,” *Phys. Rev. Lett.* **86**, 2645–2648.
- Grayson, M., D. C. Tsui, L. N. Pfeiffer, K. W. West, and A. M. Chang, 2002, “The lever-arm model: Describing resonant tunneling under bias into a fractional quantum Hall edge,” *Physica E* **12**, 80–83.
- Griffiths, T. G., E. Comferti, M. Heiblum, Ady Stern, and V. Umansky, 2000, “Evolution of quasiparticle charge in the fractional quantum Hall regime,” *Phys. Rev. Lett.* **85**, 3918–3921.
- Gweon, G. H., J. D. Denlinger, J. W. Allen, R. Claessen, C. G. Olson, H. Hochst, J. Marcus, C. Schlenker, and L. F. Schneemeyer, 2001, “ARPES line shapes in FL and non-FL quasi-low-dimensional inorganic metals,” *J. Electron Spectrosc. Relat. Phenom.* **117**, 481–502.
- Gweon, G. H., J. D. Denlinger, J. W. Allen, C. G. Olson, H. Hochst, J. Marcus, and C. Schlenker, 2002, e-print cond-mat/0107211.
- Haldane, F. D. M., 1979, “Coupling between charge and spin degrees of freedom in the one-dimensional Fermi gas with backscattering,” *J. Phys. C* **12**, 4791–4799.
- Haldane, F. D. M., 1981, “‘Luttinger liquid theory’ of one-dimensional quantum fluids: I. Properties of the Luttinger model and their extension to the general 1D interacting spinless Fermi gas,” *J. Phys. C* **14**, 2585–2609.
- Haldane, F. D. M., 1983, “Fractional quantization of the Hall effect—a hierarchy of incompressible quantum fluid states,” *Phys. Rev. Lett.* **51**, 605–608.
- Halperin, B. I., 1984, “Statistics of quasiparticles and the hierarchy of fractional quantized Hall states,” *Phys. Rev. Lett.* **52**, 1583–1586.
- Halperin, B. I., P. A. Lee, and N. Read, 1993, “Theory of the half-filled Landau level,” *Phys. Rev. B* **47**, 7312–7342.
- Han, J. H., 1997, Ph.D. thesis (University of Washington).
- Han, J. H., and D. J. Thouless, 1997a, “Dynamics of compressible edge and Bosonization,” *Phys. Rev. B* **55**, R1926–R1929.
- Han, J. H., and D. J. Thouless, 1997b, “Green’s-function approach to the edge spectral density,” *Phys. Rev. B* **56**, 15 806–15 813.
- Harris, J. M., Y. F. Yan, and N. P. Ong, 1992, “Experimental test of the  $T^2$  law for the Hall angle from  $T_c$  to 500 K in oxygen-reduced  $\text{YBa}_2\text{Cu}_3\text{O}_{6+x}$  crystals,” *Phys. Rev. B* **46**, 14 293–14 296.
- He, Song, P. M. Platzman, and B. I. Halperin, 1993, “Tunneling into a two-dimensional electron-system in a strong magnetic field,” *Phys. Rev. Lett.* **71**, 777–780.
- Heidenreich, R., B. Schroer, R. Seiler, and D. Uhlenbrock, 1975, “The sine-Gordon equation and the one-dimensional electron gas,” *Phys. Lett.* **54A**, 119–122.
- Hilke, M., D. C. Tsui, M. Grayson, L. N. Pfeiffer, and K. W. West, 2001, “Fermi liquid to Luttinger liquid transition at the edge of a two-dimensional electron gas,” *Phys. Rev. Lett.* **87**, 186806.
- Hill, I. G., and A. B. McLean, 1997, “Metallicity of In chains on Si(111),” *Phys. Rev. B* **56**, 15 725–15 728.
- Imura, K., 1999, “Tunneling into fractional quantum Hall liquids,” *Europhys. Lett.* **47**, 233–239.
- Imura, K., and N. Nagaosa, 1997, “Effects of long-range Coulomb interaction on the quantum transport in fractional quantum Hall edges,” *Phys. Rev. B* **55**, 7690–7701.
- Jain, J. K., 1989a, “Composite-fermion approach for the fractional quantum Hall effect,” *Phys. Rev. Lett.* **63**, 199–202.

- Jain, J. K., 1989b, "Incompressible quantum Hall states," *Phys. Rev. B* **40**, 8079–8082.
- Jain, J. K., 1990, "Theory of the fractional quantum Hall effect," *Phys. Rev. B* **41**, 7653–7665.
- Jerome, D., and H. J. Schulz, 1990, "Organic conductors and superconductors," *Adv. Phys.* **31**, 299–490.
- Kane, C., 1998, "Resonant tunneling between quantum Hall states at filling  $\nu=1$  and  $\nu=1/3$ ," e-print cond-mat/9809020.
- Kane, C., L. Balents, and M. P. A. Fisher, 1997, "Coulomb interactions and mesoscopic effects in carbon nanotubes," *Phys. Rev. Lett.* **79**, 5086–5089.
- Kane, C. L., and M. P. A. Fisher, 1992a, "Transport in a one-channel Luttinger liquid," *Phys. Rev. Lett.* **68**, 1220–1223.
- Kane, C. L., and M. P. A. Fisher, 1992b, "Resonant tunneling in an interacting one-dimensional electron-gas," *Phys. Rev. B* **46**, 7268–7271.
- Kane, C. L., and M. P. A. Fisher, 1992c, "Transmission through barriers and resonant tunneling in an interacting one-dimensional electron gas," *Phys. Rev. B* **46**, 15 233–15 262.
- Kane, C. L., and M. P. A. Fisher, 1994, "Nonequilibrium noise and fractional charge in the quantum Hall effect," *Phys. Rev. Lett.* **72**, 724–727.
- Kane, C. L., and M. P. A. Fisher, 1995, "Impurity scattering and transport of fractional quantum Hall edge states," *Phys. Rev. B* **51**, 13 449–13 466.
- Kane, C. L., and M. P. A. Fisher, 2003, "Shot noise and the transmission of dilute Laughlin quasiparticles," *Phys. Rev. B* **67**, 045307.
- Kane, C. L., M. P. A. Fisher, and J. Polchinski, 1994, "Randomness at the edge: Theory of quantum Hall transport at filling  $\nu=2/3$ ," *Phys. Rev. Lett.* **72**, 4129–4132.
- Kang, W., H. L. Stormer, K. W. Baldwin, L. N. Pfeiffer, and K. W. West, 1993, "How real are composite fermions," *Phys. Rev. Lett.* **71**, 3850–3853.
- Khveshchenko, D., 1999, "Quantum point contact in a compressible quantum Hall liquid," *Solid State Commun.* **111**, 501–505.
- Khveshchenko, D., 2000, "Ballistic transport through a narrow constriction in the presence of a composite-fermion electromagnetic environment," *Phys. Rev. B* **61**, 5610–5614.
- Kopietz, P., 1996, "Nonrelativistic fermions coupled to transverse gauge fields: The single-particle Green's function in arbitrary dimensions," *Phys. Rev. B* **53**, 12 761–12 768.
- Kouwenhoven, L. P., and P. L. McEuen, 1995, unpublished.
- Kurdak, C., D. C. Tsui, S. Parihar, M. B. Santos, H. C. Manoharan, S. A. Lyon, and M. Shayegan, 1994, "Surface resonant-tunneling transistor—A new negative transconductance device," *Appl. Phys. Lett.* **64**, 610–612.
- Landau, L. D., 1956, "The theory of the Fermi liquid," *Zh. Eksp. Teor. Fiz.* **30**, 1058–1064 [*Sov. Phys. JETP* **3**, 920–925 (1957)].
- Landau, D. P., 1957, "Oscillations in a Fermi liquid," *Zh. Eksp. Teor. Fiz.* **32**, 59–66 [*Sov. Phys. JETP* **5**, 101–108 (1957)].
- Landau, D. P., 1958, "On the theory of a Fermi liquid," *Zh. Eksp. Teor. Fiz.* **35**, 97–103 [*Sov. Phys. JETP* **8**, 70–74 (1958)].
- Laughlin, R. B., 1983, "Anomalous quantum Hall effect—An incompressible quantum fluid with fractionally charged excitations," *Phys. Rev. Lett.* **50**, 1395–1398.
- Lee, D. H., and X.-G. Wen, 1991, "Edge excitations in the fractional-quantum-Hall liquids," *Phys. Rev. Lett.* **66**, 1765–1768.
- Lee, D. H., and X.-G. Wen, 1998, "Edge tunneling in fractional quantum Hall regime," e-print cond-mat/9809160.
- Lee, P. A., 1990, "Resistance fluctuations in narrow AlGaAs/GaAs heterostructures—Direct evidence of fractional charge in the fractional quantum Hall-effect—Comment," *Phys. Rev. Lett.* **65**, 2206–2206.
- Lee, P. A., N. Nagaosa, T. K. Ng, and X. G. Wen, 1998, "SU(2) formulation of the  $t$ - $J$  model: Application to underdoped cuprates," *Phys. Rev. B* **57**, 6003–6021.
- Lee, P. A., T. M. Rice, and P. W. Anderson, 1973, "Fluctuation effects at a Peierls transition," *Phys. Rev. Lett.* **31**, 462–465.
- Lesovik, G. B., 1989, "Excess quantum noise in 2d ballistic point contacts," *Pis'ma Zh. Eksp. Teor. Fiz.* **49**, 513–515 [*JETP Lett.* **49**, 592–594 (1989)].
- Levi, B. G., 1996, "One-dimensional systems show signs of interacting electrons," *Phys. Today* **49** (9), 19–21.
- Levitov, L. S., A. V. Shytov, and B. I. Halperin, 2001, "Effective action of a compressible QH state edge: Application to tunneling," *Phys. Rev. B* **64**, 075322.
- Li, Y. P., D. C. Tsui, J. J. Heremans, J. A. Simmons, and G. W. Weimann, 1990, "Low-frequency noise in transport through quantum point contact," *Appl. Phys. Lett.* **57**, 774–776.
- Liefrink, F., J. I. Dijkhuis, M. J. M. DeJong, L. W. Molenkamp, and H. van Houten, 1994, "Experimental study of reduced shot-noise in a diffusive mesoscopic conductor," *Phys. Rev. B* **49**, 14 066–14 069.
- Lopez, A., and E. Fradkin, 1999, "Universal structure of the edge states of the fractional quantum Hall states," *Phys. Rev. B* **59**, 15 323–15 331.
- Luther, A., and V. J. Emery, 1974, "Backward scattering in the one-dimensional electron gas," *Phys. Rev. Lett.* **33**, 589–592.
- Luther, A., and I. Peschel, 1974, "Single-particle states, Kohn anomaly, and pairing fluctuations in one dimension," *Phys. Rev. B* **9**, 2911–2919.
- Luttinger, J. M., 1960, "Analytic properties of single-particle propagators for many-fermion systems," *Phys. Rev.* **121**, 942–949.
- Luttinger, J. M., 1963, "An exactly soluble model of a many-fermion system," *J. Math. Phys.* **4**, 1154–1162.
- Maasilta, I. J., and V. J. Goldman, 1997, "Line shape of resonant tunneling between fractional quantum Hall edges," *Phys. Rev. B* **55**, 4081–4084.
- MacDonald, A. H., 1990, "Edge states in the fractional-quantum-Hall-effect regime," *Phys. Rev. Lett.* **64**, 220–223.
- Mahan, G. D., 2000, *Many-Particle Physics* (Kluwer Academic/Plenum, New York).
- Mandal, S. S., and J. K. Jain, 2001, "How universal is the fractional-quantum-Hall-edge Luttinger liquid?" *Solid State Commun.* **118**, 503–507.
- Mandal, S. S., and J. K. Jain, 2002, "Relevance of inter-composite-fermion interaction to the edge Tomonaga-Luttinger liquid," *Phys. Rev. Lett.* **89**, 096801.
- Matthis, D. C., and E. H. Lieb, 1965, "Exact solution of a many-fermion system and its associated boson field," *J. Math. Phys.* **6**, 304–312.
- Menyhard, N., and J. Solyom, 1973, "Application of the renormalization group technique to the problem of phase transition in one-dimensional metallic system. I. Invariant couplings, vertex, and one-particle Green's function," *J. Low Temp. Phys.* **12**, 529–545.
- Metzner, W., C. Castellani, and C. Di Castro, 1998, "Fermi systems with strong forward scattering," *Adv. Phys.* **47**, 317–445.

- Metzner, W., and C. Di Castro, 1993, "Conservation laws and correlation functions in the Luttinger liquid," *Phys. Rev. B* **47**, 16 107–16 123.
- Milliken, F. P., C. P. Umbach, and R. A. Webb, 1996, "Indications of a Luttinger liquid in the fractional quantum Hall regime," *Solid State Commun.* **97**, 309–313.
- Moon, K., H. Yi, C. L. Kane, S. M. Girvin, and M. P. A. Fisher, 1993, "Resonant tunneling between quantum Hall edge states," *Phys. Rev. Lett.* **71**, 4381–4384.
- Moser, J., J. R. Cooper, D. Jerome, B. Alavi, S. E. Brown, and K. Bechgaard, 2000, "Hall effect in the normal phase of the organic superconductor (TMTSF)<sub>2</sub>PF<sub>6</sub>," *Phys. Rev. Lett.* **84**, 2674–2677.
- Ng, T. K., 1997, "Functional integral approach to quasiparticles in Fermi liquid theory," e-print cond-mat/9706033.
- Nozières, P., 1964, *Theory of Interacting Fermi Systems* (Benjamin, New York).
- Overhauser, A. W., 1965, "Note on the band theory of magnetism," *Physics (Long Island City, N.Y.)* **1**, 307–309.
- Pfeiffer, L. N., K. W. West, H. L. Stormer, J. P. Eisenstein, K. W. Baldwin, D. Gershoni, and J. Spector, 1990, "Formation of a high quality two-dimensional electron gas on cleaved GaAs," *Appl. Phys. Lett.* **56**, 1697–1699.
- Pruisken, A. M. M., B. Skoric, and M. A. Baranov, 1999, "(Mis-)handling gauge invariance in the theory of the quantum Hall effect. III. The instanton vacuum and chiral-edge physics," *Phys. Rev. B* **60**, 16 838–16 864.
- Rantner, W. and X. G. Wen, 2001, "Electron spectral function and algebraic spin liquid for the normal state of underdoped high  $T_c$  superconductors," *Phys. Rev. Lett.* **86**, 3871–3874.
- Read, N., 1989, "Order parameter and Ginzburg-Landau theory for the fractional quantum Hall effect," *Phys. Rev. Lett.* **62**, 86–89.
- Ren, Y., and P. W. Anderson, 1993, "Asymptotic correlation functions in the one-dimensional Hubbard model with applications to high- $T_c$  superconductivity," *Phys. Rev. B* **48**, 16 662–16 672.
- Reznikov, M., R. de Picciotto, T. G. Griffiths, M. Heiblum, and V. Umansky, 1999, "Observation of quasiparticles with one-fifth of an electron's charge," *Nature (London)* **399**, 238–241.
- Roddaro, S., V. Pelegrini, F. Beltram, G. Biasiol, L. Sorba, R. Raimondi, and G. Vignale, 2003, "Nonlinear quasiparticle tunneling between quantum Hall edges," *Phys. Rev. Lett.* **90**, 046805.
- Rosenow, B., and B. I. Halperin, 2002, "Nonuniversal behavior of scattering between fractional quantum Hall edges," *Phys. Rev. Lett.* **88**, 096404.
- Saminadayar, L., D. C. Glattli, Y. Jin, and B. Etienne, 1997, "Observation of the  $e/3$  fractionally charged Laughlin quasiparticle," *Phys. Rev. Lett.* **79**, 2526–2529.
- Schrieffer, J. R., D. J. Scalapino, and J. W. Wilkens, 1963, "Effective tunneling density of states in superconductors," *Phys. Rev. Lett.* **10**, 336–339.
- Schulz, H. J., 1991, "Correlated fermions in one dimension," *Int. J. Mod. Phys. B* **5**, 57–74.
- Schulz, H. J., 1995, "Fermi liquids and non-Fermi liquids," in *Proceedings of Les Houches Summer School LXI*, edited by E. Akkermans, G. Montambaux, J. Pichard, and J. Zinn-Justin (Elsevier, Amsterdam); e-print cond-mat/9503150.
- Schwartz, A., M. Dressel, G. Gruner, V. Vescoli, L. Degiorgi, and T. Giamarchi, 1998, "On-chain electro-dynamics of metallic (TMTSF)<sub>2</sub>X salts: Observation of Tomonaga-Luttinger liquid response," *Phys. Rev. B* **58**, 1261–1271.
- Segovia, P., D. Purdie, M. Hengsberger, and Y. Baer, 1999, "Observation of spin-charge separation in one-dimensional metallic chains," *Nature (London)* **402**, 504–507.
- Shen, Z. X., and J. R. Schrieffer, 1997, "Momentum, temperature, and doping dependence of photoemission line shape and implications for the nature of the pairing potential in high- $T_c$  superconducting materials," *Phys. Rev. Lett.* **78**, 1771–1774.
- Shytov, A. V., L. S. Levitov, and B. I. Halperin, 1998, "Tunneling into the edge of a compressible quantum Hall state," *Phys. Rev. Lett.* **80**, 141–144.
- Simmons, J. A., H. P. Wei, L. W. Engel, D. C. Tsui, and M. Shayegan, 1989, "Resistance fluctuations in narrow AlGaAs-GaAs heterostructures—Direct evidence of fractional charge in the fractional quantum Hall effect," *Phys. Rev. Lett.* **63**, 1731–1734.
- Sing, M., V. G. Grigoryan, G. Paasch, M. Knupfer, J. Fink, B. Lommel, and W. Assmus, 1999, "Plasmon excitations in quasi-one-dimensional K<sub>0.3</sub>MoO<sub>3</sub>," *Phys. Rev. B* **59**, 5414–5425.
- Skoric, B., and A. Pruisken, 1999, "The fractional quantum Hall effect: Chern-Simons mapping, duality, Luttinger liquids and the instanton vacuum," *Nucl. Phys. B* **559**, 637–672.
- Solyom, J., 1973, "Application of the renormalization group technique to the problem of phase transition in one-dimensional metallic systems. II. Response functions and the ground state problem," *J. Low Temp. Phys.* **12**, 547–558.
- Solyom, J., 1979, "The Fermi gas model of one-dimensional conductors," *Adv. Phys.* **28**, 201–303.
- Solyom, J., and A. Zawadowski, 1974, "Are the scaling laws for the Kondo problem exact?" *J. Phys.* **4**, 80–90.
- Someya, T., H. Akiyama, and H. Sakaki, 1995, "Tightly confined one-dimensional states in T-shaped GaAs edge quantum wires with AlAs Barriers," *Appl. Phys. Lett.* **66**, 3672–3673.
- Stern, F. and S. Das Sarma, 1984, "Electron-energy levels in GaAs-Ga<sub>1-x</sub>Al<sub>x</sub>As heterojunctions," *Phys. Rev. B* **30**, 840–848.
- Tarucha, S., T. Honda, and T. Saku, 1995, "Reduction of quantized conductance at low-temperatures observed in 2 to 10  $\mu\text{m}$ -long quantum wires," *Solid State Commun.* **94**, 413–418.
- Theumann, A., 1967, "Single-particle Green's function for a one-dimensional many-fermion system," *J. Math. Phys.* **8**, 2460–2467.
- Thouless, D. J., and Y. Gefen, 1991, "Fractional quantum Hall effect and multiple Aharonov-Bohm periods," *Phys. Rev. Lett.* **66**, 806–809.
- Tomonaga, S., 1950, "Remarks on Bloch's method of sound waves applied to many-fermion problems," *Prog. Theor. Phys.* **5**, 544–569.
- Tsui, D. C., H. L. Stormer, and A. C. Gossard, 1982, "Two-dimensional magnetotransport in the extreme quantum limit," *Phys. Rev. Lett.* **48**, 1559–1562.
- Turley, P. J., D. P. Druist, E. G. Gwinn, K. Maranowski, K. Campmann, and A. C. Gossard, 1998, "Tunneling through point contacts in the quantum Hall effect," *Physica B* **251**, 410–414.
- Varma, C. M., P. B. Littlewood, S. Schmitt-Rink, E. Abrahams, and A. Ruckenstein, 1989, "Phenomenology of the normal state of CU-O high-temperature superconductors," *Phys. Rev. Lett.* **63**, 1996–1999.
- Voit, J., 1995, "One-dimensional Fermi liquids," *Rep. Prog. Phys.* **58**, 977–1116.

- Wan, X., K. Yang, and E. H. Rezayi, 2002, "Reconstruction of fractional quantum Hall edges," *Phys. Rev. Lett.* **88**, 056802.
- Wegscheider, W., W. Kang, L. N. Pfeiffer, K. W. West, H. L. Stormer, and K. W. Baldwin, 1994, "High-mobility transport along single quasi-1d quantum wires formed by cleaved edge overgrowth," *Solid-State Electron.* **37**, 547–550.
- Wegscheider, W., L. Pfeiffer, M. Dignam, A. Pinczuk, K. West, and R. Hall, 1994, "Lasing in lower-dimensional structures formed by cleaved edge overgrowth," *Semicond. Sci. Technol.* **9**, 1933–1938.
- Wegscheider, W., G. Schedelbeck, G. Abstreiter, M. Rother, and M. Bichler, 1997, "Atomically precise GaAs/AlGaAs quantum dots fabricated by twofold cleaved edge overgrowth," *Phys. Rev. Lett.* **79**, 1917–1920.
- Wen, X. G., 1990a, "Chiral Luttinger liquid and the edge excitations in the fractional quantum Hall state," *Phys. Rev. B* **41**, 12 838–12 844.
- Wen, X. G., 1990b, "Electrodynamical properties of gapless edge excitations in the fractional quantum Hall states," *Phys. Rev. Lett.* **64**, 2206–2209.
- Wen, X. G., 1991a, "Gapless boundary excitations in the quantum Hall states and in the chiral spin states," *Phys. Rev. B* **43**, 11 025–11 036.
- Wen, X. G., 1991b, "Edge transport properties of the fractional quantum Hall states and weak-impurity scattering of a one-dimensional charge-density wave," *Phys. Rev. B* **44**, 5708–5719.
- Wen, X. G., 1992, "Theory of the edge states in fractional quantum Hall effect," *Int. J. Mod. Phys. B* **6**, 1711–1762.
- Wen, X. G., 1995, "Topological orders and edge excitations in fractional quantum Hall states," *Adv. Phys.* **44**, 405–473.
- Wen, X. G., and Q. Niu, 1990, "Ground-state degeneracy of the fractional quantum Hall states in the presence of a random potential and on high-genus Riemann surface," *Phys. Rev. B* **41**, 9377–9396.
- Wen, X. G., and A. Zee, 1992, "Classification of Abelian quantum Hall states and matrix formulation of topological fluids," *Phys. Rev. B* **46**, 2290–2301.
- Willett, R. L., M. A. Paalanen, K. W. West, L. N. Pfeiffer, and D. J. Bishop, 1990, "Anomalous sound propagation at  $\nu = 1/2$  in a 2D electron gas: Observation of a spontaneously broken translational symmetry?" *Phys. Rev. Lett.* **65**, 112–115.
- Willett, R. L., R. R. Ruel, K. W. West, and L. N. Pfeiffer, 1993, "Experimental demonstration of a Fermi surface at one-half filling of the lowest Landau level," *Phys. Rev. Lett.* **71**, 3846–3849.
- Wu, M. K., J. R. Ashburn, C. J. Torng, P. H. Hor, R. L. Meng, L. Gao, Z. J. Huang, Y. Q. Wang, and C. W. Chu, 1987, "Superconductivity at 93 K in a new mixed-phase Yb-Ba-Cu-O compound system at ambient pressure," *Phys. Rev. Lett.* **58**, 908–910.
- Yacoby, A., H. L. Stormer, N. S. Wingreen, L. N. Pfeiffer, K. W. Baldwin, and K. W. West, 1996, "Nonuniversal conductance quantization in quantum wires," *Phys. Rev. Lett.* **77**, 4612–4615.
- Yang, S.-R. E., M. C. Cha, and J. H. Han, 2000, "Numerical test of disk trial wave function for a half-filled Landau level," *Phys. Rev. B* **62**, 8171–8179.
- Yao, A., H. W. C. Postma, L. Balents, and Cees Dekker, 1999, "Carbon Nanotube intramolecular junctions," *Nature (London)* **402**, 273–276.
- Yu, Yue, 2000, "From composite fermions to the Calogero-Sutherland model: Edge of the fractional quantum Hall liquid and the dimension reduction," *Phys. Rev. B* **61**, 4465–4468.
- Yu, Yue, Wenjun Zheng, and Zhongyuan Zhu, 1997, "Microscopic picture of a chiral Luttinger liquid: Composite fermion theory of edge states," *Phys. Rev. B* **56**, 13 279–13 289.
- Zaslavsky, A., D. C. Tsui, M. Santos, and M. Shayegan, 1991, "Resonant tunneling of two-dimensional electrons into one-dimensional subbands of a quantum wire," *Appl. Phys. Lett.* **58**, 1440–1442.
- Zhang, S. C., T. H. Hansson, and S. Kivelson, 1989, "Effective-field-theory model for the fractional quantum Hall effect," *Phys. Rev. Lett.* **62**, 82–85.
- Zhang, S. C., and J. P. Hu, 2001, "A four-dimensional generalization of the quantum Hall effect," *Science* **294**, 823–828.
- Zheng, W. J., and Yue Yu, 1997, "Temperature-dependent crossover in fractional quantum Hall edges in the presence of Coulomb interaction," *Phys. Rev. Lett.* **79**, 3242–3245.
- Zou, Z., and P. W. Anderson, 1988, "Neutral fermion, charge-boson excitations in the resonating-valence-bond state and superconductivity in  $\text{La}_2\text{CuO}_4$ -based compounds," *Phys. Rev. B* **37**, 627–630.
- Zülicke, U., and A. H. MacDonald, 1996, "Electronic spectral functions for quantum Hall edge states," *Phys. Rev. B* **54**, R8349–R8352.
- Zülicke, U., and A. H. MacDonald, 1997, "Toward realistic effective models of quantum-Hall edges," *Physica E* **1**, 105–107; **3**, 229(E).
- Zülicke, U., and A. H. MacDonald, 1999, "Periphery deformations and tunneling at correlated quantum Hall edges," *Phys. Rev. B* **60**, 1837–1841.
- Zülicke, U., A. H. MacDonald, and M. D. Johnson, 1998, "Observability of counterpropagating modes at fractional quantum Hall edges," *Phys. Rev. B* **58**, 13 778–13 792.
- Zwick, F., S. Brown, G. Margaritonodo, C. Merlic, M. Onellion, J. Voit, and M. Grioni, 1997, "Absence of quasiparticles in the photoemission spectra of quasi-one-dimensional Bechgaard salts," *Phys. Rev. Lett.* **79**, 3982–3985.